UNIVERSITY OF OKLAHOMA

GRADUATE COLLEGE

STRATEGIES FOR CATALYTIC UPGRADING OF VAPOR STREAMS FROM THERMAL FRACTIONATION OF BIOMASS

A THESIS

SUBMITTED TO THE GRADUATE FACULTY

in partial fulfillment of the requirements for the

Degree of

MASTER OF SCIENCE

By

TYLER STEVEN VANN
Norman, Oklahoma
2016

STRATEGIES FOR CATALYTIC UPGRADING OF VAPOR STREAMS FROM THERMAL FRACTIONATION OF BIOMASS

A THESIS APPROVED FOR THE
SCHOOL OF CHEMICAL, BIOLOGICAL AND MATERIALS ENGINEERING

BY

_____
Dr. Steven Crossley, Chair

_____
Dr. Daniel Resasco

_____
Dr. Lance Lobban

Acknowledgements

I would like to thank my wife Melodie for all her support during the completion of my degree. I would also like to thank the bio-fuels group at OU for assistance throughout my time here.

Table of Contents

List of Tables

List of Figures

Introduction

As a result of increasing political and environmental concerns over the use of fossil fuels, current research is being conducted into fuel alternatives.[1-3] While many publications will argue that alternative fuels research is being driven by declining petroleum reserves or increase in demand, it is the environmental impact of petroleum that should be the driving force for this movement. For that reason the goal should be to develop a fuel that can be sustainable and provide a neutral effect on the environment. One of the most intriguing research areas is the use of lignocellulosic biomass for potential fuels. Lignocellulosic biomass such as hardwood trees or switchgrass are a more promising feedstock as compared to fermentation based feedstocks which compete with the world food supply. Current technology is based on the pyrolysis process of the lignocellulosic biomass such as wood, grasses and other plant material.[4, 5] In pyrolysis the biomass is heated to high temperatures (450-600°C) for less than a minute in an oxygen free environment. During this process the biomass decomposes into smaller organic compounds and water that can be condensed into what is known as bio-oil. Due to the nature of biomass the resultant bio-oil has a high oxygen content which would make it incompatible with a petroleum based refinery. For that reason the bio-oil needs to be deoxygenated before insertion into a refinery process. Many research groups around the world are investigating this upgrading step.[6, 7] Once the pyrolysis vapors are condensed the resultant liquid is highly unstable.[8] This low pH liquid is capable of catalyzing many unwanted polymerization reactions. An upgrading (i.e. removal of harmful functional groups) in the vapor phase would be critical in the stabilization of the bio-oil.

Initially commercial upgrading was done via catalytic fast pyrolysis (CFP) which was based on upgrading via zeolites in the vapor phase, specifically the MFI framework zeolite. One drawback to this process is the fast rate of deactivation of the zeolite catalyst.[9, 10] There are many current studies that try to improve zeolite catalyst lifetime by various strategies.[11] The underlying problem with many of these strategies is that the feedstock pyrolysis vapor composition is the same regardless of upgrading strategy. Under most conditions the complex mixture is too much for any one catalyst to withstand. For these reasons it was then proposed that fractionation of the bio-oil is needed for optimum upgrading.[12] Obviously using distillation techniques it would be extremely difficult to achieve a desirable separation. Once again the complexity of the bio-oil mixtures will lead to bio-oil polymerization and corrosion of the apparatus due to the high acidity. Other separation techniques have been proposed, but the economic feasibility for such separations seems to be under question. As it can be easily seen biomass pyrolysis techniques have many hurdles to overcome before they become a realistic alternative to conventional petroleum based fuels.

Thermal Fractionation of Biomass

As stated, conventional biomass pyrolysis is a one-step process where the biomass is heated in a matter of seconds to 500°C. It has been proposed that a staged thermal fractionation (ie sequential heating treatments at higher temperatures) in an inert environment could decompose the biomass components (hemicellulose, cellulose, lignin) in fractions due to increased thermochemical stability. Initially the biomass would be heated to between 250-270°C, where the hemicellulose fraction should begin to decompose. As hemicellulose decomposes numerous light oxygenated compounds

such as acetic acid, acetaldehyde, and acetol as well as water should be volatilized. To a lesser extent it would also be expected that small amounts of the cellulose fraction would decompose as well leading to the production of the sugar-derived furanic compounds. For the purpose of this work this step and subsequent catalytic upgrading will be termed Stage 1 torrefaction. The resultant solid from Stage 1 is then heated to 360°C. At these higher temperatures the decomposition of cellulose should begin.[13] The major product of cellulose heating at higher temperatures is levoglucosan. Along with levoglucosan the stage should also result in other furanic compounds from sugar decomposition. This heating treatment has been coined Stage 2 torrefaction. At this point the solid that remains is heated to over 500°C or fast pyrolysis conditions. In the last stage the thermally stable lignin portion finally begins to decompose. Lignin is a complex mixture of many aromatic alcohols or monolignols, as they decompose large amount of aromatic alcohols with ether functional groups are volatilized. These compounds, which are known as methoxyphenolics, make up the largest portion of Stage 3 Pyrolysis. Other compounds seen in the final stages are light oxygenates, furanics, and carbon dioxide, all of which are small in comparison to the large amounts of methoxyphenolics. In Figure 1 a simple diagram has been constructed to illustrate the three (3) stage process and the resultant compound families from each stage.

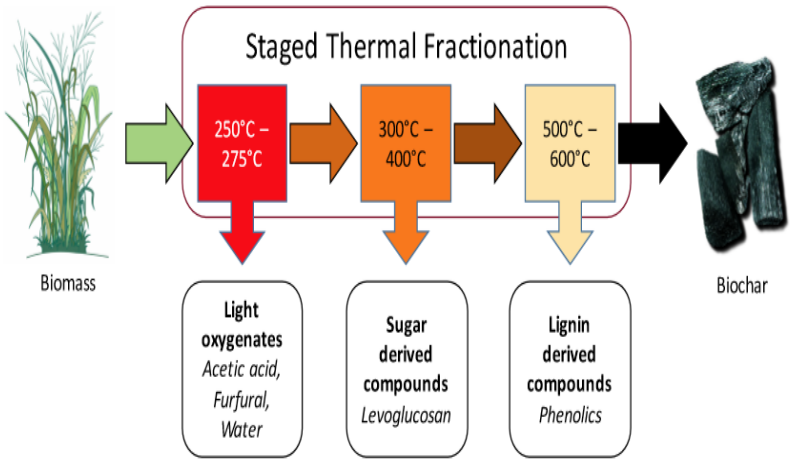

Figure 1. Basic configuration for thermal fractionation of lignocellulosic biomass and resultant compound families. (Waters 2016)

If the proposed separation and Figure 1 can be achieved then it would be logical to treat the upgrading of each stream separately. For any given vapor stream, the compound families and thus chemistries to upgrade them varies greatly. In this work a number of vapor phase and liquid stabilization strategies are proposed for each of the three stages.

Upgrading Strategies for Torrefaction Streams

Obviously, each of the different streams will require a unique upgrading strategy based on the respective composition of that stream. The initial heating at 270°C should results in a large amount of water being produced in addition to the organic compounds. For this reason the catalyst of choice will need to be capable of desired chemistries in the presence of the water vapor. Many strategies have been proposed for the upgrading of these highly acidic streams and will be discussed in Chapter 3. From the 2nd stage it is assumed that most of the cellulose will be dehydrated into levoglucosan (LGA). Most

upgrading strategies are greatly hindered by the presence of LGA in the vapor stream. It would thus be desirable to remove the levoglucosan from the vapor stream prior to any catalytic upgrading. A strategy for this will be presented in Chapter 6. Without LGA, the majority of Stage 2 will consist of furanic and to a smaller extent phenolic compounds. The final vapor stream should be mostly phenolics from lignin. A substantial amount of studies have been conducted targeting hydrodeoxygenation and alkylation chemistries in both the liquid and vapor phase.[14-16] These strategies will be discussed in Chapter 5.

Chapter 1: Methodologies

Pyroprobe System

The majority of the work carried out was done by use of CDS Analytical Pyroprobe Model 5250T fitted with a cryogenic trap and autosampler. This instrument is capable of heating samples in an inert environment on a milligram scale. Vapors from the respective streams traveled through heated (300°C) Silco-Steel transfer lines. Silco-steel was used exclusively to limit the amount of side reactions that can occur of traditional stainless steel. The model 5250 has a quartz heating chamber that is heated by a platinum coil to the specified time and temperature range. All experiments, whether it be for oak torrefaction or other pyrolysis experiments, were conducted in a similar manner.

In the case of catalytic upgrading of these vapor streams an ex situ catalytic reactor was constructed. This reactor using 6”x0.25”O.D. quartz reactor tubes heated by a Thermocraft oven at temperatures ranging from 250-600°C. The temperature of the reactor was maintained by a Omega Type K thermocouple attached to the exterior of the reactor tube near the catalyst bed. Depending on the mode (Pyro vs Trap) of the pyroprobe the flow rates through the reactor varied between 20-90 mL/min helium. A separate hydrogen stream was added to allow for 0-200 mL/min of hydrogen as needed. The system was also modified to allow a pure hydrogen flow of 50 mL/min for catalyst reduction prior to the introduction of torrefaction vapors. The quartz reactor consisted of 0.2 g of borosilicate acid washed beads (150-212 μm) from Sigma Aldrich and 1.0-10.0 mg of the catalyst. Typically the catalysts were pelletized to a range of 90-250 μm to allow for even distribution in the glass beads. This mixture of glass beads and

catalyst was added to the top of a small amount of quartz wool and capped with a similar amount of wool on top of the bed. A six-port valve on the pyroprobe allowed for bypass of the reactor system for experiments where pyrolysis vapors were sent straight to the GC-MS/FID system.

The previously described reactor set-up was developed out of necessity based on the results from reactions carried out in the commercial reactor provided by CDS. From experiments conducted using hydrgoen it was clearly evident that the 316 stainless steel reactor provided was not inert and high convervions of many products were seen in non-catalytic runs. It was hypothesized that the trace amounts of oxides found in 316-SS were reduced in the presence of hydrogen. As these reactions occur at a low partial pressure of reactants in the carrier gas the surface area of the steel tube would be adequate to cause unwanted conversion.

In all cases the vapors were sent to an online GC-MS/FID system. A Shimadzu QP2010 system fitted with a RTX-1701 column (60m x 0.25mm, 0.25 μm film thickness). A suitable GC column ramp rate was created to allow for separation of the numerous products seen in pyrolysis. This ramp consisted of a hold at 45°C for 4 minutes and then heated to 280°C at 3°C/min and then held for 20 minutes. The entire program lasted for 99 minutes for each sample. A 90:1 split ratio was used for the column flow. This would result in a column flow of 1 mL/min. Helium (UHP Airgas) carrier gas was used for all experiments.

The FID and MS detectors were used for both quantification and identification of all the vapor phase products. The mass spectrum allowed for identification of product peaks based on a library search as well as literature sources.[17] The mass spectrometer

is set to scan masses from 35.00-250.00 at 0.5 seconds per scan. Flame Ionization methods could then be used for quantification of these now identified peaks. A novel ECN model developed for the purpose of quantification of pyrolysis was used extensively in this work. The base model was developed by doctorate candidate Nhung Duong and modified as new compounds were identified in the vapor streams. This model accounted for different types of carbon-oxygen bonds found in pyrolysis and catalytically upgraded streams. It is well known that different C-O bonds can affect the intensity of the FID signal.[18]

Each experiment in the pyroprobe consisted of 0.6-4.0 mg of sample being placed in the heating chamber. The exact mass was dependent on the sample being examined, larger sample were often needed to provide adequate peak sizes in the chromatography. Red oak samples were traditionally weighed to be between 0.7-1.0 mg. For stage 2 & 3 a similar amount of stages 1 & 2 residual solid was used as the feed. Other samples ran fit in the specified mass range to prevent any saturation of the detector on the GC system. The red oak used was purchased locally and ground to 0.25-0.45 mm and dried in a vacuum at 60°C overnight. In previous studies the red oak composition was 21,47 and 27 wt% for lignin, hemicellulose and cellulose respectively.[19] The nature of non-oak samples can be found in the respective chapters. The sample was added to the top of a small amount of quartz wool in the reactor tube to prevent any particles from falling out of the sample tube as it was placed into the heating chamber.

Chapter 2: Red Oak Thermal Fractionation

Stage 1 Torrefaction

As stated previously, in the first stage of the torrefaction process the goal is to remove mostly water as well as the lighter oxygenated compounds such as acetic acid, acetaldehyde, and to a lesser extent, sugar derived furanic compounds such as furfural. The thermal conditions for this stage are 270°C for 20 minutes. The exact composition of Stage 1 compounds as determined by GC-MS/FID analysis can be seen in Figure 2 based on 1 mg of raw oak. As this is FID analysis, carbon dioxide and water would not be accounted for. It is known from unpublished work in the University of Oklahoma research group that the water content in this stage is approximately 65%. Once the composition was determined a plan for catalytic upgrading could be developed based on the available compound groups.

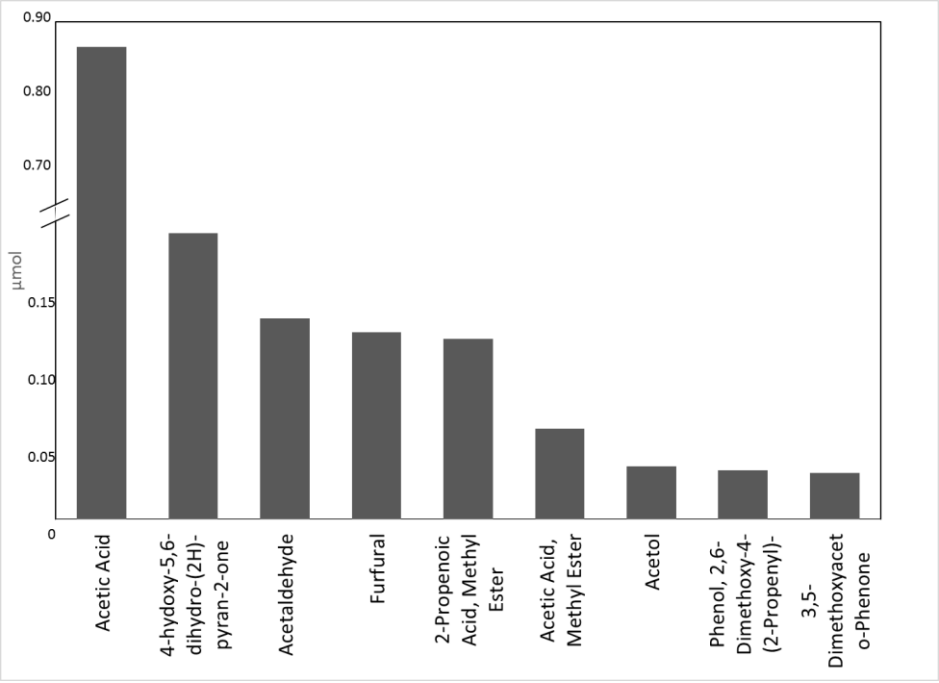

Figure 2: Product Distribution from Stage 1 Torrefaction. Normalized per 1 mg of biomass

As expected the major compounds from the first stage torrefaction are hemi-cellulose degradation products. The largest organic product is acetic acid at over 0.86 μmol/mg of biomass torrefied. Importantly, small amounts of pyranic and furanic species are seen. Any upgrading strategy therefore will need to be suitable for the larger furanic molecules as well. Based on this composition of the stream, we can take a structured approach to react each of the different compounds. A summary of the targeted chemistries can be seen in Chapter 3.

Stage 2 Torrefaction

In the second stage, thermal treatment of the Stage 1 residue is at 350°C for five (5) minutes. During this stage it is expected by earlier work that the cellulose and the remaining hemicellulose fractions should thermally decompose. As this is the expected degradation pattern in Stage 2, large amounts of sugar derived compound should make up the vapors, the largest of which should be levoglucosan. To a smaller extent, furanics which are also a sugar derived class of molecules should be observed. As it can be seen in Figure 3, Stage 2 is indeed made up mostly of these sugar derived products.

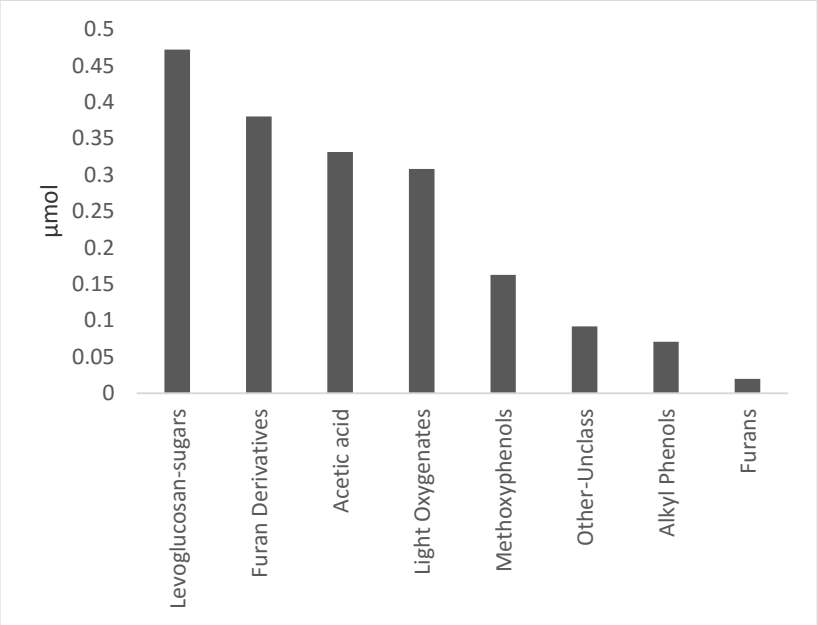

Figure 3: Composition of Stage 2 torrefaction vapors on a µmol of each compound per mg of biomass fed

It is of note that one correction was made to the data that is found in Figure 3. Actual data indicates that the levoglucosan peak is around 20x smaller. It was corrected because under these conditions a cryogenic trap is needed after torrefaction to allow for GC analysis. When this trap is heated to 300°C, it is believed that this temperature is not sufficient for the levoglucosan to be volatilized and thus detectable by the GC. Model studies were completed with pure levoglucosan pyrolysis that indicated around 95% of the levoglucosan that is pyrolyzed never makes it off of the liquid nitrogen trap. Thus during stage 2 it was assumed that the levoglucosan present is actually 20x larger than what is detected by the GC-MS/FID.

Stage 3 Torrefaction

The final step in the thermal fractionation process is the pyrolysis of the Stage 2 solid residue at 500°C for 60 seconds. It is expected that at these temperatures, the thermally

stable lignin would finally begin to decompose and give a vapor stream comprised primarily of phenolic species and a small amount of light gases. Figure 4 shows the major compound groups in the vapor stream in both a compound and carbon mole basis.

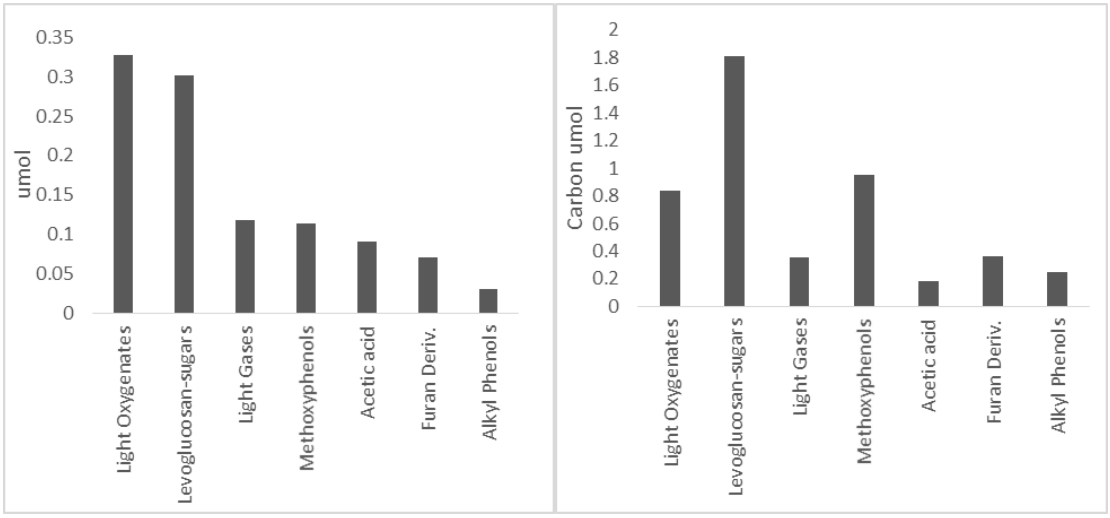

Figure 4: Left-Molar composition of Stage 3 Pyrolysis at 500°C. Right-Carbon molar composition of Stage 3 Pyrolysis at 500°C.

Interestingly, the major compound is not the phenolic species that were expected. The sugar derived levoglucosan is the major component of the system. On a compound molar basis it is light oxygenates, mainly acetaldehyde and acetol, that make up the largest component. As these are low carbon compounds, the total number of carbon moles in the species is not as high. It would appear based on this data that one of two directions needs to be taken. Firstly, it is possible that the thermal treatment in Stage 2 need to be increased. A higher temperature may lead to increased decomposition of the cellulose in that stage. Another direction would be to leave the stages as they are currently and make use of selective adsorption techniques to trap out the levoglucosan. This will be discussed in more detail in Chapter 6. If the stream can be purified to mostly phenolics a more efficient upgrading technique can be implemented.

Chapter 3: Upgrading of Stage 1 Torrefaction Vapors

Targeted Chemistries for Stage 1

Based on the compositions discussed in Chapter 2 for the Stage 1 thermal treatment, the upgrading strategy needs to be built around the large amount of acetic acid that is present. Initially the strategies being investigated followed what was seen in previous work completed at the University of Oklahoma, Pham et al. concluded that ketonization of the acids and esters could prove to be a promising route for stabilization of the bio-oil.[20-22]. Pham's work resulted in numerous publications discussing the kinetics and mechanism of acetic acid ketonziation over a Ru/TiO_2 catalyst. When undergoing ketonization two acid molecules will form a carbon–carbon bond sacrificing one molecule of carbon dioxide. This reaction is promising for many reasons. Firstly, many of the unwanted condensation reactions that occur in raw bio-oil are catalyzed by the acids that are present. This ketonization will act to raise the pH of the resultant liquid bio-oil and thus decrease the rate of oligomerization. Secondly, these ketones can be used as building blocks for further upgrading reactions. A ketone can be reacted with furfural, for example via aldol condensation, to form a higher molecular weight compound that is closer to the fuel range. A schematic of this reaction can be seen in Figure 5. This method has been discussed in great detail by work by Dumesic et al.[23, 24]

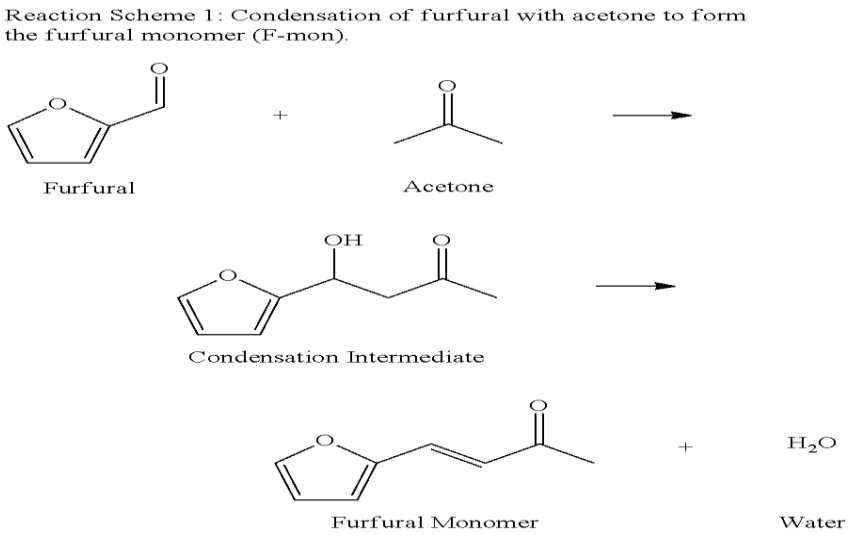

Figure 5: Dumesic, J. U.S. Patent for Making a C6-C15 hydrocarbon via dehydration of a carbohydrate such as glucose using acid catalyst to yield a furan derivative, followed by aldol condensation, then hydrodeoxygenation; renewable jet fuel

Another potential route for further upgrading of the ketone product would be to undergo hydrogenation to an alcohol. Alcohols are known to be great alkylating agents. Alkylation, similar to aldol condensation reactions, are way to increase the carbon number distribution in the liquid product.

Catalytic Upgrading of Stage 1 with Ru/TiO_2

To follow up on the work of Pham et al. the catalyst to be used for Stage 1 upgrading was chosen to be Ru/TiO_2. In their work they have shown that Ru/TiO_2 is highly effective for the ketonization of acetic acid to acetone in the liquid and vapor phase. 5 wt% Ru/TiO_2 was prepared via the incipient wetness technique, which has been discussed thoroughly in earlier work.[14, 25] To study the effect of Ru/TiO_2 on the Stage 1 torrefaction vapors an *ex situ* catalyst bed of 1 mg of catalyst mixed in 200mg of acid-washed glass beads was utilized. The catalyst was reduced in 50 mL/min pure

hydrogen at 400°C for two hours prior to use. Under reaction conditions the flowrate was set to be 20 mL/min of hydrogen in 20 mL/min of helium and a reactor temperature of 400°C was used.

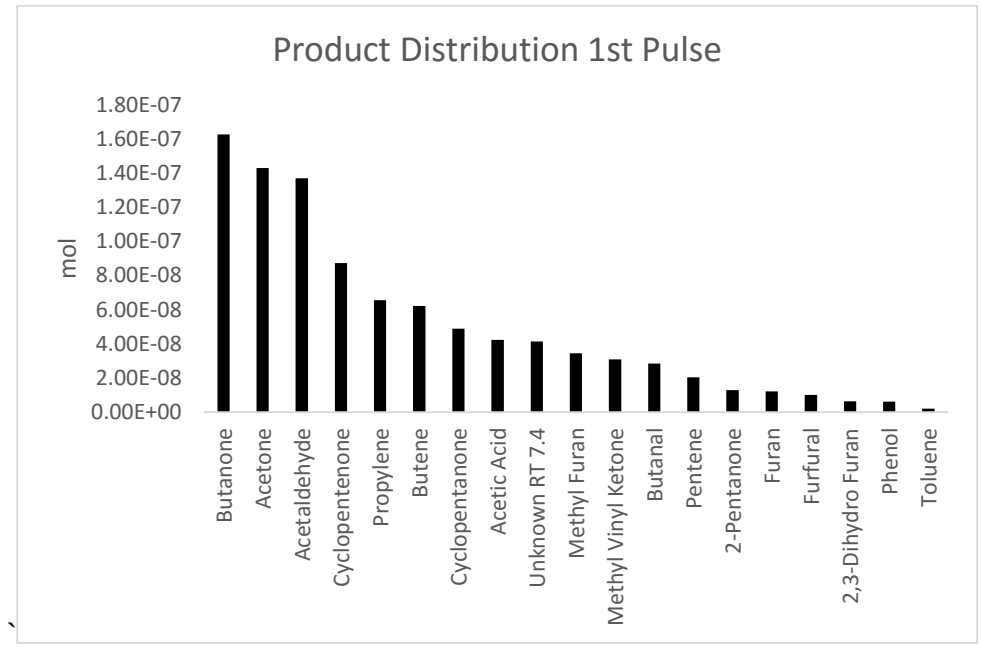

Figure 6: Major Products of 1st pulse of Stage 1 torrefaction with 5% Ru/TiO_2 catalyst.

The results of the upgrading for the first biomass pulse have been summarized in Figure 6. Remarkably, the yield to the desired products was extremely high for this upgrading step. As expected, high levels of ketonization were observed. The butanone and acetone are ketonization products from acetic acid and propenoic acid-methyl ester. It is not yet understood why the butanone product seems to be favored over the self-ketonization product acetone. Although the ketonization of the acids was prevalent, the most significant finding from this work was the reactions related to furfural. A large amount of the furfural underwent a ring re-arrangement to form 2-cyclopenten-1-one and cyclopentanone via Piancantelli rearrangement. The reaction of furfural to

cylcopentanone via Piancantelli Rearrangement has been observed over Pt/C catalyst in the liquid phase.[26] The mechanism has also been an intriguing reaction for application in bio-fuel production.[27] To our knowledge this is the first such example of this reaction in the vapor phase over Ru/TiO_2. The cyclopentanone produced via this reaction can then be used in numerous subsequent reactions to produce fuel range products.[28] It has been proposed in this group that the most likely source of the 2-methyl furan, is from selective hydrodeoxygentation. While this reaction has not been probed extensively in the vapor phase for Ru/TiO_2, similar reaction pathways have been examined in previous work with other bimetallic catalysts.[29]

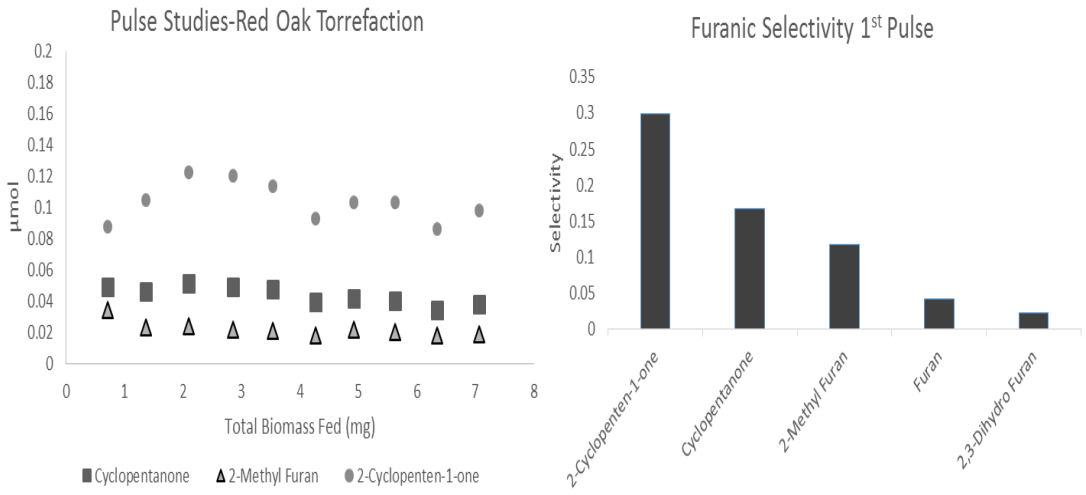

Figure 7: Left : Furfural Products as a function of biomass fed. Right: Product yields derived from Furfural on the first biomass pulse

Figure 7 gives insight into the reactions over furfural over the Ru/TiO_2 catalyst. Initially we see that 2-cyclopenten-1-one is the main product. This product can also be hydrogenated to form cyclopentanone. Originally this peak was difficult to quantify as it overlapped retention times with furfural, (reactant compound). Deconvolution was completed by tracking specific m/z in the mass spectrum. Masses 82 and 96 and unique

to 2-cyclopenten-1-one and furfural respectively. A model compound injection was done to determine the ratio peak intensities between these two compounds. This ratio could then be used to split the FID area into the two respective peaks. Figure 8 clearly shows the overlap between the two peaks. As stated in the FID spectrum only one peak is observed. The discovery of this phenomena greatly increased the yield to ring re-arrangement products over initial calculations

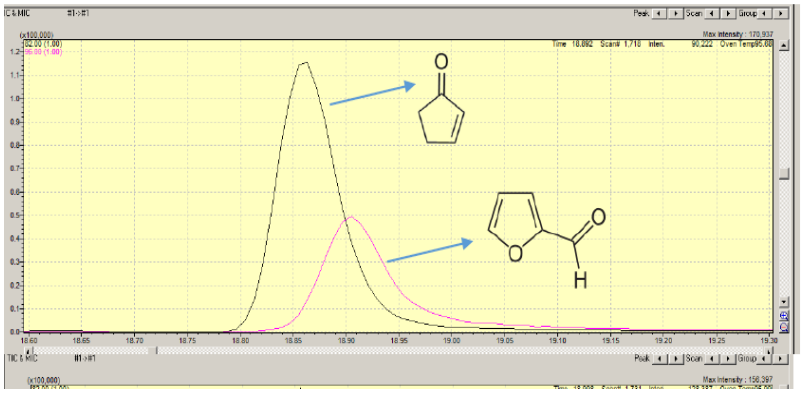

Figure 8: 1st Pulse of Stage 1 Upgrading with Ru/TiO_2. Overlapping of Furfural/Cyclopentenone Peak

From the molar amounts of products observed attributed to furanic reactions, another interesting observation was noticed. The molar amounts of these products was greater than the furfural measured to be in the torrefaction vapors. It was clearly evident that another compound must be playing a role in these reaction. From blank experiments we see the following phenomena:

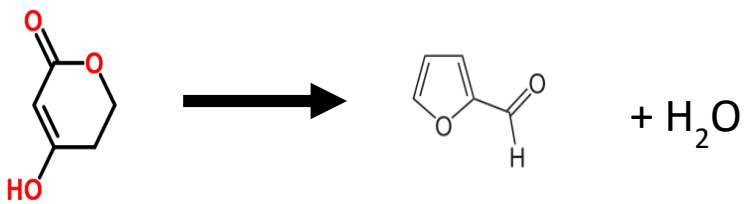

This dehydration of the pyranic species is occurring with increased residence time in the heated transfer lines. An increase in furfural molar amount in blanks through an empty reactor vs. straight into the GC system verifies this phenomena. At higher temperatures such as in pyrolysis it is likely that this phenomena would be easily overlooked.

Of great importance in this work is catalyst deactivation. As one of the main reasons for separation of the different chemical compounds via thermal fractionation is to improve catalyst life it will be important to observe the catalyst life as a function of the biomass that is passed over it.

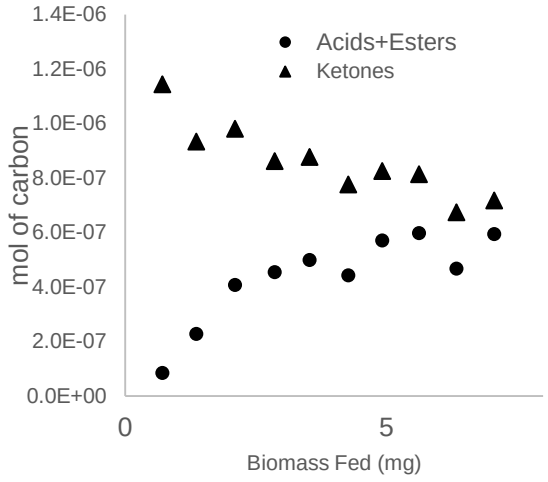

Figure 9: The mole of carbon found in each of the compounds as a function of the biomass that is pulsed over the reactor

As it can be seen in Figure 9, after an initial deactivation phase the catalyst becomes fairly stable and the amount of ketones produced seems to level off. This is very promising for the purposes of this work. When the full bio-oil is pulsed over Ru/TiO_2 deactivation is rapid. Also of note is that many of the reactions observed, such

as the Piancantelli Rearrangement, are only made possible when the streams are purified via the thermal fractionation that is outlined.

Size Selective Conversion by use of Zeolite Catalysts

From examination of the composition of the stage 1 torrefaction stream it is evident that a wide variety of compound sizes are present. The difference between the major organic product, acetic acid, with a kinetic diameter of 4.4 angstrom and the large furanics (5.3A) provide an opportunity to attempt to react these compound selectively based on size. Huber et al. discussed a similar approach using a wide variety of zeolite catalysts for biomass upgrading.[9] Zeolites can be synthesized with dozens of different pore sizes and structures. For this strategy the goal would be to pick a zeolite with pores large enough for the acetic acid to easily diffuse and limit the amount of furanics and pyranics. Most suitable zeolites with these characteristics are 8-membered ring zeolites with either a 2 or 3-dimensional pore structure. The major fault of these candidates is the large internal intersections found inside the crystal. After investigation SAPO-34 was seen as a suitable candidate for screening with the stage 1 torrefaction vapors. The pore size (5.0 angstrom Norman Radii) from the chabazite allows for easy accessibility for the acetic acid while blocking the majority of the other components. As this technique has not previously discussed in literature the expected product was not known. Ketonization would be desirable but has not yet been investigated with model compounds. Also it would be assumed that any aromatics formed inside the pores would be too large to escape leading to undesirable coke. SAPO-34 has traditionally been used methanol-to-olefin (MTO) reactions.[30] If similar chemistries could be

achieved with acetic acid the resultant olefins could be used in a variety of ways. One such technique is discussed in more detail in Chapter 5.

In reality what is seen with SAPO-34 (ACS chemical, 2.1 mg) when used for Stage 1 torrefaction upgrading is that a small amount of light gases are produced and quick deactivation is observed. It is believed that the high temperatures used (500°C) favors aromatization of the hydrocarbon pool and once the aromatics are formed they cannot escape the pores and lead to quick deactivation. An interpretation of FID area in Figure 10 illustrates that compared to ZSM-5, furfurals appear to not be reacting inside pore structure in SAPO-34. The initial pulse shows some loss of furfural attributed to reactions on the external surface of the catalyst. Acetic acid appears to react for a number of pulses on the other hand. The difference in apparent deactivation would lead to the conclusion that different amounts of active sites are available to the respective components.

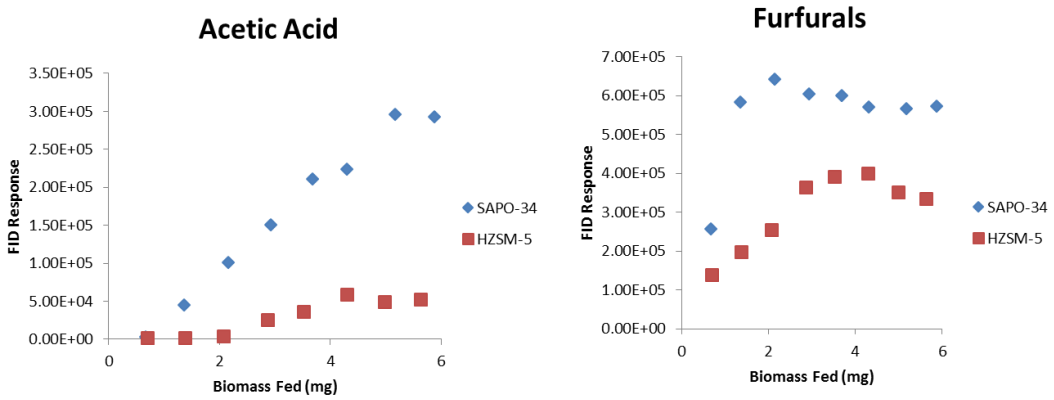

Figure 10: Comparison of FID signal with different pore size catalysts as a function of biomass torrefied. Squares: HZSM-5 Diamonds: SAPO-34

In a related study, a sequential bed was used with SAPO-34 then a second bed with HZSM-5 at 500°C. 4.5 and 2.0 mg of the SAPO-34 and HZSM-5 were used to

examine if the light gases created from SAPO-34 could increase the yield of furanics to BTX (Benzene-Toluene-Xylene) products via Diels-Alder condensation. (Diels-Alder discussed further in Chapter 5)

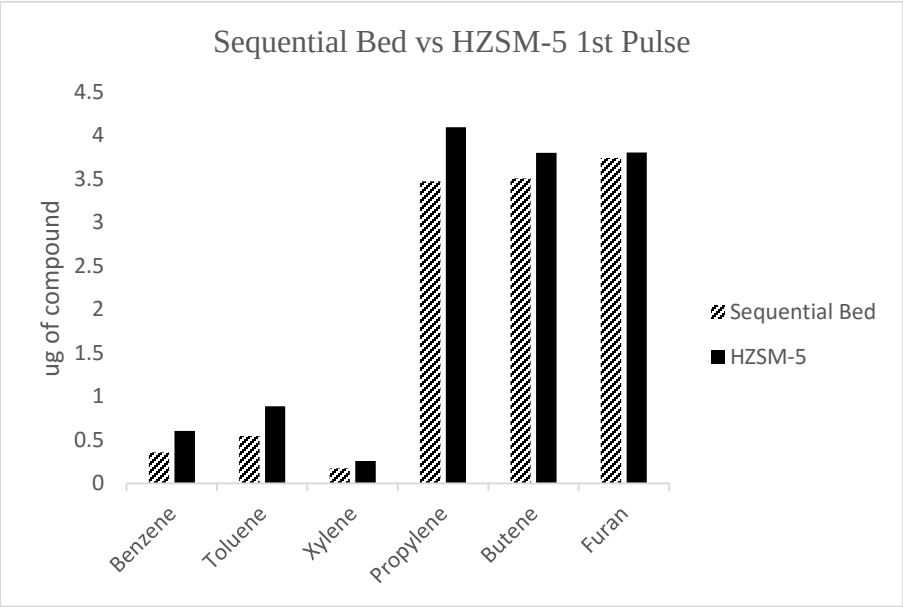

Figure 11: Comparison of Sequential Bed on Aromatic Production

Figure 11 represents the aromatic and light gas species observed in the initial pulse of stage 1 torrefaction vapors. It can be seen that no enhancement to aromatic production is seen. Subsequent pulses also yielded no increase in aromatics as compared to HZSM-5. It is of note that this represents a small fraction of the reactant vapors (<10%). Most the organic species are still ending up as coke, similar to what is seen if HZSM-5 is used alone for Stage 1 upgrading. The small differences in BTX production would also indicate that it is the furanics that are likely ending up as the aromatic product and even when no acetic acid is present in the HZSM-5 the aromatic yield is not affected greatly. No significant amounts of acetone are observed in this

case. It would appear that most of the acetic acid ultimately ends up as coke deposited on the catalyst as discussed previously.

Sequential Bed Reactions Targeting Acylation of Furanics

Mechanistic studies conducted by Gumidyala et al. for the ketonization of acetic acid over zeolites, specifically HZSM-5, have shown the formation of an acyl group to be a crucial step. The proposed mechanism can be seen in Figure 12.

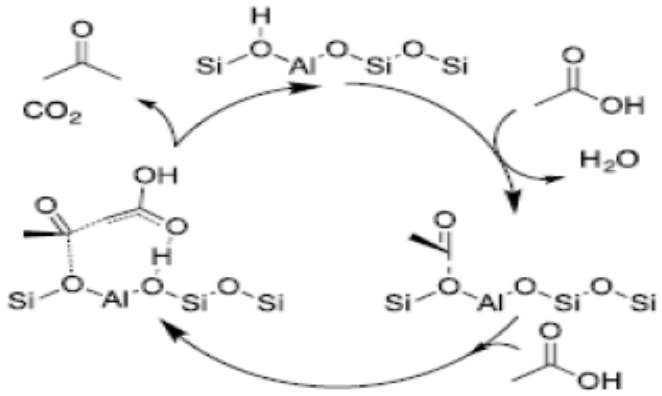

Figure 12: Proposed mechanism of acetic acid ketonization over HZSM-5

The formation of the acyl at low temperatures led to question of whether this acyl group could be used in acylation as opposed to ketonization. It would be highly desirable to use this acyl group for acylation of furanic and phenolic compounds. This serves two purposes. One, it eliminates the carbon lost via CO_2 during ketonization. Secondly, the acylation leads to higher carbon molecular weight compounds through C-C bond formation to send to the gasoline pool. Gumidyala in a series of studies with model compounds has shown that acylation of furanics and phenolics is indeed possible using ZSM-5 as the catalyst. For 1st stage torrefaction implications he also has shown that the acylation of furfural is not practical. A mixture of acetic and furfural leads to high levels

of coke. It has been shown that furan is a promising candidates for acylation and can be easily be obtained from furfural via decarbonylation.[31] This strategy was investigated with the real streams in a dual bed catalytic reactor. The first bed consisted of 5 mg of Pd/SiO_2 at 250°C to decarbonylate the furfural in the stream to furan. Figure 13 shows the resultant vapor stream after reaction with just the first Pd/SiO_2 bed. We see that most of the furfural is adsorbed on the catalyst and it is not seen in the form of decarbonylation products (furan) or unreacted. Also from Figure 13 it can be seen that the acetic acid yield is reduced by 50%. It is likely the temperatures are too low for full desorption from the catalyst surface. Nonetheless, the resultant stream although much smaller in molar amount still contains the desirable characteristics of having acetic acid and a small amount of furan/methyl furan. It is possible that optimization of conditions or reactors with greater partial pressures could increase yields significantly.

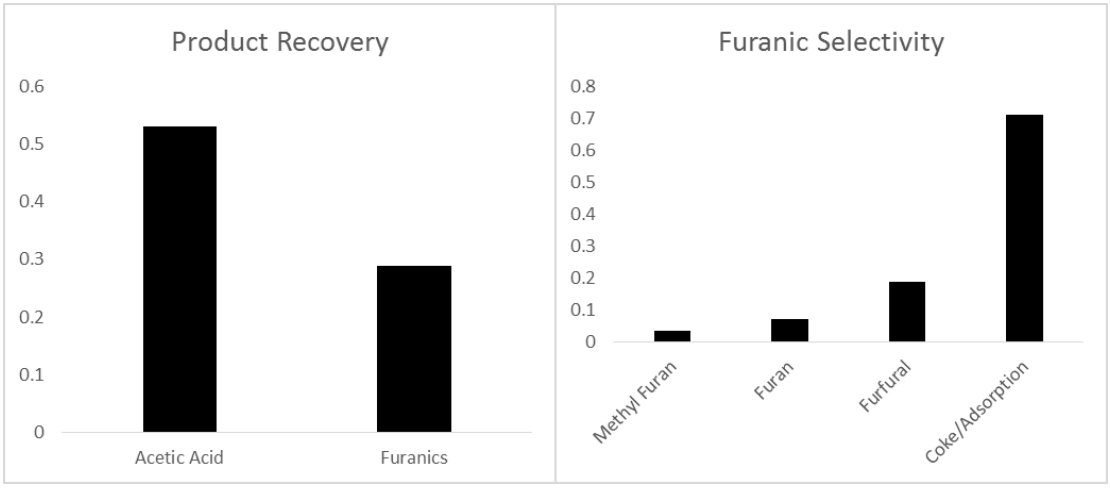

Figure 13: Left: Product Recovery based on blank levels. Right: Yields of the furanic/pyranic species to products observed via GC-MS/FID

The next step was to add the second catalyst bed. Directly, below a Pd/SiO_2 a HZSM-5 (Zeolyst CBV8014) was created with 1.5 mg of catalyst. The results of this

process can be seen in Figure 14. Unexpectedly, no acylation was observed. The furanic species have disappeared from the spectrum leading to the conclusion that they formed coke on the zeolite.

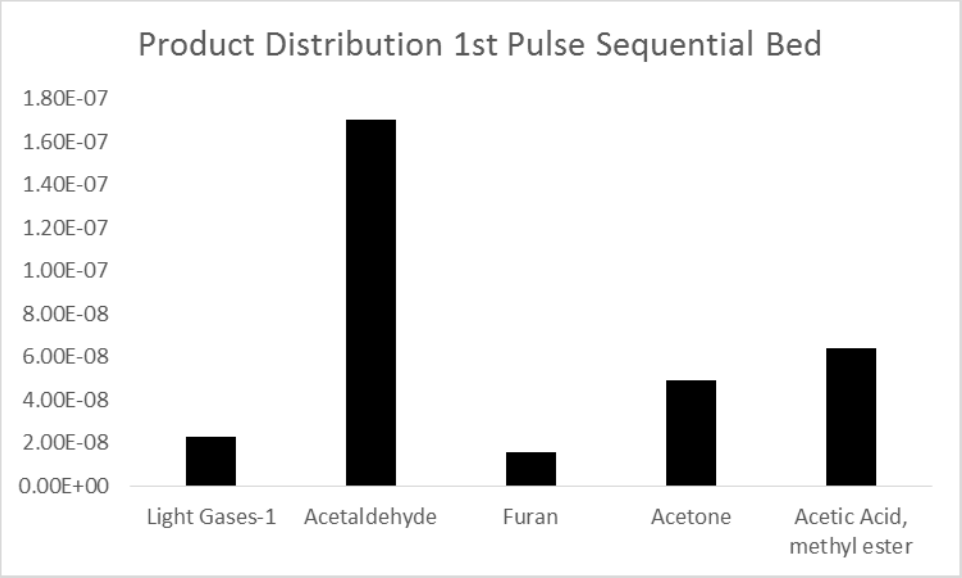

Figure 14: Product Distribution from First pulse of dual beds using 2.0 mg Pd/SiO_2 and 1.5 mg HZSM-5 in moles

Also, the acetic acid reacted to form a methyl ester product. In stage 1 torrefaction the mass of observed products is seen to be around 0.125mg/mg of biomass fed. After the dual beds are utilized the mass drops down to 0.017, an almost 90% reduction. It is likely that these types of experiments will be difficult moving forward with the current pyroprobe set up. While model compound studies have shown promise for these reactions, it is likely that the drastic differences in partial pressure with the real torrefaction streams in the pyroprobe is hampering the catalyst activity. Research is currently underway to verify the dual bed approach can be utilized if partial pressures are in a more realistic range for the scaled up process.

Chapter 4: Selective Oxidation of Furfural to Furoic Acid using Gold Support Catalysts and Subsequent Decomposition of Magnesium Carboxylate Salts

[a]Manuscript currently under preparation. Oxidation work was carried out by Daniel Santhanaraj, TGA-MS experiments by Lawrence Barrett. Text and Salt Decomposition by Tyler Vann

Tyler Vann, Daniel Santhanaraj, Lawrence Barrett, Daniel Resasco, Steven Crossley*

School of Chemical, Biological and Materials Engineering, University of Oklahoma, Norman, OK, 73019, USA
*Corresponding author: Tel.: +1 405 325 5930 E-mail address: stevencrossley@ou.edu

Preface

In conjunction with vapor phase stage 1 work completed at the University of Oklahoma in this study many aspects of the upgrading in the liquid phase are being investigated as well. In this chapter a manuscript of work describing a liquid phase technique applicable to stage 1 torrefaction upgrading can be seen.

Abstract

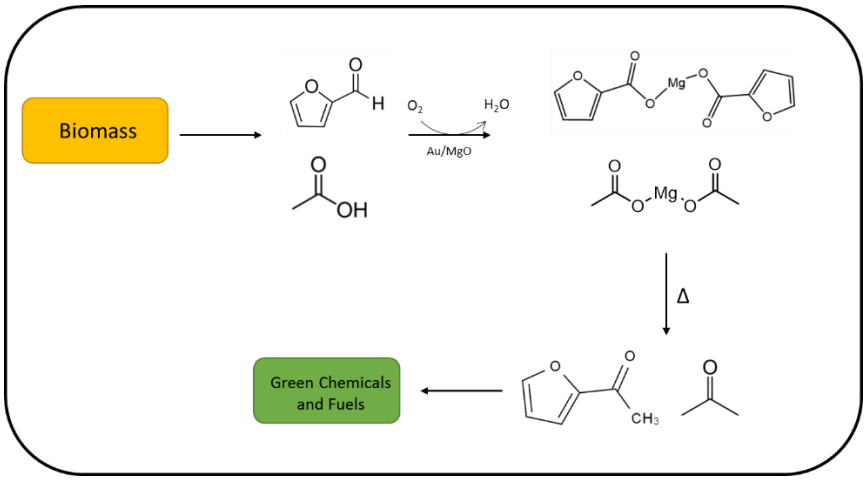

Although furfural is a well-known product from the thermal decomposition of lignocellulosic biomass, a suitable strategy for upgrading to yield a fuel range product has been a challenging topic. In this work a straightforward and re-useable approach for selective oxidation of furfural to yield furoic acid has been investigated using supported gold catalysts. Using gold supported on magnesium oxide or alumina in a water solvent results in the formation of furoic acid. If MgO is present in the aqueous solution, magnesium furoate salts are formed from reaction with $Mg(OH)_2$. As the reaction occurs and furoic acid is produced the MgO acts to titrate the acid. These salts can then be thermally decomposed in the presence of other salts such as magnesium acetate to yield a ketone product. The molar ratios of each of the salts can then be tailored to preferentially form the cross-ketone and is presented in this contribution. Detailed product identification and quantification has been carried out to analyze the decomposition products. It is well known that ketones are an instrumental building block in the formation of carbon-carbon bonds in biomass refining.

Introduction

An increased emphasis on the production of renewable fuels and chemicals has led to the development of a wide variety of techniques for the preparation of materials traditionally derived from crude oil. Biomass feedstocks can be converted into a wide variety of platform chemicals by use of heterogeneous catalysis or fermentation methods.[3, 32] Of particular interest, sugar derived molecules such as furfural and hydroxymethyl furfural (HMF) are common products from the degradation of polymers such as starch, cellulose and hemicellulose.[33] These molecules have been shown to be an important building block for a wide variety of specialty chemicals and fuels.[26, 34]

Hydrogenation and HDO reactions have been studied in great depth to produce compounds such as furfuryl alcohol and methyl furan over a wide variety of metal catalysts.[31, 35, 36] Another technique gaining attention particularly in the green chemical industry is the selective oxidation of HMF to form 2,5-Furandicarboxylic acid (FDCA), which has been proposed as a potential substitute for terephthalic acid used the production of poly(ethylene terephthalate) or PET.[37] This substitute, termed as PEF, poly(ethylene 2,5-furanoate), has been shown to compare quite well with traditional PET.[38] It is likely that similar oxidative chemistries could also be carried out with furfural. The subsequent furoic acid (FA) could be used for a number of targeted chemicals for both biofuel and fine chemical production.

The oxidation of HMF or furfural would be most economically favorable with use of oxygen/air as opposed to other oxidation techniques. In general this oxidation can occur a select group of supported Pt, Pd and Au catalysts in the aqueous phase.[39, 40] [41]It has been shown that high yields can only be obtained by the addition of a base to form an alkaline solution. Without a basic solution the catalysts in the platinum group and gold are highly susceptible to oxygen poisoning. The base is used for the neutralization of the acids which would otherwise adsorb strongly onto the metal surface and lead to fast deactivation. Traditionally, sodium or potassium hydroxide has been added to the reaction solution to product the respective salts. Historically, quantitative yields of FDCA have been shown with Pt/Al_2O_3 at 60°C with 0.2 bar oxygen pressure with KOH maintaining a pH of 8-11.[40, 42] . Supported gold nano-catalysts are also gaining traction for use in the oxidation of both HMF and furfural.[43, 44] For these products to be useful in biofuel production the resultant carboxylate or

acid would then need to be upgraded by other means to produce a chemical with the necessary carbon backbone length to be blended into the fuel pool. It would thus be desirable to obtain backbones >C6.

Research in the area of divalent salt decomposition such as Ca^{2+} or Mg^{2+} has been well documented.[45-47] The products from such decomposition result in a symmetric ketone as well as CO_2 and regeneration of the metal oxide through a process known as ketonic decarboxylation, the mechanism of which has been a topic of great debate for the last half century. Importantly for a green process, the regeneration of the oxide thus leads to renewable process capable of increasing the carbon backbone of the compounds, which is obviously desirable in the production of fuel range products. Mixtures of different carboxylate salts have also been shown to produce cross-ketone products.[48, 49] This is of particular importance due to the large varieties of carboxylic acids that are present or can be produced from traditional bio-oil.

In this contribution, selective oxidation of furfural at moderate temperatures was carried out using Au-supported catalysts (MgO or Al_2O_3. The role of an alkaline solution using $Mg(OH)_2$ as the base during the reaction has also been investigated. The decomposition of the resultant carboxylate salts was then examined using gas chromatographic and thermogravimetric analysis techniques.

Results and Discussion

Selective Oxidation of Furfural

Many research groups have shown the importance of an alkaline solution on the selective oxidation of sugar derived products such as glucose and 5-(Hydroxymethyl) furfural (HMF). In previous oxidation studies a carbonate buffer, KOH or NaOH

titration is used to raise the pH into the desired pH range (9-10).[50-52] In this work to achieve the desired pH range, magnesium oxide was dissolved into the water solution. It is well known that MgO in water forms $Mg(OH)_2$ and thus an alkaline solution. This technique should have the same effect as traditional methods to raise the pH of the solution to improve catalyst stability and reaction rates.

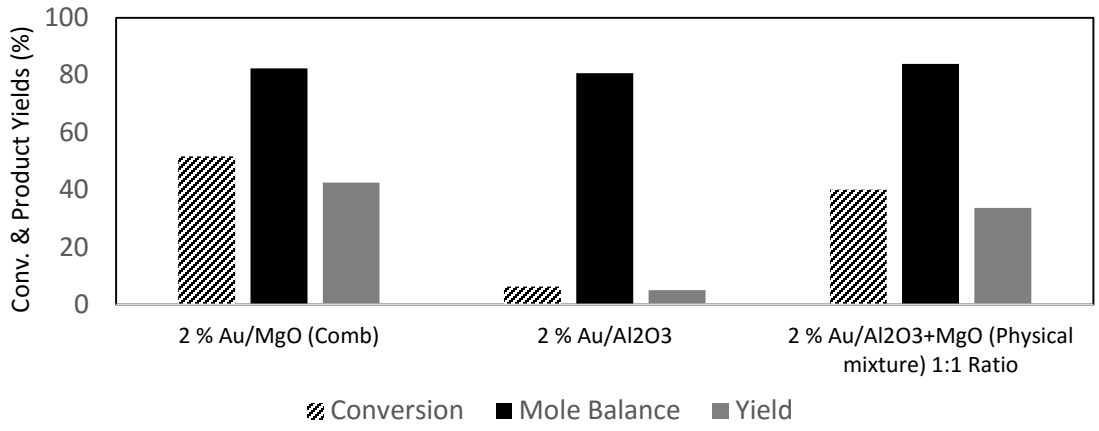

Figure 15: Summary of conversion and yields for selective oxidation reactions over Au-Supported Catalysts after thirty minutes or reaction time

A 2%Au/MgO catalyst was prepared for the selective oxidation of furfural to furoic acid. Reactions were carried out in an aqueous solution at 95°C with an initial furfural concentration of 0.22M and 50 milligrams of the catalyst. After thirty minutes of reaction time a furfural conversion of 51% was observed as shown in Figure 15. HPLC analysis of the liquid indicated that the product yield of 43% with 100% selectivity to the oxidized product. Due to the nature of the HPLC analysis it was not initially known if the product was simply furoic acid or magnesium furoate. It has been shown that $Mg(OH)_2$ formed via dissolved MgO can act to titrate the acid in a water solvent to form these magnesium salts. In this study it is likely salt formation is

prevalent. No other products were observed via HPLC. In a similar manner 2%Au/Al_2O_3 was also investigated under the same reaction conditions. A sharp conversion drop to only 6% was observed with a yield of 5% to the desired product. This would help support the salt formation hypothesis. The lack of the base to titrate the formed acid product leads to over-oxidation of the gold catalyst and almost immediate deactivation.

To test this hypothesis and show the importance of $Mg(OH)_2$ in solution, the reaction was carried out using a physical mixture of 2%Au/Al_2O_3 and MgO, 1:1 on a mass basis. The introduction of the MgO increases furfural conversion after thirty minutes up to 40% with similar selectivity and product yield to previous experiments. It becomes immediately apparent the necessity of having a gold surface clear of these oxygen poisons. Without the $Mg(OH)_2$ potential yields are greatly hampered by catalyst deactivation. A summary of the conversions and yields for each run can be seen in Figure 15. While magnesium oxide was used extensively in this study, current literature would suggest other divalent cations or monovalent cations would also be a suitable alternative as a source for the hydroxide in solution. Although the differences in decomposition behavior would tend to support the use of divalent cations such as magnesium and calcium. The carboxylate salts formed during the course of reaction cannot be directly used for any potential application in terms of biofuels or chemicals. Therefore, it is essential to convert these salts into stable hydrocarbons through C-C bond formation.

Thermogravimetric Analysis

Of particular importance to the feasibility of this reaction system is the magnesium salt formation and subsequent decomposition. For further upgrading purposes the magnesium furoate needs to decompose to form the organic product and regenerate the MgO to be recycled back into the system. Many studies have been conducted on the nature of magnesium and other carboxylate salt decomposition.[53, 54] While the mechanism is still unclear, salt decomposition ultimately leads to ketonic decarboxylation and thus a useful ketone as a desired product. This method has been used previously in the production of acetone from calcium acetate on a commercial scale.

It was previously unknown whether magnesium furoate would decompose to form the self-ketonization product of Di-2-furylmethanone. Literature suggests that for most acids lacking an α-hydrogen the main product would be the conjugate olefin. This product comes from the instability of the of free-radical intermediates, CO is lost and results in the eventual formation of the alkene product.[45, 46]

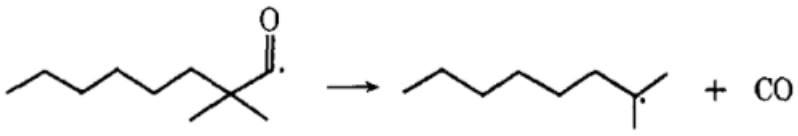

Scheme 1: Decarbonylation of free radical formed from carboxylate lacking α-hydrgoen during ketonic decarboxyation

A well-known exception to this mechanism is that of benzoate salt.[45] While lacking an α-hydrogen the resultant phenyl radical is highly energetically unfavorable as compared to the benzoyl radical. For this reason carbon monoxide is not lost and the

symmetrical ketone of diphenyl ketone is seen in roughly equimolar amounts to benzene.

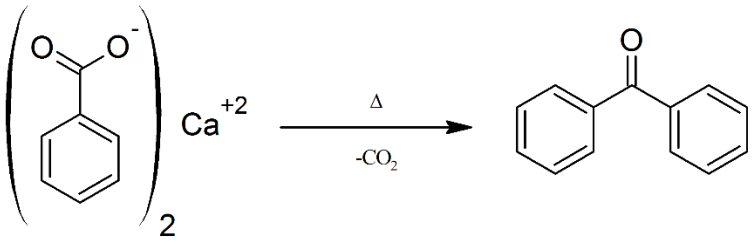

Scheme 2: Ketonic decarboxylation of calcium benzoate

The question becomes whether furoate will behave similar to the benzoate salt or other salts lacking an α-hydrogen. In this study, magnesium furoate was heated to 500°C in an analytical pyroprobe, with the resultant vapors being analyzed by GC-MS/FID. Selectivity to furan was observed to be 98%. Less than 2% of the symmetrical ketone was observed. It would appear that similarly to the majority of other acids lacking an α-hydrogen the instability of the resultant free radical leads to decarbonylation and greatly suppresses any ketonization reactions. As opposed to forming furan, the desired decomposition product for further upgrading would be a ketone. For this reason it is likely that another salt, such as magnesium acetate, will need to be present to achieve the desirable reactions. After initial heating of biomass to form torrefaction liquids, a large amount of acetic acid is present along with furfural. During the partial oxidation reaction additional $Mg(OH)_2$ in solution could be used to titrate the acetic acid making the needed salts for ketonization of the furoate.

It would then be necessary to study how a mixture of these salts would behave when exposed to elevated temperatures in an inert atmosphere. To do this a physical mixture of magnesium acetate and magnesium furoate (mass basis 4:1) was investigated

using thermogravimetric analysis. While magnesium salts are formed from the partial oxidation of furfural, it should be noted magnesium furoate for TGA was prepared starting with commercial furoic acid in solution. Magnesium acetate was also available commercially. The decomposition behavior as a function of temperature can be seen in Figure 16. Two distinct mass losses can be observed. The first a mass loss of approximately 29% at a temperature range of 100-175°C can be attributed to the loss of adsorbed water on the magnesium salts. The second mass loss starting at 280°C is due to the decomposition of the acetate and furoate groups. This is strongly believed to be due to ketonization occurring to produce the ketone and magnesium carbonate. The lack of two distinct weight loss periods at higher temperatures would indicate that almost immediately the carbonate decomposes into magnesium oxide and CO_2. Given the reaction scheme below the theoretical mass loss is 74%.

$$6.9\ Mg\ Acetate + 1\ Mg\ Furoate \rightarrow 7.9\ MgO + 7.9\ CO_2 + 7.9\ Mixed\ Ketones$$

An actual mass loss of 72% was observed in the given temperature range. The small discrepancy is most likely due to the formation of aldol condensation products on the MgO surface that fail to desorb. This reaction has been well studied in literature and would be prevalent at these elevated temperatures. Overall the decomposition pattern here agrees quite well with what has previously been seen previously for magnesium acetate.

Mass spectral data was also collected on the resultant vapors. As expected, initially only water is observed as the salts are dehydrated. At a temperature of approximately 400°C the ketone products of acetone and acetyl furan are observed as well as carbon dioxide from the decomposition of magnesium carbonate. No significant

amount of furan or self-ketonization of the furoate was observed. It appears that most of the furoate underwent ketonization with the abundant acetate groups. The molar ratios of acetate to furoate make the probability of forming the cross ketone highly favorable.

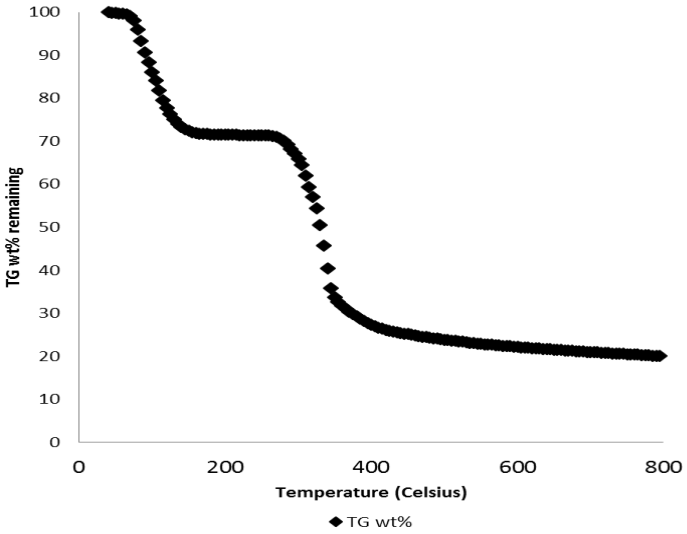

Figure 16: TGA weight loss analysis of 4:1 physical mixture of magnesium acetate:furoate

Pyroprobe Experiments

To further study the products from the decomposition of the magnesium salts, samples were prepared at numerous molar ratios and subjected to heating via an analytical pyroprobe in inert helium and the vapor products were analyzed by both flame ionization detection and mass spectral analysis. FID analysis allowed for quantification of the products and they were identified via the mass spectrum. Based on the TGA data a heating temperature of 400°C for three minutes was chosen. Three samples were prepared for analysis. Samples A & B were prepared using commercial acetic acid and furoic acid in solution with molar ratios (AA/FA) of 10:1 and 3.9:1 respectively. Sample C was a physical mixture of magnesium acetate and magnesium

furoate at a molar ratio of 6.9:1. In this case the respective magnesium salts were prepared with either acetic or furoic acid alone.

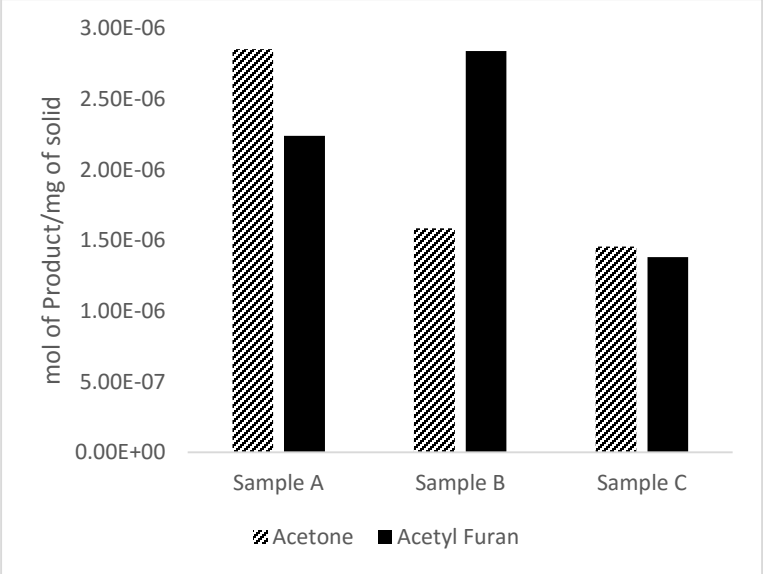

Figure 17: Product yields from salt decomposition using analytical pyroprobe at 400°C for three minutes

A summary of the product distributions can be seen in Figure 17. In agreement with TG-MS studies the main products observed were the acetone and acetyl furan through ketonization of the –oate groups. It can clearly be seen by altering the reactant concentrations during the salt formation period can shift the selectivity to the acetyl furan. The incorporation of the acetic acid into this six carbon backbone molecule would be highly preferred over forming acetone. An optimal acetate/furoate concentration could be determined from minimum acetone production. Many strategies have been proposed for the upgrading of ketones similar to these into a suitable fuel product.[6, 23, 55-59] Most of these studies suggest aldol condensation as a promising route to increase the carbon number and eliminate carbon lost due to CO_2 or CO production.

With Sample C we can clearly see a loss in yield when the physical mixture of salts is treated. It is believed this phenomena is due to the nature of the magnesium salts that are formed. When the acetate and furoate functional groups are bound to the same magnesium ion it is likely that the proximity increases the yield of the cross-ketone product (acetyl furan). Another source of the loss in yield to both products could be due to the presence of $Mg(OH)_2$ in the sample. Young et al. reported in the early 20th century the negative effects of excess hydroxide on acetone yield.[60]

Conclusion

Furfural was selectively oxidized with a conversion of over 50% and a high selectivity to the furoate product in the presence of gold on magnesium oxide. A similar result was obtained with Au/Al_2O_3 although importantly an alkaline solution is necessary. The positive impact of $Mg(OH)_2$ in the aqueous solution on catalyst activity was explicitly shown. $Mg(OH)_2$ has an important role in titrating the formed acids to keep the catalyst surface free of oxygen poisons. Without $Mg(OH)_2$ deactivation of Au/Al_2O_3 was prevalent due to oxygen poisoning.

As a result of the titration of the produced acids with $Mg(OH)_2$ magnesium salts are formed and can be purified from the aqueous solution by filtering and a dewatering process. These salts can then be exposed to high temperatures in inert atmospheres and undergo ketonization likely by a free radical mechanism to form higher molecular weight building blocks for green chemical or biofuel production. While magnesium furoate was not capable of ketonization alone a mixture with magnesium acetate shown promising yields of a furoate ketonization product.

Experimental

Catalyst Synthesis

Magnesium oxide for this work was synthesized by mixing $Mg(NO_3)_2$ and de-ionized water vigorously at 80°C for fifteen minutes. An equimolar amount of citric aside was solution was then introduced and heated at 90°C until concentrating in to gel form. The resultant gel was then calcined under static air at 550°C overnight to obtain the MgO

The 2%Au/MgO catalyst was prepared by dissolving 0.04 g of Gold (III) chloride hydrate in 40 mL of water. One gram of magnesium oxide prepared from the combustion method was then added and stirred for 30 minutes. Approximately 0.4 mL of 28% aqueous ammonia was then added to obtain a pH in the 10-11 range. The solution was then stirred for six hours followed by a reflux for 30 min at 100°C. To obtain the final catalyst the solid was washed with deionized water and then dried at 200°C for four hours. 2%Au/alumina was prepared in the same manner.

Furfural Partial Oxidation

50 mg of a given catalyst was added to a 25 mL three necked round bottom flask. 6 mL of 0.17 M furfural was then added. Oxygen (Airgas) flow at 10 mL/min was then bubbled into the solution. The reactor temperature was maintained at 95°C using a silicon oil bath and hot plate. A magnetic stirrer was used at 750 rpm throughout the reaction for a total time of thirty minutes. Product compositions were measured using HPLC on water instrument equipped with both UV and refractive index (RI) detectors and the separation was done by Aminex HPX-87H column from Bio-Rad Laboratories. The column flow rate was fixed to 0.6 ml/min of 5mM sulfuric acid

solution. The concentration of unreacted furfural and furoic acid were quantified from the standard calibration curve.

Magnesium Salt Synthesis

The preparation of magnesium furoate was completed using commercial 2-furoic acid (Sigma Aldrich) and magnesium oxide prepared via the combustion method. Approximately 0.28 g of 2-furoic acid was dissolved in deionized water. MgO was then added at a 1:5 (MgO:Acid) weight ratio. The solution was then heated to 100°C to allow for evaporation of the water. The dried solid was then filtered and washed with acetone multiple times to remove any excess furoic acid. The sample was then placed in a desiccator to mitigate the adsorption of water vapor from the air as the compounds are highly hygroscopic.

In a similar manner the Mg Acetate+Furoate samples were synthesized. Acetic acid and furoic acid were added to approximately 6 mL of water in a 10:1 or 1:1 molar ratio. Magnesium oxide was then added at twice the stoichiometric amount. At this point the synthesis followed what has previously been discussed.

Pyrolysis Experiments

For each run 1-4.0 milligrams of salt was pyrolyzed at 400°C for three minutes in helium using a CDS Analytical pyroprobe model 5250. The resultant vapors were passed through heated transfer lines at 300°C to a Shimadzu QP2010 GC-MS/FID system fitted with a RTX-1701 column (60m x 0.25mm with 0.25 µm film thickness). Helium (Airgas, Ultra High Purity) carrier gas was used at 90 mL/min with a 90:1 injector split ratio. The GC oven temperature program consisted of a hold for 4 min at 45°C then was ramped at 3°C/min up to 280°C and held for another 20 min. The mass

spectrum allowed for identification of each product. The FID chromatogram was used to quantify each compound. A previously developed effective carbon number (ECN) model was used in lieu of a traditional calibration to allow for mass quantification. This model has been used extensively for the quantification of compounds found in oak pyrolysis.

TGA of Physical Mixture

A physical mixture of synthesized magnesium furoate and commercial magnesium acetate (Sigma) was prepared at a 1:4 mass ratio . The mixture was then analyzed by thermogravimetric analysis using a Netzch 449F1 Jupiter. The sample was heated from 40°C to 800°C at 2°C/min, under 40 mL/min of UHP Argon. The outlet gases were also analyzed by an Aeolos 32 mass spectrometer.

Chapter 5: Upgrading of Stages 2 & 3 Torrefaction Vapors

Stage 2 Upgrading using Ga/ZSM-5

Targeted Chemistries for Stage 2

While levoglucosan is the major product in this vapor stream, the upgrading strategy is not built around the upgrading of levoglucosan. Vapor phase upgrading of this compound would be extremely difficult and catalyst lifetimes would be small. For this reason the main goal for upgrading of Stage 2 will be the transformation of the furanic derived species to useful aromatic products. This process has drawn a great deal of interest in recent years.[61-63] One of the most promising strategies for upgrading is by use of a microporous zeolite. The MFI zeolite has shown the most promise for these reactions. Huber et al. have completed numerous studies that show the effectiveness of this catalyst on furanic upgrading. In their work they conclude that ZSM-5 is the optimal catalyst as the pore structure limits the amount of polycyclic compounds that can be formed, as these compounds are too large to escape the catalyst pores. For this reason mostly benzene, toluene and xylenes (BTX) are formed. Their group found that most of the reactions follow Diels-Alder classes of reactions and a summary can be seen in Figure 18.

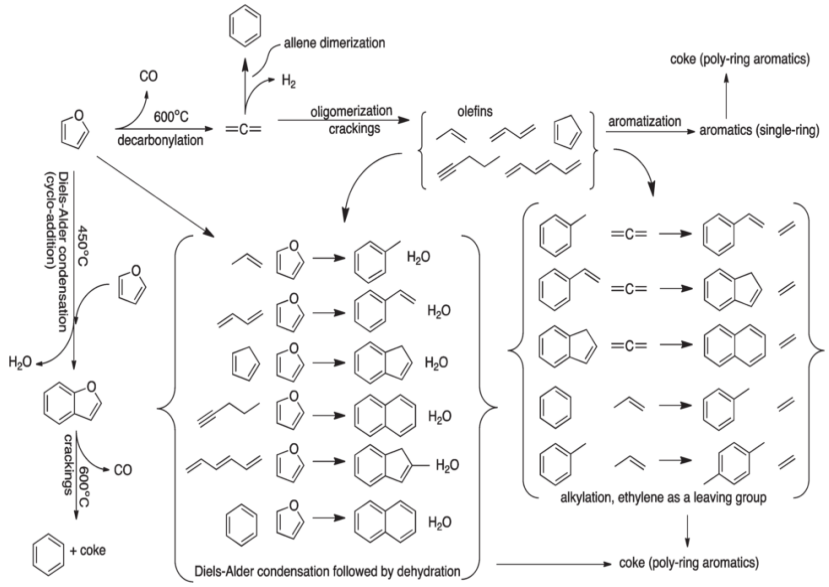

Figure 18: Cheng and Huber. Production of targeted aromatics by using Diels-Alder classes of reactions with furans and olefins over ZSM5

In previous work Dauenhauer et al. found that the Bronsted acids catalyze the dehydration reaction, the rate determining step, and thus could promote these Diels-Alder cycloaddition reactions.[64, 65] In a later paper, Huber et al. concluded that gallium promoted zeolites could be used to increase rates of decarbonylation, oligomerization and aromatic production.[66, 67] As previously discussed the size-selective techniques in Chapter 3 could also be used as an olefin source. In our group we have done work with full pyrolysis vapors with Ga/HZSM-5 that indicate that aromatic production does indeed increase. Other reactions have shown enhanced activity with Gallium as well.[68] For these reasons the catalyst for Stage 2 vapor phase stabilization was chosen to be Ga/HZSM-5.

Pyroprobe Results

In earlier work by Stevens, A. and Crossley, S. the optimal pretreatment and reaction conditions for aromatic production was found for upgrading of pyrolysis vapors with Ga/HZSM-5. It was assumed that these conditions would also be applicable for Stage 2 upgrading. Ga/HZSM-5 was first reduced in 1 bar H_2 550°C for one hour. The catalyst was then cooled to 500°C for reaction. The gas flow rates during these reactions were the same as what was used in Stage 1 upgrading (20mL/min H_2+20mL/min He). As with other pyroprobe studies approximately 0.75-0.90 mg of biomass solid was heated.

The resultant vapor stream from pulse 1 Stage 2 upgrading with Ga/HZSM-5 under the aforementioned conditions can be seen in Figure 19.

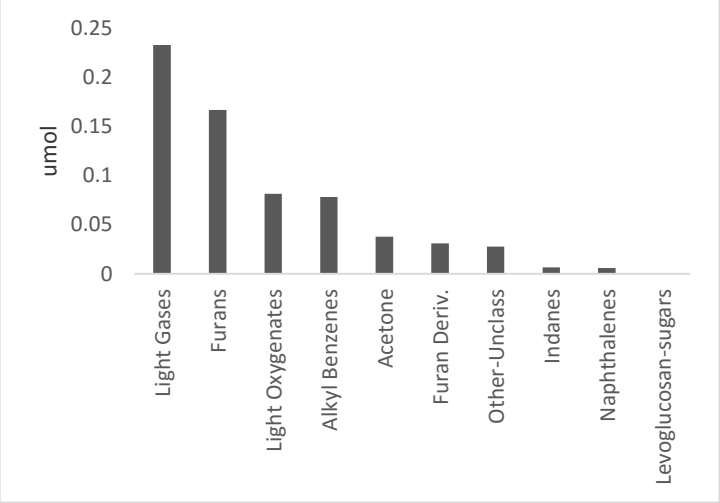

Figure 19: Composition of 1st pulse of Stage 2 torrefaction with 3%Ga/HZSM-5 catalyst.

Upon first examination it is immediately seen that the production of light gases is much higher than the desired amount. It is important to note that Figure 19 is on a

compound molar basis, a more accurate representation can be seen in Figure 20. In Figure 20, the data is represented on a carbon mole basis.

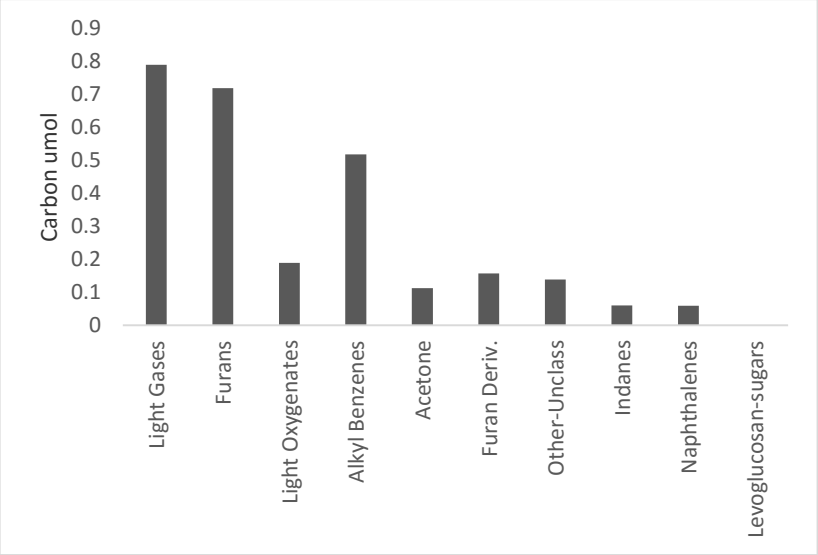

Figure 20: Composition of 1st pulse of Stage 2 torrefaction with 3%Ga/HZSM-5 catalyst on a carbon mole basis

Admittedly, the carbon amount that ends up as light gases is higher than expected. This could be due to a couple of different reasons. The most probable is that the gallium loading in the catalyst has not been optimized. For this trial, the gallium loading used was 3% and no attempt has been made to optimize the catalyst for these conditions. It would be expected that there is an optimal gallium loading and experiments should be conducted to find this amount. With the amount of light gases and furans present it would be reasonable to hypothesize that these compounds could be reacted via Diels-Alder, similar to what is seen in Figure 18, if catalyst conditions were appropriate. The catalyst amount was also low at 1.4 mg, so an increased amount should lead to an increase in aromatic yield and this will be examined moving forward. Also promising is that a small amount of ketonization is observed with this catalyst. The

acetone that is produced can then be used similarly to what is discussed with the ketones from Stage 1 upgrading.

Although the levoglucosan accounted for during upgrading was seen to be zero, it has been determined that most of this is not due to upgrading from the Ga/HZSM-5. The most likely explanation for the loss of the levoglucosan is due to the same liquid nitrogen trap problem as stated before. The levoglucosan will not desorb from the liquid nitrogen trap at 300°C. It has been seen in full pyrolysis experiments with the pyroprobe using Ga/HZSM-, that while a small amount of the levoglucosan will react most of the levoglucosan does not. The levoglucosan that does fit into the pore of the zeolite most likely leads to increased coking as well. In a best case scenario for this upgrading strategy the levoglucosan will remain unreacted and can be separated from the resultant liquid and treated separately.

As with Stage 1 upgrading the catalyst lifetime was also studied. While initially the conversion and thus production of alkyl benzenes was acceptable, after a few milligrams of the Stage 1 solid was fed to the reactor the catalyst deactivated. It is difficult to make many conclusions with this upgrading step. While it appears to deactivate quickly, that could be a function of two things. One would be the very small amount of catalyst that is used. With such a small amount there were only a few sites available for reaction to take place. Secondly, with such a large amount of levoglucosan in this stage it could deactivate the catalyst very quickly. Work is underway to try and purify this stream before introduction to the Ga/HZSM-5 and will be discussed in more detail.

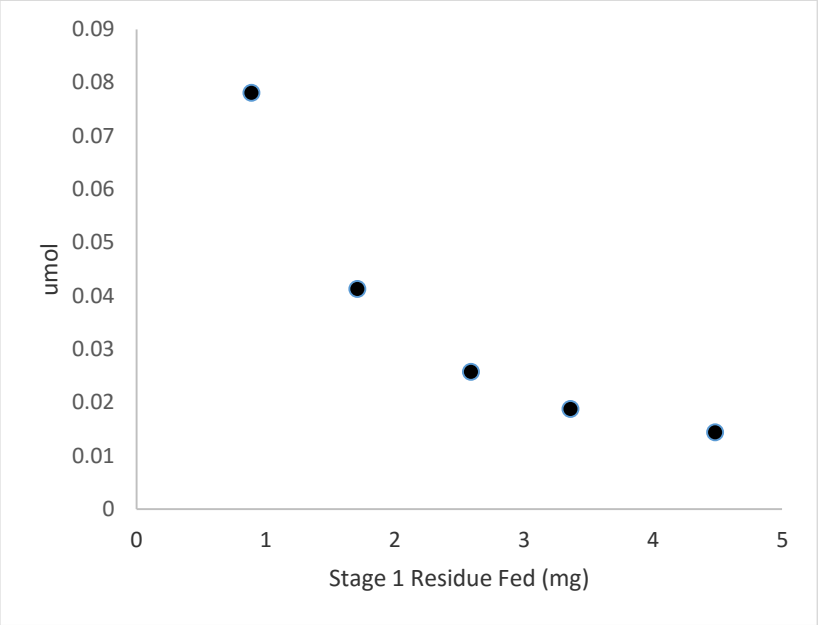

Figure 21: Alkyl benzenes production as a function of the biomass that is pulsed through the reaction system

Stage 3 Upgrading Using Ru/TiO_2

Targeted Chemistries for Stage 3

Resasco et. al have proposed that a suitable upgrading in the liquid phase for phenolics would be through hydrodeoxygenation (HDO) over metal catalysts and possible subsequent alkylation with alchohols as discussed in many recent studies.[15, 58, 69, 70] Using this pathway many of the phenolic species are converted to more stable cyclic compounds such as cylcohexanes, cylcohexanones, and cyclohexanols. With high H_2/feed ratios, metal catalysts have shown significant improvement over conventional acid or metal oxide catalysts for C-O bond cleavage and decreased coking.[1] Traditional metal catalysts do have drawbacks though. Lighter oxygenates and carbon molecules connected via ester bonds usually end up as light gases which are undesirable. On the other hand, acid functionality can act to create C-C bonds through

reactions such as ketonization similar to what is seen in Stage 1 of this work. In a previous study by Boonyasuwat et al. using the bifunctional Ru/TiO_2 (the same catalyst from Stage 1 in this work) lignin derived model compounds can be successfully upgraded into more stable products. In the study guaiacol was used as a model compound for lignin reacting over a variety of supported Ruthenium catalysts. A general pathway for the reactions occuring can be seen in Figure 22.

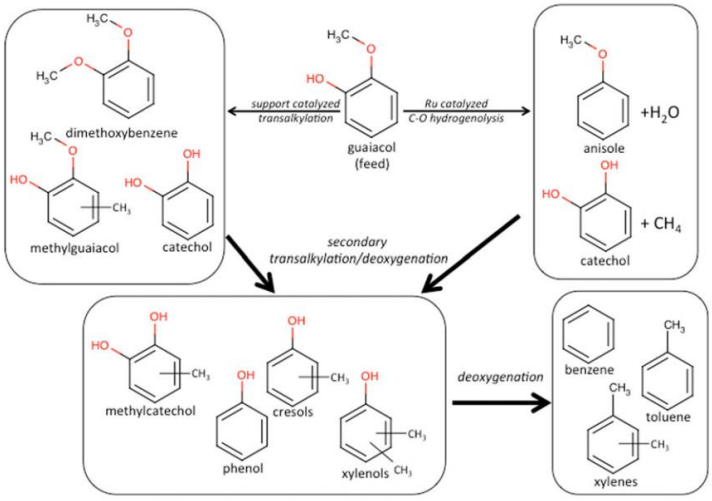

Figure 22: Generalized reaction pathways occurring over the supported Ru catalysts used by Boonyasuwat et al.

Boonyasuwat found that Ru/TiO_2 exhibited superior activity and stability for the conversion of guaiacol when compared to other Ru supported catalysts. They also found that carbon retention of the methoxy group was better over acidic supports such as TiO_2. This observation was attributed to transalkylation reactions that occur over Lewis acid sites on the TiO_2. Based on these model compound studies it was concluded that Ru/TiO_2 would be a suitable choice for the stabilization of the Stage 3 vapors.

Pyroprobe Results

Pyroprobe studies were conducted with 1.4 mg of Ru/TiO_2 at 400°C for Stage 3 stabilization. Prior to experiments the catalyst was reduced in hydrogen at atmospheric pressure for 2 hours at 400°C. Under reaction conditions the gas flowrate was set to 90 and 20 mL/min for He and H_2 respectively. The first pulse vapor composition as detected by FID analysis can be seen in Figure 23.

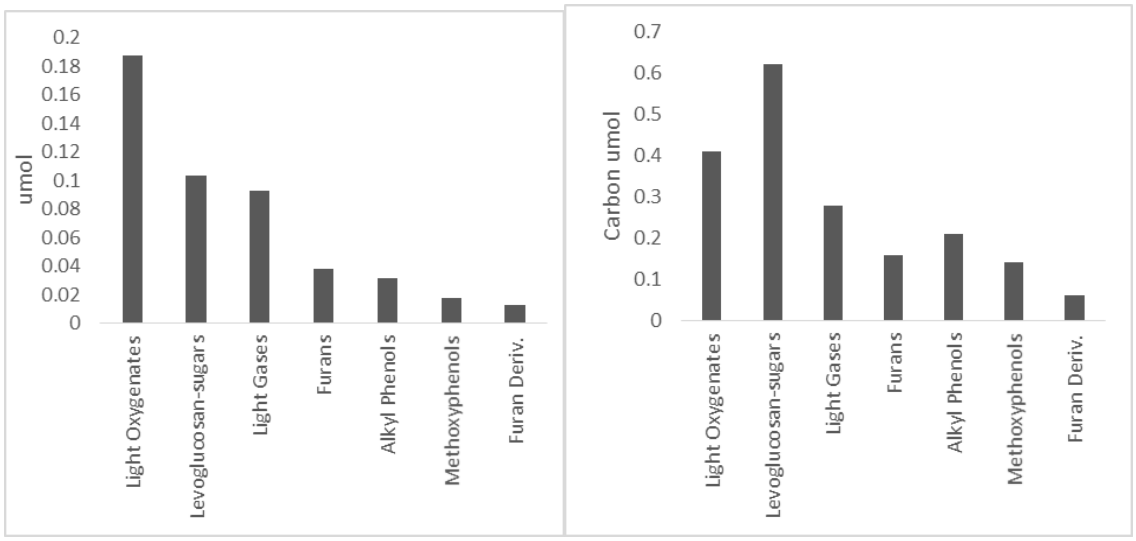

Figure 23: Composition of the 1st pulse for Stage 3 pyrolysis upgrading over 1.4 mg Ru/TiO_2

Compared to the upgrading of the other two stages, the Stage 3 is currently the farthest from being optimized. From the experimental data for this stage is does not appear that the desired reactions are occurring. While there is a slight increase in the selectivity to alkyl phenols as compared to the feed levels the difference is almost negligible. The complexity of the mixture in Stage 3 is most likely leading to high coking levels similar to what is seen with full pyrolysis vapors. To alleviate this problem a purification of the stream will most likely be needed. A proposed two-stage purification process of the Stage 3 vapors may lead to higher activity of the Ru/TiO_2. A

simple depiction of this two-stage purification process can be seen in Figure 24. The basic principle is to remove both the harmful levoglucosan and light oxygenates from the vapor stream before the Ru/TiO_2 catalyst bed. Firstly, selective adsorption via activated carbon at 300°C has shown promise to remove the levoglucosan from the stream (Chapter 6). In a real process situation this levoglucosan could then be recovered from the activated carbon in a liquid washing step. Once the levoglucosan is removed, the vapor phase is a mixture of mostly light oxygenates and methoxyphenolics. This stream can then be passed over either a zeolite with a passivated outer shell or a small pore zeolite that will not allow diffusion of the larger phenolic compounds. The basic principle is the same in both cases, it is desired to have the light oxygenates react to create less reactive compounds such as ketones or aromatics. Once this occurs the Ru/TiO_2 lifetime and activity should increase as the major reactive components will be the methoxyphenolics. If it is found this strategy does not achieve the targeted reactions, further investigation into alternate catalysts may be needed.

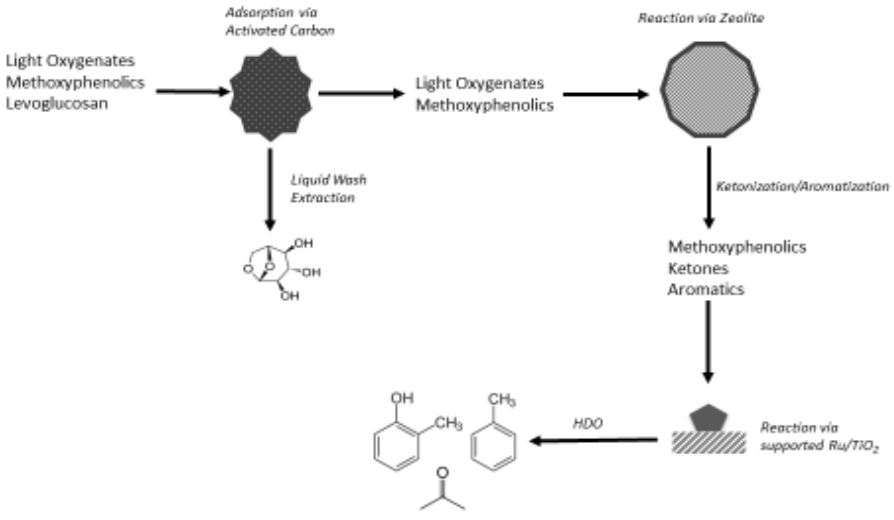

Figure 24: Schematic for proposed purification process of the Stage 3 pyrolysis vapors.

Proposed Strategy for Levoglucosan Upgrading

As shown, one of the major products from biomass thermal decomposition is levoglucosan stemming from cellulose. Catalytically levoglucosan (LGA) provides one of the greatest challenges for developing useful products. For a wide variety of vapor phase reactions using traditional biomass upgrading catalysts LGA greatly hinders desired reaction chemistries. The logical route for upgrading of LGA is the first purifying it from the rest of the pyrolysis vapors. This can likely be done with the use of activated charcoal as an adsorbent as mentioned in Chapters 4 & 6. The handling of this purified levoglucosan stream then becomes a topic of great interest.

One of the most studied techniques for levoglucosan is hydrolysis to form glucose.[71, 72] At this point the glucose can be fermented in traditional ways or as recently student partially oxidized to from gluconic acid which is a useful intermediate in a wide variety of applications.[52] Other strategies have also been proposed for levoglucosan upgrading but to this point a suitable method has not been proposed.[73-75]

A strategy to produce levoglucosenone (LGO) the sugar enone product of cellulose from levoglucosan has also been studied recently.[76] LGO can also be seen in lower yields from fast pyrolysis of cellulose and biomass. To enhance LGO production many acid catalysts have been studied such as $MgCl_2$ and $FeCl_3$ as well as inorganic salts such as $(NH_4)_2SO_4$ and $(NH_4)_2HPO_4$.[77, 78] A more simple approach was proposed from Lu et al. involving the pyrolysis of cellulose or levoglucosan in the presence of a sulfated titania catalyst. Results in an analytical pyroprobe indicated promising selectivity to LGO from the mixed pyroprobe using LGA, although no true

yields were reported. Currently research in the area of vapor phase upgrading of LGO is limited. It was of interest to understand if some of the targeted ring rearrangement reactions that are seen with furanic derivatives could be carried out with LGO as well.

The analytical pyroprobe with *ex situ* reactor was used to study this phenomena. Based on initial pyrolysis at 500°C of commercial LGO a yield of 42% by weight was observed using the ECN model. Also importantly no thermal decomposition products were observed as >99% of the total FID area was in the LGO peak. For catalytic experiments 0.6-2mg of LGO was placed into a pyrolysis reactor tube using a microsyringe. Importantly each sample was made minutes prior to heating to prevent any polymerization in the reactor tube. LGO is unstable at the temperatures (slightly in excess of room temperature) seen in the pyroprobe. Liquid LGO is stored best in a freezer at <-20°C. 4.25 mg of Ru/TiO_2 was catalyst with carrier flows set in a similar manner to other pyrolysis experiments with 90 and 20 mL/min of helium and hydrogen respectively. Figure 25 depicts the conversion based on disappearance in the pulse experiments.

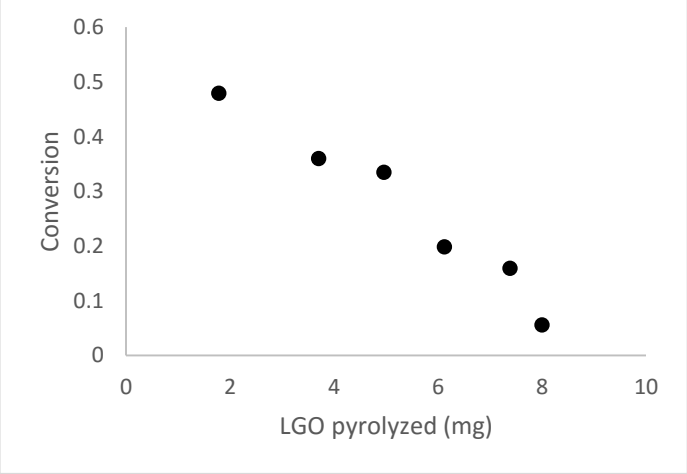

Figure 25: Levoglucosan conversion using 4.25 mg of Ru/TiO_2

Initially an approximately 48% conversion of the LGO is observed. The main products identified by GC/MS analysis are C5 ring derivatives such as 2-cyclopenten-1-one and cyclopentene-1,3-dione. The total mass yield of these product makes up 19% of the reacted LGO and an unknown bicyclic compound makes up another 20%. The missing 61% is assumed to be lost both due to coke deposited onto the catalyst and condensation in the reactor transfer lines. The product distribution excluding the bicyclic compound for the first pulse of LGO can be seen in Figure 26. No noticeable change in the distribution trends were observed as a function of the number of LGO pulses. All products appeared to decrease at similar levels.

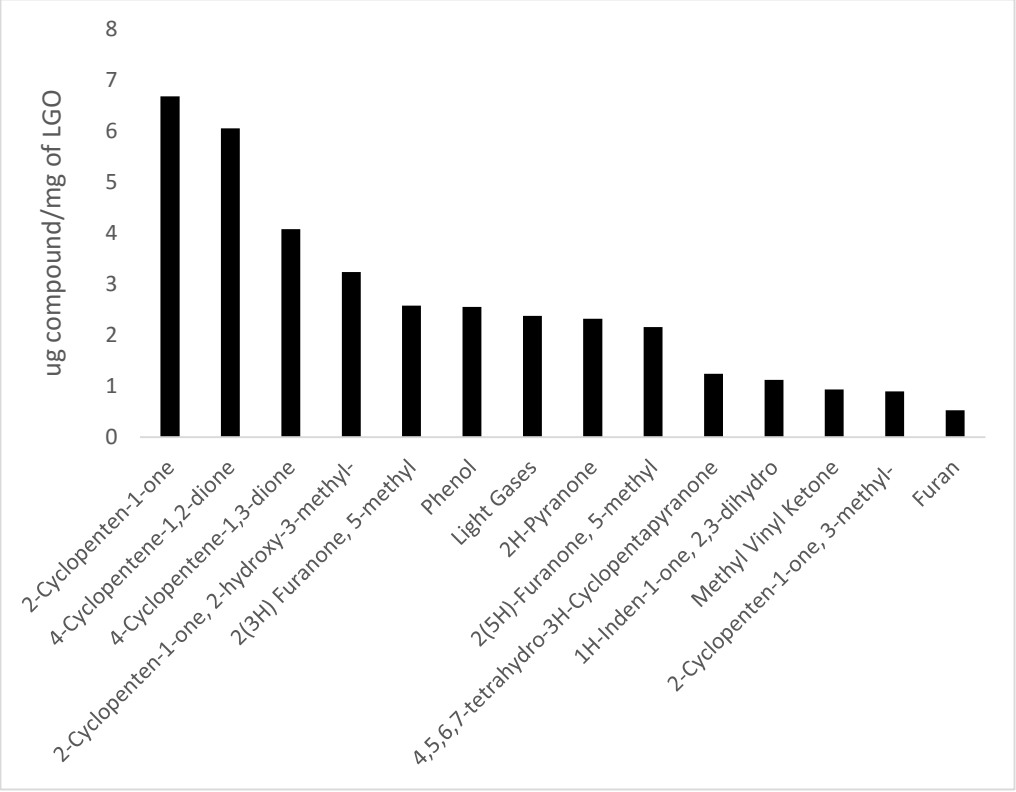

Figure 26: Product Distribution of 1st Pulse form LGO pyrolysis with upgrading using 4.25 mg Ru/TiO_2 with hydrogen slipstream

As these were just initial experiments it is likely that this process can be optimized in a variety of ways to both increase the yields to desirable products and decrease catalyst deactivation. The limits on hydrogen partial pressure inside the pyroprobe reactor system hamper the ability to work at higher H_2/reactant ratios. Higher ratios could be more favorable in limiting deactivation. Nonetheless, the mere fact that a variety of useful ketone products were seen warrants further investigation into reactions involving LGO as current levoglucosan strategies are far from optimal.

Chapter 6: Selective Adsorption of Vapor Products from Red Oak Pyrolysis

Introduction

As discussed in previous chapters, one of the major problems with catalytic upgrading of a complex pyrolysis or torrefaction oil is the wide variety of functional families that are present. To this point there is not a suitable catalyst capable of handling these streams without fast deactivation. This was one of the main goals of the thermal fractionation techniques. Separation of the compound groups allows for a targeted catalyst and chemistries to be implemented. As we have seen, even though thermal fractionation of biomass is a promising route for this separation the respective cuts are not "clean". In other words, most of the streams still contain a variety of different functional groups. For this reason other separation techniques must be investigated. One would assume that even with these cleaner streams compared to conventional pyrolysis a simple distillation would not be practical. In this work one technique that has shown promise is the selective adsorption of these vapor products onto activated carbon.

A selective adsorption or "trapping" has shown to be capable of separation of the phenolic functional group that is seen as a result of lignin degradation. This would be particularly useful in stages 1 and 2 where the catalysts have been mostly optimized for lighter oxygenates and sugar derivatives. Keeping the catalyst clean of these phenolic compounds should lead to a decrease in deactivation and allow for the targeted reactions such as ketonization to occur. Another compound of interest to trap would be levoglucosan (LGA) in stages 2 & 3. It has been established that a vapor phase upgrading of LGA seems impractical. As discussed previously in Chapter 5, the mostly

likely routes for upgrading of the LGA stream occur in the liquid phase. It is believed that the separation of LGA from the vapor streams can be done for the most part thermally by condensation. A high boiling point compound (384°C) such as LGA would be likely condensed given enough surface area of a suitable media.

In model compound studies here at the University of Oklahoma completed by Schneberger et al. it has been shown that over activated carbon different compounds adsorb on activated carbon at varying strengths.

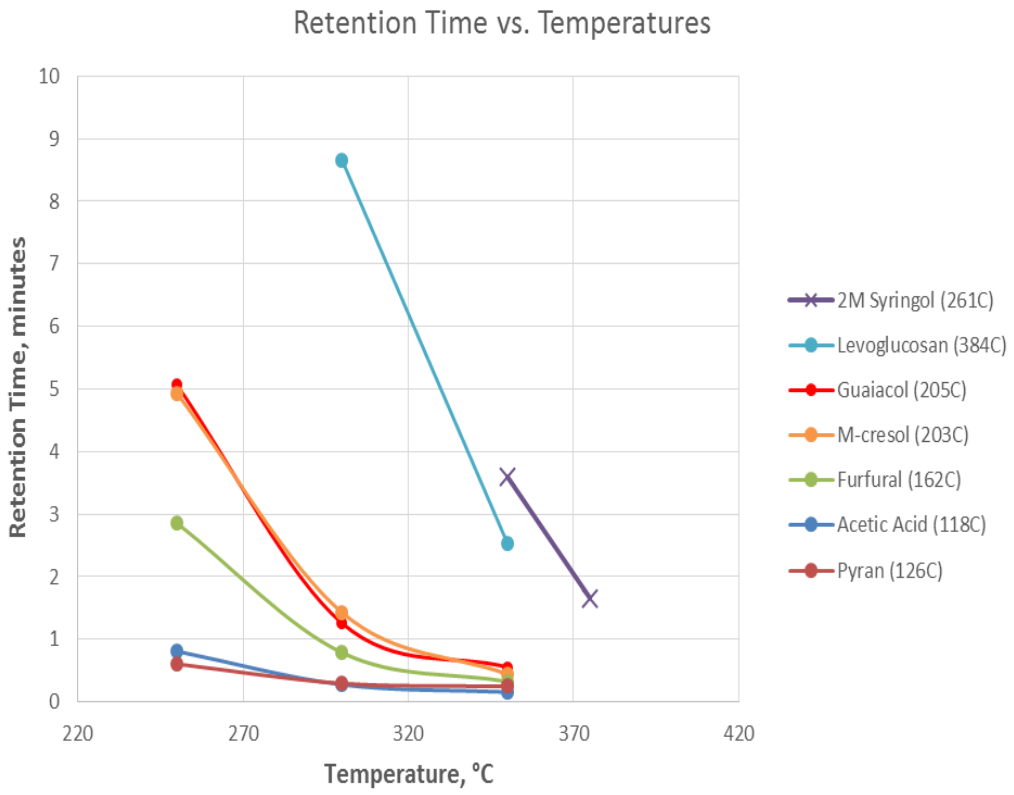

Figure 27: Schneberger et al. Model compound studies with activated carbon trap.

In Figure 27 it can clearly be seen phenolic compounds appear to have a stronger affinity for the carbon trap. A longer retention time would be indicative of a higher bond strength between the compound and the activated carbon. Also of significance is

the fact that syringol and levoglucosan do not desorb at 250°C. A low temperature trap would likely lead to a vapor stream with significantly reduced amounts of these compounds and similar derivatives. An examination of the syringol (b.p 261°C) would also lead to the conclusion that the separation is not simply a thermal phenomenon. It has the highest retention time but with a boiling point of over 120°C less than the levoglucosan. It has been hypothesized that the aromatic ring of the phenolics plays a large role in the adsorption of these compounds. While moving forward the mechanism of adsorption will be of importance it was not the main goal of this work and mechanistic studies were not completed to this point.

Pyroprobe Studies

With the knowledge gathered from the model compound studies it was then desirable to test this hypothesis with the real vapor streams. The pyroprobe was utilized to investigate whether this trapping could be carried out. The set-up was similar to what was done with catalytic experiments previously discussed. In lieu of a catalyst in the quartz reactor, two milligrams of activated carbon (20-40 mesh, phosphoric acid activated, Sigma) was diluted with 200 milligrams of borosilicate beads. The surface area of this adsorbent was reported to be 600 m^2/gram. A range of temperatures was investigated from 270-330°C. An ideal separation would consist of a reduction levoglucosan-sugars and methoxyphenolics. In agreement with catalytic experiments 0.7-1.0 mg of red oak was pyrolyzed at 500°C. It was assumed that if this technique showed promising results with the full pyrolysis it could also be implemented in a similar manner with the different stages of thermal fractionation.

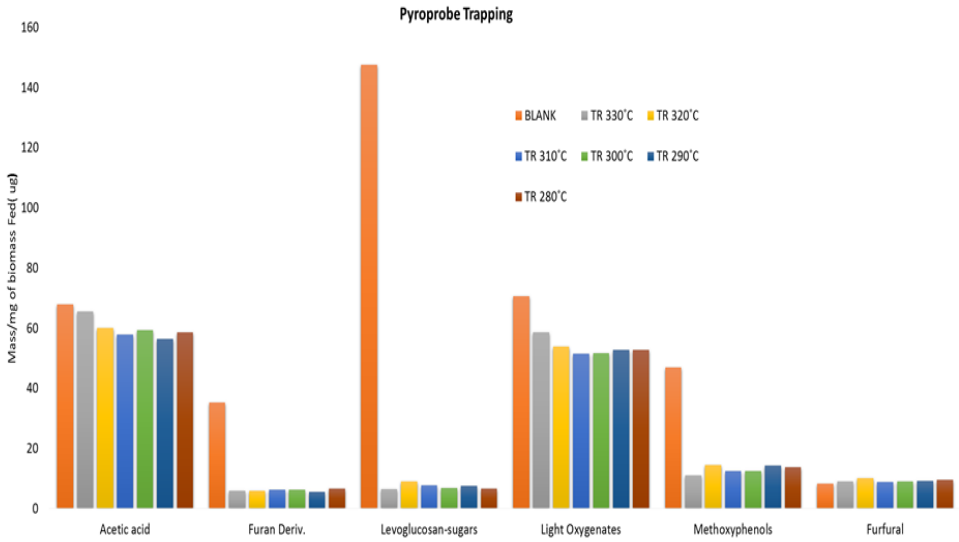

Figure 28: Pyroprobe Selective Trapping Studies with Red Oak Pyrolysis

Figure 28 provides a summary of the trapping studies that were conducted in the pyroprobe. In agreement with the model compound studies a desirable separation can be achieved. It can quickly be seen that the LGA yields seen by FID were greatly reduced in the presence of the activated carbon adsorbent. As expected methoxyphenolics were also greatly reduced. Acetic acid and other light oxygenates were for the majority unaffected by the presence of the trap. From 270-330°C a significant difference could not be seen. This would likely lead to the conclusion that an even lower temperature could be used such as <250°C.

Two important aspects of this process were not investigated thoroughly due to limitations of the pyroprobe and reactor system. Firstly, the underlying assumption is that any of the absorbed species can be recovered either by solvent wash or thermal heating. With the small scale of the pyroprobe these studies were not feasible. Although unlikely, studies would also need to be conducted to ensure that no reactions take place on the surface of the activated carbon. Secondly, the main goal is to increase the

catalyst lifetime and yield to desirable products. While catalytic studies were attempted in the pyroprobe system, the results were inconclusive. The main limitation is that while the FID can analyze the initial pulse of biomass it is incapable of catching anything that bleeds off the adsorbent in the >1.5 hours the GC program is running. These compounds would just end up in the noise of the FID/MS system. As such it would appear that this phenomena occurs as the catalyst lifetimes did not appear to be affected. In this system all of the undesirable components will still end up making it to the catalyst bed and thus deactivate the catalyst. A system modification would be needed to divert the desorbed gases after the initial pulse has passed through the trap. This method should provide a route to investigate the true effect selective trapping has on catalyst performance.

Chapter 7: Role of Diffusion Path on the Catalytic Upgrading of Biomass Pyrolysis Vapors over ZSM-5[a]

[a]Manuscript by Stevens, A and Vann, T et al. *Role of Diffusion Path on the Catalytic Upgrading of Biomass Pyrolysis Vapors over ZSM-5.* Experiments and initial text draft prepared by Adam Stevens and Abhishek Gumidyala, additional data work-up and text by Tyler Vann

Preface

In addition to work carried out on the staged thermal fractionation of biomass, catalytic upgrading of full pyrolysis vapors has been completed with the same pyroprobe reaction system. Chapters 7 & 8 detail some of this work that was done in conjunction with Adam Stevens. These finding will have significant carryover to upgrading of torrefaction vapors with zeolite catalysts as well.

Abstract

The goal of this study was to determine the role of the internal diffusion path for lignocellulosic biomass pyrolysis vapors over a ZSM-5 catalyst. By using differing crystallite size catalysts and desilicated mesoporous catalysts, the internal diffusion path a reactant would cover could be varied. It was found that by having a shorter diffusion path, i.e. smaller crystallite size and mesoporous zeolite, alkyl benzene and naphthalene production was increased dramatically. By shortening the diffusion path, initial products have a higher chance of exiting the pores of the catalyst before further reacting to form polyaromatics which are the precursors of coke. It was also discovered that extra-framework alumina present after the creation of mesopores have the capacity of plugging the pores of the catalyst and effectively blocking the internal acid sites and thus the catalyst requires an acid-wash to remove any blockages of the pores.

Introduction

With rising concerns on the effects of CO_2 in the atmosphere from the use of fossil fuels, governments and companies worldwide have invested heavily into developing a carbon neutral process to supplement the transportation fuel industry. When biomass, more specifically lignocellulosic biomass, undergoes fast pyrolysis, the cellulose, hemicellulose, and lignin that compose the biomass begins to thermally decompose to lighter molecules. While these compounds may be highly valuable, they are also oxygenated, unstable, and react easily to polymerize and form side-products. Biomass pyrolysis yields numerous products including acetic acid, light oxygenates, furfurals, methoxyphenols, and levoglucosan/sugars; many of which are acidic/corrosive and harmful to equipment and those who may be handling the raw bio-oil. Separation of these products is nearly impossible due to the high distribution of products and an added difficulty is encountered when the pyrolysis vapors are condensed because polymerization occurs almost immediately. While there are many difficulties inherent with this process, research has been done to develop novel methods of overcoming these challenges.

Catalytic fast pyrolysis (CFP) is a rising method of taking the biomass and converting it to usable chemicals and products; more specifically gasoline and diesel range molecules. Immediately after the biomass is pyrolyzed, the vapors are passed over a solid catalyst to deoxygenate the molecules while attempting to retain the carbon. This overcomes the problems with raw liquid biofuel and creates a much more stable product that can be stored and potentially further upgraded. Some CFP reactions are done in situ[2, 79] while others are done ex situ[8, 80-82]. In general, zeolite catalysts

have been found to be very effective in the deoxygenation of biofuels and so is the major focus of this study.

The challenge of determining the optimal zeolite catalyst for this process has been taken on by many research groups. Zeolites that have been investigated include, HY, ZSM-5, H-Beta, ZSM-11, MCM-22, and SAPO-34; among others. Multiple research groups have found that the family of zeolites that converted the pyrolysis vapors best, towards aromatics, was the MFI family particularly ZSM-5.[9, 83, 84] It has been found that by using ZSM-5, dehydration, decarboxylation, decarbonylation, oligomerization, and dehydration reactions can be performed within the same zeolite to deoxygenate the highly oxygenated products produced from fast pyrolysis. The pore size of ZSM-5 is also optimal to facilitate aldol condensation toward aromatics. This is possible due to the confining effect imposed by the pore walls on the reactants.[85] To further improve ZSM-5 performance, it can be modified through the use of metals, external coatings, and changing the morphology to increase the activity of the catalyst or change the reaction mechanism.

Some of the proposed methods to increase the activity of a zeolite and/or decrease the rate of deactivation focus on affecting the diffusion path molecules have to travel to reach an active site within the pores or escape the pores. These include varying the crystallite size or introducing mesopores into the framework of the zeolite.[86-90] By decreasing the diffusion path, the zeolite is expected to show higher activity toward aromatics and less coking of the catalyst. In a previous work done by our group, it was shown that small crystal zeolites had greater stability and production of alkyl aromatics from light oxygenates due to the increased removal of products.[86] Mesoporous ZSM-

5 zeolites were investigated by Wang et. al. as a catalyst for upgrading of pyrolysis vapors. They found that creating mesopores post-synthesis at increasing concentrations of NaOH to get larger mesopores increased the aromatic production noticeably.[88] In this work an in-depth study was carried out focused on what role the diffusion path to the active sites inside the catalyst had on aromatic production.

Results and Discussion

Catalyst Characterization

Porous Structure

SEM images of the crystallite series were taken and can be seen in the supplemental material. Imaging of the parent (Sample C) and mesoporous catalyst was also done using SEM and as seen in Figure 29, the parent zeolite's surface is relatively uniform and consistent with other ZSM-5 zeolites. Samples A, B, C have approximate crystal sizes of 0.5, 5, 10 μm respectively. After attacking Sample C with NaOH to create mesopores, Figure 29**Error! Reference source not found.** shows that the surface is noticeably different. There are many large pockets and craters but the spherical form is maintained. This led us to believe that the zeolite structure was maintained and the pore structure had not collapsed. These images are supported in the literature, showing a removal of the interior zeolite.[91] After acid washing, no noticeable change was observed to the zeolite structure.

Nitrogen adsorption experiments were performed on the 3 Sample C series catalysts to determine if extra-framework alumina (EFA) created by the NaOH attack blocks the pores of the zeolite and is included in **Table 1**. The micropore volume was found to decrease due to EFA after NaOH attack, but when an acid wash was performed

removing the EFA, micropore volume returned to levels seen with the parent zeolite. The mesopore volume and external surface area increased with each step in the creation of the final catalyst. This was expected and helped confirm the creation of mesopores. The increase in surface area also leads us to believe the zeolite crystal structure was also maintained.

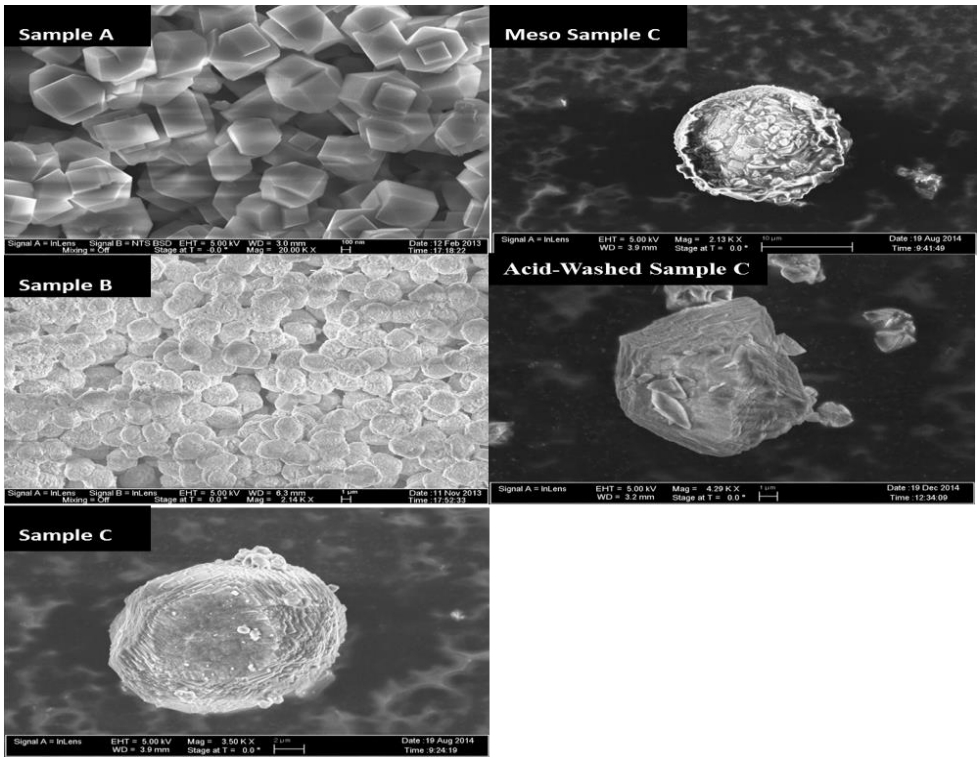

Figure 29: SEM Images of different catalysts.

Table 1 Nitrogen adsorption results for mesopore series[a]

	Micropore Volume cm^3/g	Micropore Area cm^2/g	Total Pore Volume cm^3/g	Mesopore Volume cm^3/g	External Surface Area m^2/g
Sample C	0.186	355	0.222	0.035	19.5
Meso Sample C	0.165	314.9	0.305	0.140	51.6
Acid-Washed Sample C	0.189	361	0.357	0.168	61.0

[a] measured via t-plot method

To further confirm that the crystallinity was maintained after NaOH attack, X-Ray Diffraction (XRD) was performed on the catalysts. While a minor loss in crystallinity can be seen, Table 1, it is evident that the MFI structure of the zeolite was maintained and XRD data agrees with spectrum currently found in literature.[92]

Acidity

IPA-TPD was used to determine the Brønsted acid site density of each catalyst. For the Sample C mesoporous series catalyst, it was found that the density of acid sites decreased after NaOH attack but was then increased higher than the initial parent catalyst after the acid wash; see Table 3. The decrease in acid site density when linked with what was learned from the nitrogen adsorption, gives further credence to the hypothesis of pore blockage by EFA. This correlates well with literature and the activity seen in pyroprobe experiments. Also, when compared on a per acid site basis, the acid-washed mesopore zeolite was far superior in the production of alkyl benzenes; Figure 30.

Table 2 Measured Brønsted sites and calculated Si/Al ratio for mesopore series[a]

	Sample A	Sample B	Sample C	Meso Sample C	Acid-Washed Sample C
Brønsted Acidity (mmol/gm catalyst)	0.850	0.673	0.189	0.160	0.216
Si/Al Ratio	19.6	23.7	90	103	76

[a] measured by TPD of isopropylamine

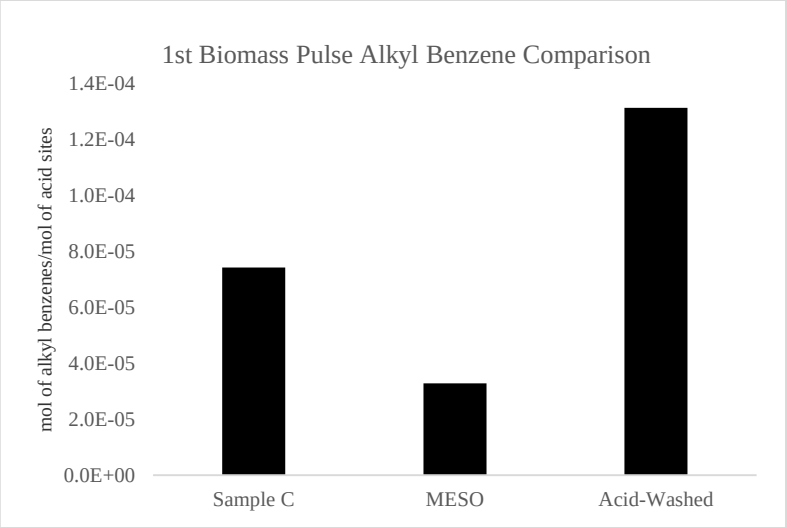

Figure 30: 1st Biomass Pulse for Mesopore Series on per Acid Site Basis

Catalyst Activity

Effect of Crystallite Size

ZSM-5 catalyst of differing crystallite sizes was synthesized to study the influence of pore diffusion on aromatic production. It was hypothesized that the internal diffusion path distance would be inversely proportional to the yield of alky benzenes products. As there is a higher ratio of internal to external sites, the molecules should not have to diffuse so far to reach the inner sites.

In pyroprobe experiments we did see improved results when using the smaller crystal size as seen in Figure 31 and Figure 32. The alkyl benzenes and naphthalenes produced from the catalyst were noticeably different and greatly improved. After a few pulses the 5μm catalyst shows significant deactivation and then appears to level off a steady conversion. For the 500nm zeolite the aromatic yield has been increased three-fold throughout the pulse experiments. The deactivation behavior for both crystallites is

not uncommon for pyrolysis vapor upgrading and correlates well with literature and previous experience with low Si/Al ratio ZSM-5 zeolites.[93]

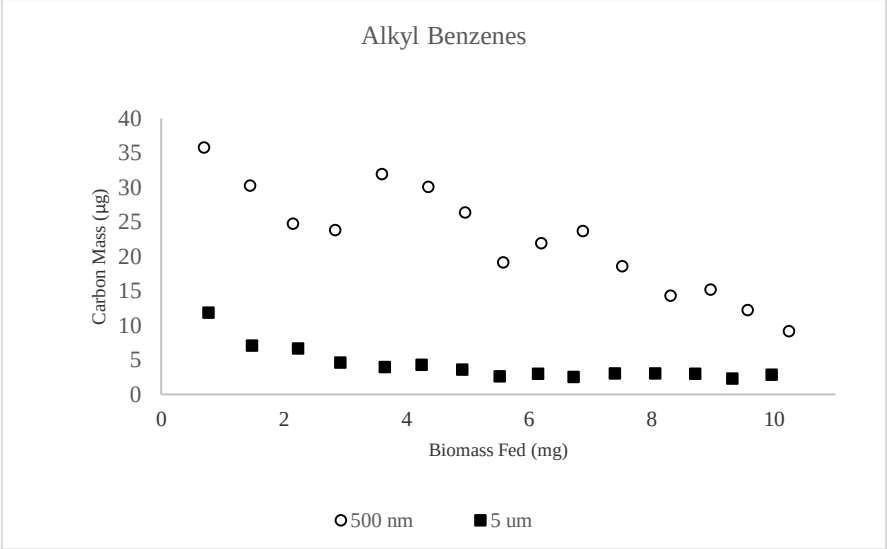

Figure 31: Crystallite Size Series-Alkyl Benzenes

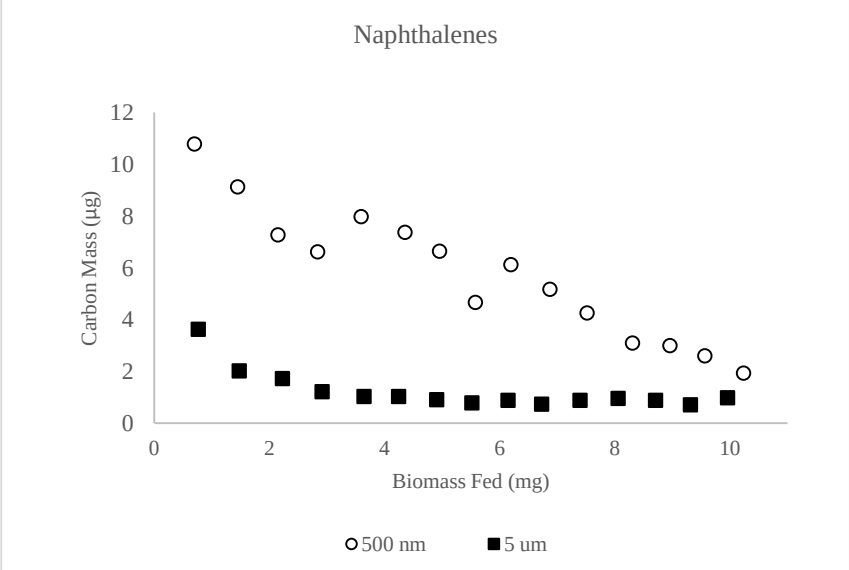

Figure 32: Crystallite Size Series- Naphthalenes

Role of Extra-Framework Alumina

When the parent zeolite (Sample C) was attacked using NaOH, there were visible differences in the surface of the zeolite when observed through SEM. From the images

it was apparent that a mesoporous material had been formed. To determine if the zeolite crystallinity was maintained after creating the mesopores, XRD was performed on the parent (Sample C) and the NaOH attacked catalyst. While a minor loss in crystallinity was observed, the XRD results suggest that the MFI structure was maintained to a large extent.

When both zeolites were used to upgrade the pyrolysis vapors on a constant mass basis, it was seen that the activity of the mesoporous ZSM-5 was much lower when compared to the parent. We hypothesized that this was due to a plugging of the pores by EFA that was redeposited after the NaOH attack. To test this the mesoporous zeolite was washed with hydrochloric acid to remove the EFA and then repeated the experiment in the pyrolysis system.

Effect of Acid Washing and Mesopores

Remarkably a nearly order of magnitude difference was observed in the initial creation of alkyl benzenes; see Figure 33. Other products like naphthalenes (Figure 34), indanes, and acetone also increased significantly over the mesoporous catalyst. The initial cause in the increase in activity is due to the acid washing removing the EFA and opening the pores and thus making more active sites accessible to the pyrolysis vapor reactants. In addition to the increase in accessible acid sites, the creation of mesopores also leads to a decrease in the diffusion path to the active site. It would be expected that trend observed with the 500nm vs 5μm would also hold true in this case. This would explain the substantial difference in alkyl benzene yield between the parent and acid-washed mesoprous zeolite. As discussed previously the shorter diffusion path should

decrease the amount of subsequent aromatic reaction to form polyaromatics and coke that remain in the zeolite pores.

One trend that was noticed is that the acetone and furans, both products of catalytic upgrading, increased as biomass was fed to the acid-washed catalyst. This is due to the compounds undergoing secondary reactions to form naphthalenes, indanes, or coke. There was no increase or decrease in the light combustible gas peak.

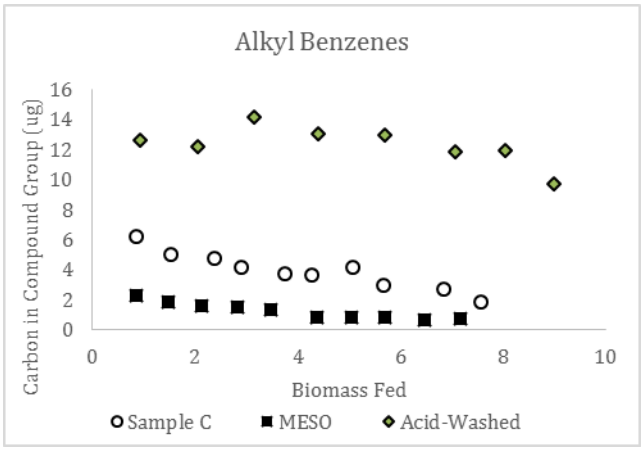

Figure 33: Mesopore Series- Alkyl Benzenes

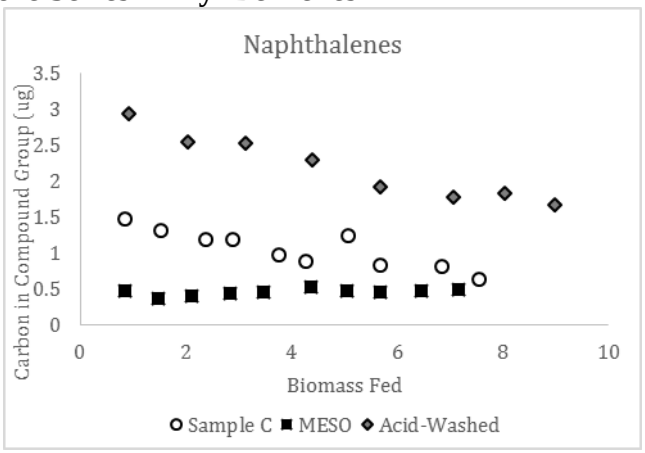

Figure 34: Mesopore Series- Naphthalenes

It appears that the creation of mesopores, which reduce the diffusion path a compound travels through the zeolite, increases the production of alkyl benzenes and

naphthalenes. The conversion of furanic compounds were increased in the mesopore zeolite as were other light oxygenates. This is due to an increased accessibility to internal active sites and both furfurals and light oxygenates are compounds that can undergo aldol condensation to form alkyl benzenes and naphthalenes.

Role of Internal vs External Active Sites

By examing specific molecules found in the pyrolysis vapors we can also examine the role of internal vs external sites on catalytic activity. Two prevalent compounds in pyrolysis vapors are acetic acid derived from hemicelluose and lignin derived syringol. It would be expected that a small compound such as acetic acid would have little difficulty diffusing into the internal pore structure of HZSM-5. Syringol on the other hand with its larger kinetic diameter has a hard time fitting inside the catalyst. Any reaction of syringol thus must be taking place on the external surface of the catalysts. In Figures 35 & 36 signifcant difference can be see in the conversion of each of the species over the different catalysts. Similar to the trends seen with the alkyl benzenes production, the mesoporous Sample C appears to have the lowest activity. Interestingly, if we look at the activity normalized to the number of acid sites available for reaction, calculated from the IPA-TPD, we see almost no difference between the three samples. This further confirms that the loss in activity in mesoporous Sample C is due to blocking of the internal sites. With the syringol the change in acid site density should have minimal effect on the conversion. This molecule should be more strongly correlated to the external surface area that is available for reaction. Using BET analysis it is known that the surface area of the mesopore series increases as NaOH attack and acid washing is carried out. From Figure 36 it can be observed that conversion does not

follow the trend of the external surface area. The increased surface area that is exposed from the NaOH attack lead to much higher conversion levels with the mesoporous samples. If we examine the intial pulses of biomass fed another interesting observation can be seen. The non acid-washed sample actually leads to a higher conversion of these large bulky molecules per external S.A., Figure 38. We credit this to the reactions taking place on the EFA that was created from the NaOH attack. Looking at the conversion it is evident that the effect of these EFA sites is only prevalent initally and then are deactivated rapidly. In other work it has been shown that it is possible to inhibit these external sites. If the methoxyphenolic compounds remain unreacted from the zeolite upgrading they can be separated from the resultant liquid and more targeted chemistries for methoxyphenolics can be utilized.

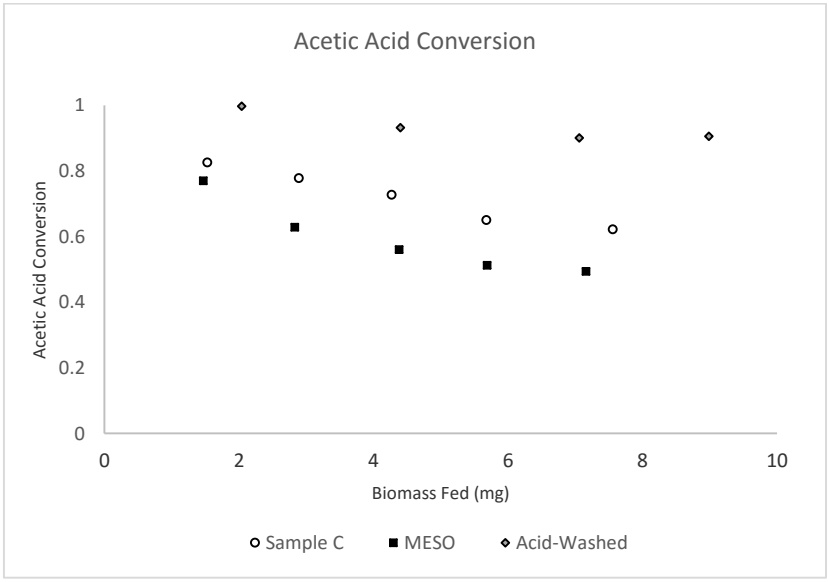

Figure 35: Mesopore Series- Acetic Acid Conversion

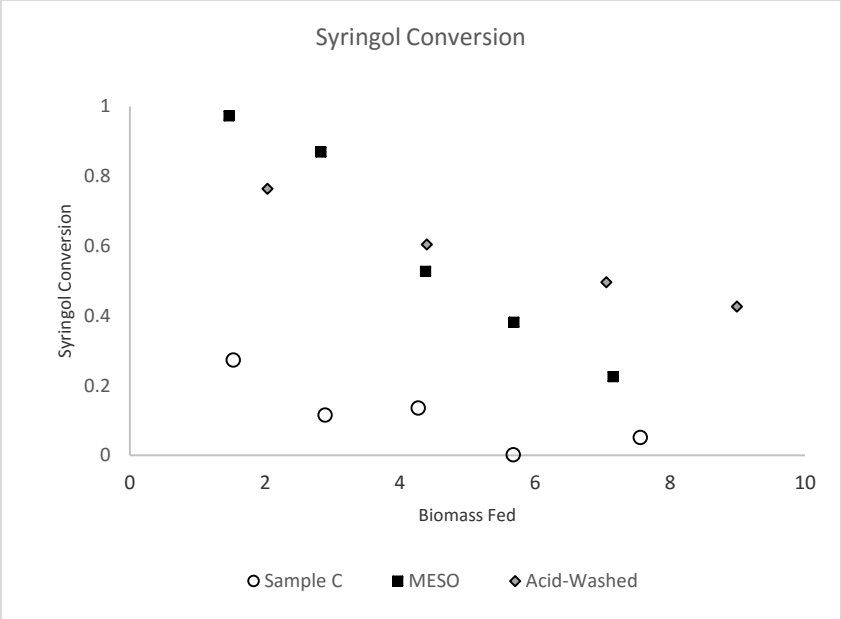

Figure 36: Mesopore Series- Syringol Conversion

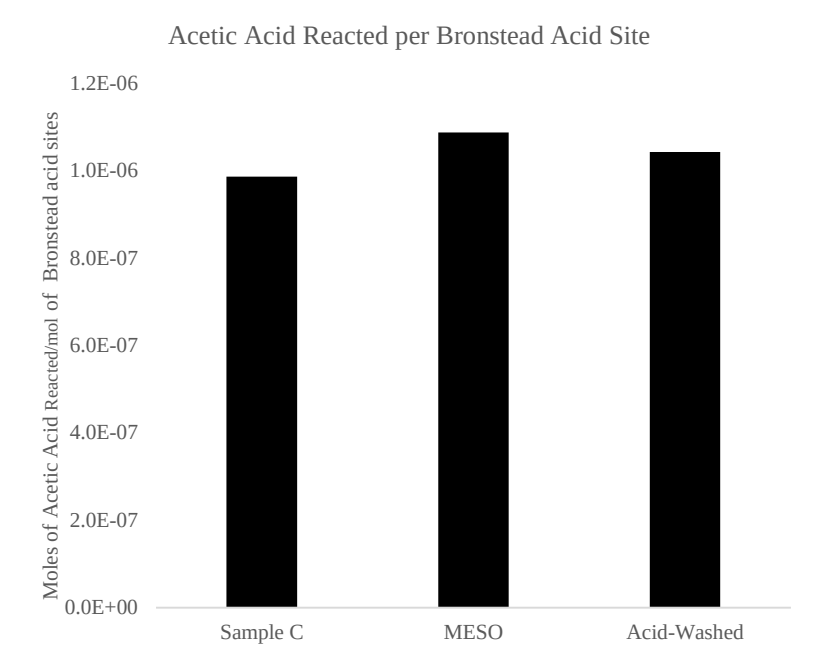

Figure 37: Mesopore Series- Acetic Acid reacted per Bronsted Acid Acid

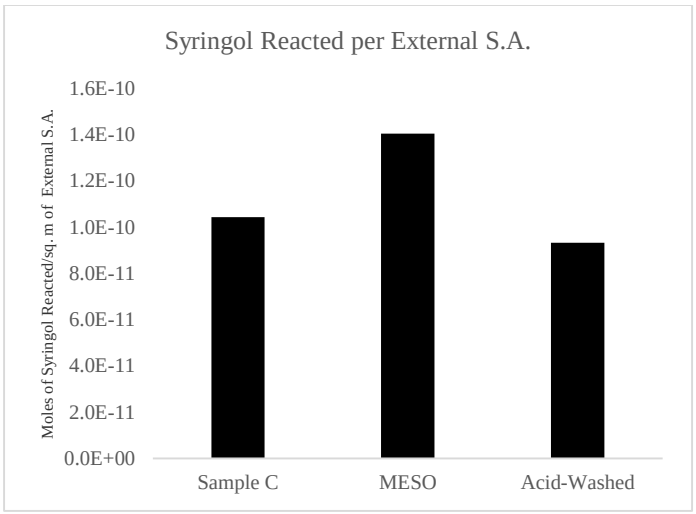

Figure 38: Syringol Reacted per External Surface Area

Deactivation

The deactivation rate of the Acid-Washed Sample C zeolite showed a slower deactivation curve for the production of alkyl benzenes. This could be due to a decrease in the production of coke through conversion of naphthalenes to higher polyaromatics which get easily trapped in the cages and pores of the ZSM-5 structure. As the diffusion path is shortened, the products of alkyl benzenes and naphthalenes are more likely to escape the pores before further reacting to form polyaromatics which lead to coke.

Conclusions

Catalytic fast pyrolysis is a constantly changing and growing topic and manipulation of the catalyst can improve the products produced. By controlling the length a pyrolysis product travels through a zeolite, it is possible to increase the production of alkyl benzenes and naphthalenes. This diffusion length can be controlled through changing the size of the zeolite crystal or by creating mesopores in the zeolite structure by NaOH attack. A subsequent acid wash is needed to remove any extra-

framework alumina that has been redeposited after mesopore creation which can plug the pores of the zeolite and block access to active sites. It was determined in this study that the length of the diffusion path can be adjusted to increase the catalytic conversion of pyrolysis products, with shorter paths found to be more favorable than longer paths. A higher production of products would in turn decrease the production of coke and increase the life of the catalyst.

Experimental Section

Catalyst Synthesis

Three different ZSM-5 crystals were hydrothermally synthesized following Armaroli et al.'s procedure. The precursor gel composition was varied keeping the synthesis conditions same as reported.[1] The reagents used for the synthesis are tetraethyl orthosilicate (98%, Sigma-Aldrich), tetrapropylammonium hydroxide (40% W/W, Alfa-Aesar), aluminum isopropoxide (98%, Sigma-Aldrich), sodium hydroxide (>98%, Sigma-Aldrich) and double distilled water. Synthesized samples were washed three times with doubly distilled water and filtered by centrifugation. The obtained cake was dried overnight (12hrs) at 85 ˚C in an oven. The dried sample is ion-exchanged from sodium form to ammonia form with 2M ammonium nitrate solution at 80˚C for 3 hours. The ion-exchange procedure was repeated 5 times to ensure complete exchange. This was followed by washing with double distilled water 3 times and drying overnight (12hrs) at 85˚C. Obtained ammonium form zeolite was calcined at 600˚C (ramp rate 2 ˚C/min) for 5 hrs to get proton form of zeolite. These three H-ZSM-5 samples will be referred as A, B and C in further discussion. Characterization results of all three synthesized samples are tabulated in Table 2 and Table 3.

Table 3 Hydrothermally synthesized samples.

Sample	Crystal size (SEM, μm)
A	0.4-0.5
B	5
C	10
Meso C	10
Acid-washed Meso C	10

Mesopore Creation

It is well established that alkaline treatment of crystalline ZSM5 can create mesopores by de-silication.[94-97] In our study, 0.2M sodium hydroxide solution was used for the alkaline treatment of Sample C. The zeolite and NaOH solution was mixed in a ratio of 1:30 for the experimental procedure.[98] The solution was well stirred at a temperature of 80˚C for 5 hours. The mixture was cooled in an ice bath and was washed with double distilled water for three times. The washed sample was oven dried at 85˚C for 12 hours. The dried sample was ion-exchanged and calcined following the procedure described in the previous section. This sample is referred to as Meso Sample C further.

Acid Washing

Acid wash of the Mesoporous Sample C was done following the procedure as published in literature.[99] The Mesoporous Sample C was washed with 0.2M hydrochloric acid in a ratio of 1:10 at a temperature of 80˚C under vigorous stirring for

3 hours. The sample was then washed three times and oven dried at 85˚C for 12 hours. This sample is termed as Acid-Washed Sample C further.

SEM

To estimate the particle diameter of all the samples scanning electron microscopy (SEM) measurements were performed by a Zeiss-NEON FEG-SEM instrument. To prepare samples for SEM, a small amount of the zeolite was dispersed in water. A drop of zeolite aqueous suspension was placed on carbon tape and dried for one hour at 75˚C before doing the experiments.

Nitrogen Adsorption

A Micrometrics ASAP 2020 Surface Area and Porosity Analyzer (Micrometrics; Norcross, GA) was used to perform nitrogen adsorption experiments to determine the total pore volume, micropore volume, and by difference the mesopore volume of the catalysts.

IPA-TPD

Isopropyl amine (IPA) temperature-programmed desorption (TPD) is a proven technique for estimating the number of Brønsted acid sites in H-form zeolites.[100, 101] IPA reacts on a Brønsted acid site of H-zeolite to produce propylene and ammonia. IPA-TPD experiments were done on all the H-Zeolite samples used in this study to investigate the amount of Brønsted acid sites. 50mg of catalyst was taken in a quartz reactor (1/4” OD) and flushed at 300˚C for two hours with helium as carrier gas (20ml/min). After flushing the sample, temperature was reduced to 100˚C and 2 μL

pulses of IPA were injected into the reactor through a septum via a syringe. Mass to charge ratio (m/e) of 44 and 58 were tracked at exit of the reactor with a MKS Cirrus 200 quadrupole mass spectrometer (MS), to ensure saturation of all the acid sites in the catalyst bed with IPA. Pulses of IPA were continued until a constant signal m/e=44 and 58 was observed. After adsorption of IPA on to the catalyst bed, it was flushed with carrier gas (20ml/min) at 100˚C for 4hrs to remove all the physically absorbed IPA. Flushing was followed by a temperature ramp from 100˚C to 600˚C at a rate of 10˚C/min. The products desorbing from the reactor with temperature ramp were tracked by MS. Quantification of the products was done by injecting standards and propylene gas pulsed using a sample loop.

XRD

For checking the crystallinity of the sample, X-ray diffraction studies using Rigaku automatic diffractor (Model D-MAX A) with a curved crystal monochromator were performed. A flat surface of the well ground samples was prepared on a plastic slide for the experiments. The instrument has Cu-Kα as a radiation source and was operated at 40kV and 35 mA between the angle range of 5-60˚.

Pyrolysis GCMS-FID

Pyroprobe Description – The instrument used for pyrolysis of biomass was the CDS analytical pyroprobe model 5250 fitted with an autosampler. Pyrolysis vapors travel through1/16 inch Silco-stainless steel transfer line tubing that is kept at 300°C.

Reactor Description – A 6” long quartz reactor was placed between two heated transfer lines for ex situ catalytic upgrading of the biomass vapors. A furnace oven was used to heat the catalyst bed to the reaction temperature. 5 mg of catalyst was used for all experiments and was mixed thoroughly with 200 mg acid washed borosilicate glass beads obtained from Sigma Aldrich (G1145) to prevent channeling through the catalyst bed. The catalysts were pelletized and sieved to a similar size as the glass beads, 90-250 μm, and held in position by a pinch in the quartz tube and two plugs of 30 mg of quartz wool. To maintain proper temperature, a thermocouple was secured to the outside of the quartz tube and placed in the middle of the catalyst bed. Quartz wool was used as insulation on top and bottom of the furnace to maintain the desired temperature.

GCMS-FID Description – To analyze the pyrolysis vapors or catalytically upgraded vapor products, a Shimadzu QP2010 GCMS-FID system was used with a RTX-1701 column 60m×0.25mm with a 0.25 μm film thickness. The oven ramp rate was programmed to hold for 4 min at 45°C then ramp at 3°C/min to 280°C and hold for 20 min. The injector temperature was set at 280°C with the injector split ratio set to 90:1. The carrier gas was helium (ultra high purity from Airgas) and the column flow rate was maintained at 1 mL/min. Products were identified using the mass fragmentation patterns and literature while yields were determined using the FID area of a peak normalized to 1 mg of biomass fed. The FID/MS split ratio was set to 10:1. A calibration was then applied to determine the μgrams of carbon/mg biomass. This was done using an effective carbon number (ECN) model that takes in to account the various effects of C-O bonds on the FID signal. Due to the large amount of compounds seen in pyrolysis vapors, traditional model compound injection calibrations were not feasible.

Experiment Conditions

The biomass samples used consisted of locally sourced red oak sawdust that was ground to 0.25-0.45 mm and dried in a vacuum (0.02 MPa) at 60˚C overnight. Typical red oak composition has been found to have a lignin, hemicellulose, and cellulose content of 21, 47, and 27 wt % respectively.[19] An estimated ash content of 2% was determined by calcination in a TGA unit at 800°C. 0.7-1.0mg of oak was packed in a quartz tube with a quartz wool plug on bottom to prevent any loss of particles when the tube drops from the autosampler into the pyrolysis chamber of the pyroprobe.

The pyrolysis chamber consists of a quartz chamber wrapped in a platinum wire that is heated to 500°C while sealed in an inert environment of helium for 60 seconds. All pyrolysis experiments were done under these conditions. In a previous work, it was found that 500°C was an optimum temperature for the catalytic upgrading of pyrolysis vapors over a ZSM-5 and so all catalytic experiments were performed under the same conditions.

Chapter 8: The Role of Gallium Modified ZSM-5 on Catalytic Upgrading of Biomass Pyrolysis Vapors[a]

[a]Manuscript by Stevens, A and Vann, T et al. *The Role of Gallium Modified ZSM-5 on Catalytic Upgrading of Biomass Pyolysis Vapors.* Experiments and initial text draft from Adam Stevens. Additional data work-up and text by Tyler Vann

Abstract

This study investigates how the addition of gallium to ZSM-5 catalyst affects the activity and life of the catalyst when upgrading lignocellulosic biomass pyrolysis vapors. It is shown that the addition of gallium causes the activity of the catalyst decreases. This is due to the gallium exchanging with Brønsted acid sites after impregnation. The gallium can then be reduced in hydrogen to form GaO+, Ga+, or GaH_{2+} which allow hydrogenation/hydrogenolysis reactions.

The introduction of reduced gallium limits the amount of coke formation. The influence of reduction temperature was also investigated and was can be seen to influence the production of alkyl benzenes and naphthalenes. To keep the gallium reduced and the catalyst from deactivating quickly, a low partial pressure slipstream of hydrogen is required and has been shown to improve catalyst life.

Introduction

Due to environmental concerns over transportation fuels and chemicals derived from petroleum sources, a push for green alternatives is driving a large amount of scientific research in this area. With the addition of rising CO_2 levels in the atmosphere, a carbon neutral source of energy would be very beneficial. Biomass is proving to be a potential candidate for that position and with advances in turning that raw bio-oil into usable diesel fuel, hopes are rising. When biomass is thermally broken

down in an inert environment, the cellulose, hemicellulose, and lignin that make up that organism are broken into monomer molecules which can then be recovered and processed into a biofuel. The raw bio-oil is composed of hundreds of oxygenated compounds which tend to corrode, polymerize, and complicate processing and storage. To overcome these difficulties, researchers have developed catalytic fast pyrolysis (CFP). This process uses a solid catalyst to react the oxygenated pyrolysis products in the vapor phase and produce simpler, less oxygenated molecules suitable for further upgrading to products similar to transportation fuel components. In this work, ex situ catalyst beds are used exclusively. Many other studies use in situ catalysis to study the activity and potential of new catalysts for upgrading pyrolysis vapors.[79] Through the use of an ex situ catalyst bed, the deactivation of a catalyst can be seen investigated.[8, 80, 82, 102]

While many different catalysts have been studied, zeolites have proved robust enough to handle the complicated nature of CFP. Groups that have studied a range of different zeolite structures have found that ZSM-5 was optimal for the production of alkyl benzenes and aromatics. [9, 82-84] This is due to the optimal pore diameter which produces a confinement effect that promotes the aromatization of reactants to form alkyl benzenes and polyaromatics. [85]

Metals have been found to assist in reactions needed for the conversion of raw bio-oil to more manageable and valuable fuels. Gallium is one such metal that has been seen to participate in the aromatization of light compounds. [103-105] It is also believed to assist in the hydrogenolysis of the C-O bond. Depending on the pre-reduction conditions, the gallium metal can be in a GaO+, Ga+, or GaH_{2+} form during

catalytic upgrading.[106-108] Model compound studies have been done on this Ga-ZSM-5 using benzaldehyde and m-cresol, both of which are compounds found in pyrolysis vapors and so results can be related toward catalytic fast pyrolysis.[109] When the Ga-ZSM-5 was run in He, there was no influence on the Brønsted acid site density according to IPA-TPD. But when it was reduced in H_2, Brønsted acid site density decreased dramatically. Without the H_2, the gallium remains in Ga_2O_3 oxide clusters, but during reduction, gallium acts as an exchangeable cation (Ga+) and is able to exchange with the Brønsted site's hydrogen atom.

It has been shown in literature that when benzaldehyde was passed over ZSM-5 in H_2 or He, the only product observed was benzene. When gallium was added to the zeolite, under helium conditions, similar results were seen; no toluene production. It wasn't until H_2 was used as the carrier gas that the gallium became active and caused a large change in selectivity toward the production of toluene and small amounts of methane. With the addition of Gallium and H_2, hydrogenation/hydrogenolysis reactions became available to retain the carbon as toluene.[109]

In a similar study, m-cresol was used with Ga-ZSM-5. Without the use of H_2, the conversion of m-cresol decreases very quickly showing fast deactivation. When adding H_2, conversion to toluene is increased and remains the dominate product over benzene while limiting deactivation. 500°C was found to be an optimal temperature for the conversion of m-cresol to toluene.[68]

Pre-reduced Ga-ZSM-5 is observed to have high conversion when compared with non-reduced Ga-ZSM-5. The gallium remains reduced for a short time but then is lost without the addition of a hydrogen stream. Without the hydrogen stream the

reactants are more likely to react and form coke products which will deactivate the catalyst. With hydrogen the surface pool that has been created is able to further react to final products and be removed from the catalyst before they are converted to coke.

Results and Discussion

Catalyst Activity

Pyroprobe

It has been shown previously that GaZSM-5 can increase the rate of decarbonylation and deoxygenation in pyrolysis model compound reactions.[68, 109] Due to these promising results GaZSM-5 was proposed as a catalyst for the upgrading of oak pyrolysis vapors. Without pre-reduction and no hydrogen stream during biomass pulses, rate decreases when gallium is introduced into the zeolite. This was to be expected when gallium is added to ZSM-5 as it acts as a cation and replaces the Brønsted acid sites in the catalyst and in turn there are fewer acid sites to convert the pyrolysis vapors. When the catalyst was pre-reduced at 575°C for 1 hr, the initial activity increase higher than without gallium but a steep deactivation curve observed. This is believed to be due to the gallium oxidation due to species present in the bio-oil vapors.

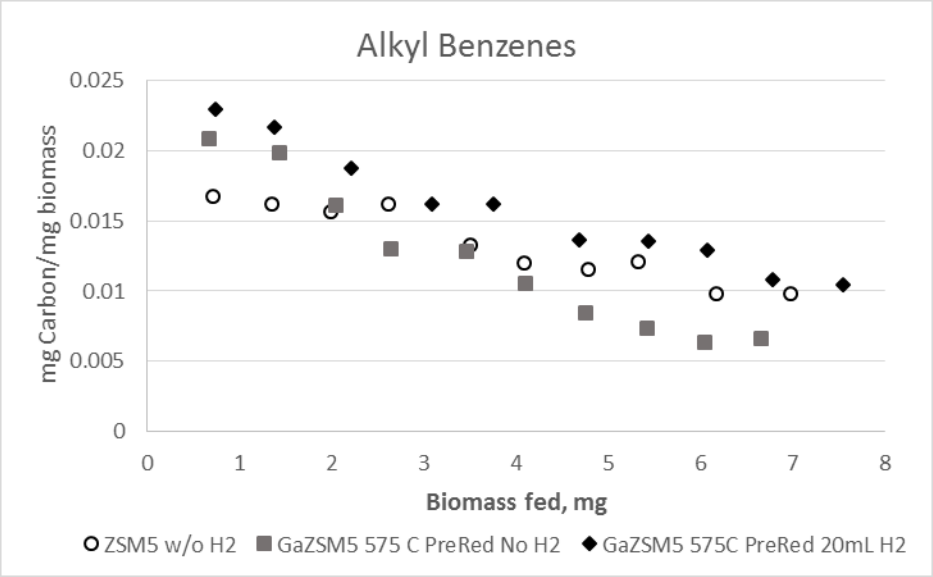

Figure 39: Alkyl Benzene Comparison, ZSM-5 vs Ga/ZSM-5 with and without hydrogen flow

Hydrogen Slipstream

Next a small partial pressure of hydrogen (20mL H_2 to 94mL He) was introduced to keep the gallium in its reduced form and it was observed that the initial activity increased higher than before as well as a decrease in the deactivation rate (Figure 39). Also to be noted was that the production of coke was visibly different when compared to a run without hydrogen; see Figure 40. This implies less carbon has been lost to coke resulting in improved overall yield.

Figure 40: Comparison of Catalyst bed; left with hydrogen, right without hydrogen

Effect of Pre-Reduction Temperature

While these results indicated promise, it was necessary to investigate if the reduction temperature of 575°C was too high, leading to sub-optimal activity. In order to determine if the pre-reduction temperature was optimized, the pre-reduction temperature was decreased to 500°C for ~12hrs. The initial activity again increased to the highest yet of alkyl benzenes and a slower rate of deactivation was observed, shown in Figure 41. With 550°C pre-reduction for 2 hours produced similar amounts of alkyl benzene products are observed.

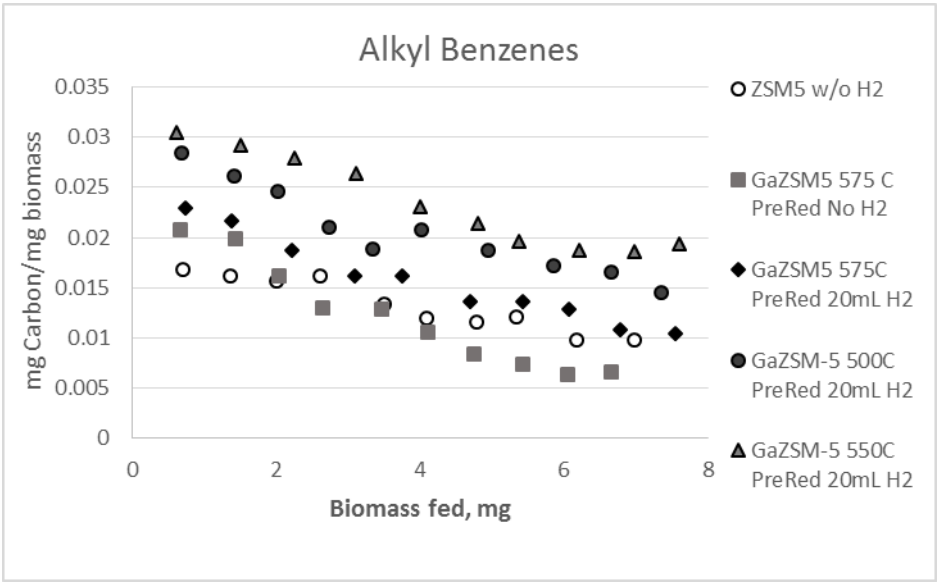

Figure 41: Alkyl Benzene Comparison for different Pre-Reduction Temperatures

One major difference in the reduction temperatures was in the production of naphthalenes. As shown in Figure 42, the highest production of naphthalenes was actually at the lowest pre-reduction temperature, 500°C. According to Dooley et al., the gallium ZSM-5 requires high reduction temperatures for the gallium to fully reduce or fully exchange the gallium.[103] At higher reduction temperatures, there would be

fewer Brønsted sites than at lower reduction temperatures and would therefore have less chance for pyrolysis vapors to be converted to alkyl benzenes and on to naphthalenes as an end product. A small exchange of gallium with Brønsted sites may be necessary to improve the activity and lower the rate of deactivation or possibly some of the gallium oxide.

At the 575°C pre-reduction the methoxyphenolic compound yield is lowest and alkyl phenolics are highest. With gallium exchanged catalyts at higher temperatures, there is a higher possibility for larger methoxylated molecules to be deoxygenated to form smaller alkyl phenolics. Under excess catalyst conditions, these would then further react to form alkyl benzenes and naphthalenes. At the lowest temperature, 500°C, furfurals were at their lowest levels and are undergoing aldol condensation to form naphthalenes because of the higher number of Brønsted sites

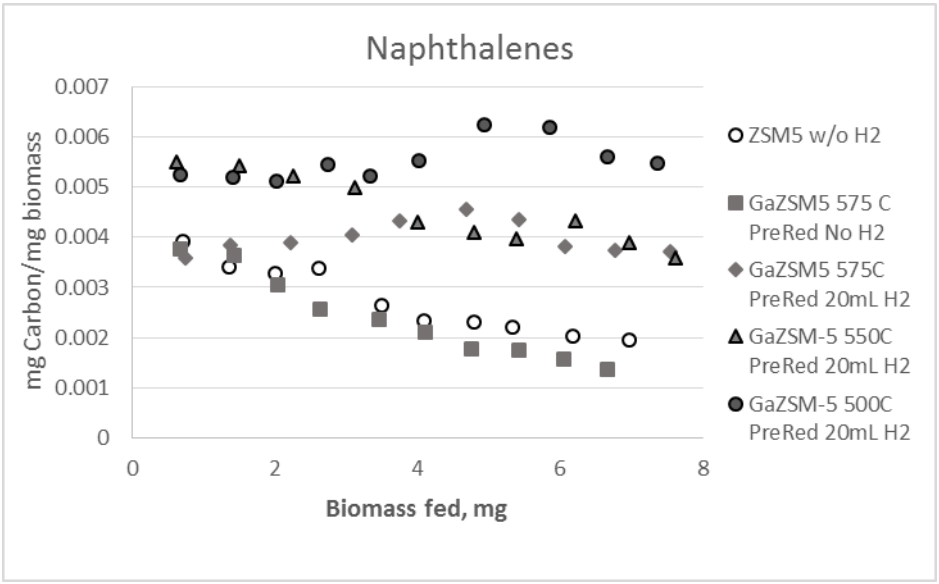

Figure 42: Naphthalene Comparison for different Pre-Reduction Temperatures

Excess Catalyst

While alkyl benzene production increases with catalyst loading, there is a maximum amount of alkyl benzenes that can be generated. One drawback of using gallium with ZSM-5 is that the combustible light gas peak was seen to increase compared to the parent zeolite. This may be due to the gallium cleaving the methoxy groups from the methoxyphenolics.

In an attempt to recapture the lost combustible light gases, 5 and 10mg of catalyst was used to reach an excess catalyst environment. As seen in Figure 43, the combustible light gases increased when 5mg was used, but when excess catalyst was reached at 10mg, the light gases were recaptured. While these compounds were recaptured, the alkyl benzenes and naphthalenes did not increase in proper proportion. It is believed that the recaptured light gases were incorporated in the polyaromatics which have a difficult time exiting the zeolite pores due to steric hindrance and are lost as coke. So it is observed that there is an optimal amount of catalyst loading that should be used per biomass to minimize coking and light gas production but also maximize alkyl benzene and naphthalene formation. One other option would be to send these light gases to a second catalyst bed to be recaptured.

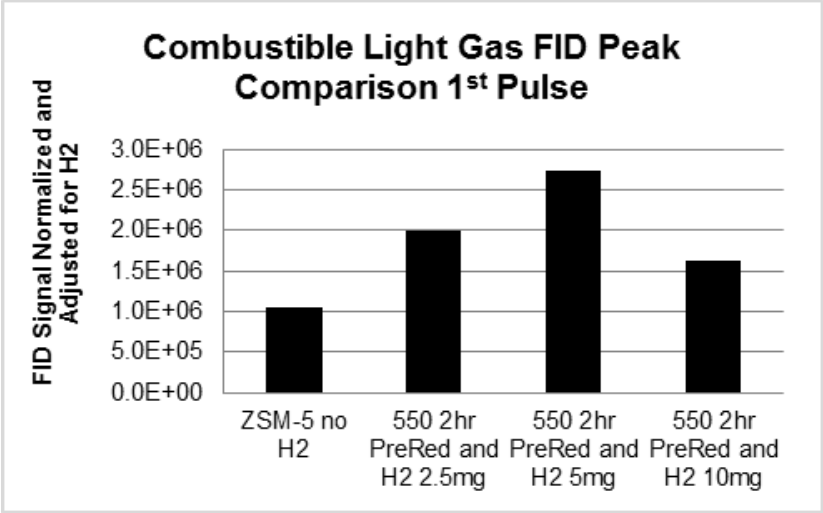

Figure 43: Combustible Light Gas Comparison for excess catalyst runs

Conclusions

While ZSM-5 has been found to be optimal in the catalytic upgrading of pyrolysis vapors, the addition of gallium has been shown to increase the activity of the catalyst. Pre-reduction of the catalyst has a large effect on the selectivity of products produced due to the percentage of Brønsted sites exchanged by gallium during reduction. A hydrogen stream is needed to keep the gallium reduced, but only low partial pressures of hydrogen are needed. It was also found that excess catalyst should not be used due to the negligible increase in alkyl benzene production to reduction of combustible light gases produced

Experimental Section

The experimental technique for this work was similar to what was previously discussed in chapter 7.

References

1. Pham, T.N., D. Shi, and D.E. Resasco, *Evaluating strategies for catalytic upgrading of pyrolysis oil in liquid phase.* Applied Catalysis B: Environmental, 2014. **145**: p. 10-23.

2. Huber, G.W., S. Iborra, and A. Corma, *Synthesis of transportation fuels from biomass: Chemistry, catalysts, and engineering.* Chemical Reviews, 2006. **106**(9): p. 4044-4098.

3. Resasco, D.E. and S.P. Crossley, *Implementation of concepts derived from model compound studies in the separation and conversion of bio-oil to fuel.* Catalysis Today, 2014.

4. Mohan, D., C.U. Pittman, and P.H. Steele, *Pyrolysis of wood/biomass for bio-oil: A critical review.* Energy & Fuels, 2006. **20**(3): p. 848-889.

5. Zhang, Q., et al., *Review of biomass pyrolysis oil properties and upgrading research.* Energy conversion and management, 2007. **48**(1): p. 87-92.

6. Kunkes, E.L., et al., *Catalytic conversion of biomass to monofunctional hydrocarbons and targeted liquid-fuel classes.* Science, 2008. **322**(5900): p. 417-421.

7. Mortensen, P.M., et al., *A review of catalytic upgrading of bio-oil to engine fuels.* Applied Catalysis A: General, 2011. **407**(1): p. 1-19.

8. Wan, S., et al., *Direct catalytic upgrading of biomass pyrolysis vapors by a dual function Ru/TiO2 catalyst.* AIChE Journal, 2013. **59**(7): p. 2275-2285.

9. Jae, J., et al., *Investigation into the shape selectivity of zeolite catalysts for biomass conversion.* Journal of Catalysis, 2011. **279**(2): p. 257-268.

10. Zhang, H., et al., *Catalytic conversion of biomass-derived feedstocks into olefins and aromatics with ZSM-5: the hydrogen to carbon effective ratio.* Energy & Environmental Science, 2011. **4**(6): p. 2297-2307.

11. Foster, A.J., et al., *Optimizing the aromatic yield and distribution from catalytic fast pyrolysis of biomass over ZSM-5.* Applied Catalysis A: General, 2012. **423**: p. 154-161.

12. Lindfors, C., et al., *Fractionation of bio-oil.* Energy & Fuels, 2014. **28**(9): p. 5785-5791.

13. Yang, H., et al., *Characteristics of hemicellulose, cellulose and lignin pyrolysis.* Fuel, 2007. **86**(12): p. 1781-1788.

14. Boonyasuwat, S., et al., *Conversion of Guaiacol over Supported Ru Catalysts.* Catalysis Letters, 2013. **143**(8): p. 783-791.

15. Gonzalez-Borja, M.A. and D.E. Resasco, *Reaction Pathways in the Liquid Phase Alkylation of Biomass-Derived Phenolic Compounds.* Aiche Journal, 2015. **61**(2): p. 598-609.

16. Zhao, C., et al., *Highly Selective Catalytic Conversion of Phenolic Bio-Oil to Alkanes.* Angewandte Chemie-International Edition, 2009. **48**(22): p. 3987-3990.

17. Faix, O., et al., *Thermal degradation products of wood.* Holz als Roh-und Werkstoff, 1991. **49**(5): p. 213-219.

18. Scanlon, J.T. and D.E. Willis, *Calculation of flame ionization detector relative response factors using the effective carbon number concept.* Journal of Chromatographic Science, 1985. **23**(8): p. 333-340.

19. Gardner, D.J., et al., *Dynamic wettability of wood.* Langmuir, 1991. **7**(11): p. 2498-2502.

20. Pham, T.N., et al., *Ketonization of Carboxylic Acids: Mechanisms, Catalysts, and Implications for Biomass Conversion.* Acs Catalysis, 2013. **3**(11): p. 2456-2473.

21. Pham, T.N., et al., *Aqueous-phase ketonization of acetic acid over Ru/TiO2/carbon catalysts.* Journal of Catalysis, 2012. **295**: p. 169-178.

22. Pham, T.N., D.C. Shi, and D.E. Resasco, *Kinetics and Mechanism of Ketonization of Acetic Acid on Ru/TiO2 Catalyst.* Topics in Catalysis, 2014. **57**(6-9): p. 706-714.

23. Chheda, J.N. and J.A. Dumesic, *An overview of dehydration, aldol-condensation and hydrogenation processes for production of liquid alkanes from biomass-derived carbohydrates.* Catalysis Today, 2007. **123**(1): p. 59-70.

24. Barrett, C.J., et al., *Single-reactor process for sequential aldol-condensation and hydrogenation of biomass-derived compounds in water.* Applied Catalysis B-Environmental, 2006. **66**(1-2): p. 111-118.

25. Omotoso, T., S. Boonyasuwat, and S.P. Crossley, *Understanding the role of TiO2 crystal structure on the enhanced activity and stability of Ru/TiO2 catalysts for the conversion of lignin-derived oxygenates.* Green Chemistry, 2014. **16**(2): p. 645-652.

26. Hronec, M. and K. Fulajtarova, *Selective transformation of furfural to cyclopentanone.* Catalysis Communications, 2012. **24**: p. 100-104.

27. Piutti, C. and F. Quartieri, *The Piancatelli Rearrangement: New Applications for an Intriguing Reaction.* Molecules, 2013. **18**(10): p. 12290-12312.

28. Hronec, M., et al., *Cyclopentanone: A raw material for production of C 15 and C 17 fuel precursors.* Biomass and Bioenergy, 2014. **63**: p. 291-299.

29. Sitthisa, S., W. An, and D.E. Resasco, *Selective conversion of furfural to methylfuran over silica-supported Ni-Fe bimetallic catalysts.* Journal of Catalysis, 2011. **284**(1): p. 90-101.

30. Dahl, I.M. and S. Kolboe, *On the reaction mechanism for propene formation in the MTO reaction over SAPO-34.* Catalysis Letters, 1993. **20**(3-4): p. 329-336.

31. Sitthisa, S. and D.E. Resasco, *Hydrodeoxygenation of Furfural Over Supported Metal Catalysts: A Comparative Study of Cu, Pd and Ni.* Catalysis Letters, 2011. **141**(6): p. 784-791.

32. Lin, Y.-C. and G.W. Huber, *The critical role of heterogeneous catalysis in lignocellulosic biomass conversion.* Energy & Environmental Science, 2009. **2**(1): p. 68-80.

33. Román-Leshkov, Y., et al., *Production of dimethylfuran for liquid fuels from biomass-derived carbohydrates.* Nature, 2007. **447**(7147): p. 982-985.

34. Rosatella, A.A., et al., *5-Hydroxymethylfurfural (HMF) as a building block platform: Biological properties, synthesis and synthetic applications.* Green Chemistry, 2011. **13**(4): p. 754-793.

35. Sitthisa, S., et al., *Kinetics and mechanism of hydrogenation of furfural on Cu/SiO2 catalysts.* Journal of Catalysis, 2011. **277**(1): p. 1-13.

36. Rao, R.S., R.T.K. Baker, and M.A. Vannice, *Furfural hydrogenation over carbon-supported copper.* Catalysis Letters, 1999. **60**(1-2): p. 51-57.

37. Casanova, O., S. Iborra, and A. Corma, *Biomass into Chemicals: Aerobic Oxidation of 5-Hydroxymethyl-2-furfural into 2, 5-Furandicarboxylic Acid with Gold Nanoparticle Catalysts.* ChemSusChem, 2009. **2**(12): p. 1138-1144.

38. Gandini, A., et al., *The furan counterpart of poly (ethylene terephthalate): an alternative material based on renewable resources.* Journal of Polymer Science Part A: Polymer Chemistry, 2009. **47**(1): p. 295-298.

39. Gorbanev, Y.Y., et al., *Gold-Catalyzed Aerobic Oxidation of 5-Hydroxymethylfurfural in Water at Ambient Temperature.* ChemSusChem, 2009. **2**(7): p. 672-675.

40. Vinke, P., H. Van Dam, and H. Van Bekkum, *Platinum catalyzed oxidation of 5-hydroxymethylfurfural.* Studies in surface science and catalysis, 1990. **55**: p. 147-158.

41. Gupta, N.K., et al., *Hydrotalcite-supported gold-nanoparticle-catalyzed highly efficient base-free aqueous oxidation of 5-hydroxymethylfurfural into 2, 5-furandicarboxylic acid under atmospheric oxygen pressure.* Green Chemistry, 2011. **13**(4): p. 824-827.

42. Vinke, P., et al., *On the oxygen tolerance of noble metal catalysts in liquid phase alcohol oxidations the influence of the support on catalyst deactivation.* Studies in Surface Science and Catalysis, 1991. **59**: p. 385-394.

43. Taarning, E., et al., *Chemicals from renewables: aerobic oxidation of furfural and hydroxymethylfurfural over gold catalysts.* ChemSusChem, 2008. **1**(1-2): p. 75-78.

44. Della Pina, C., et al., *Selective oxidation using gold.* Chemical Society Reviews, 2008. **37**(9): p. 2077-2095.

45. Hites, R.A. and K. Biemann, *Mechanism of ketonic decarboxylation. Pyrolysis of calcium decanoate.* Journal of the American Chemical Society, 1972. **94**(16): p. 5772-5777.

46. Renz, M., *Ketonization of carboxylic acids by decarboxylation: mechanism and scope.* European journal of organic chemistry, 2005. **2005**(6): p. 979-988.

47. Pulido, A., et al., *Ketonic decarboxylation reaction mechanism: a combined experimental and DFT study.* ChemSusChem, 2013. **6**(1): p. 141-151.

48. Case, P.A., A.R. van Heiningen, and M.C. Wheeler, *Liquid hydrocarbon fuels from cellulosic feedstocks via thermal deoxygenation of levulinic acid and formic acid salt mixtures.* Green chemistry, 2012. **14**(1): p. 85-89.

49. Landoll, M.P. and M.T. Holtzapple, *Thermal decomposition of mixed calcium carboxylate salts: Effects of lime on ketone yield.* Biomass and Bioenergy, 2011. **35**(8): p. 3592-3603.

50. Lilga, M.A., R.T. Hallen, and M. Gray, *Production of oxidized derivatives of 5-hydroxymethylfurfural (HMF).* Topics in Catalysis, 2010. **53**(15-18): p. 1264-1269.

51. Gorbanev, Y.Y., S. Kegnæs, and A. Riisager, *Effect of support in heterogeneous ruthenium catalysts used for the selective aerobic oxidation of HMF in water.* Topics in Catalysis, 2011. **54**(16-18): p. 1318-1324.

52. Santhanaraj, D., et al., *Gluconic Acid from Biomass Fast Pyrolysis Oils: Specialty Chemicals from the Thermochemical Conversion of Biomass.* Chemsuschem, 2014. **7**(11): p. 3132-3137.

53. Niu, S., et al., *Thermogravimetric analysis of the relationship among calcium magnesium acetate, calcium acetate and magnesium acetate.* Applied Energy, 2010. **87**(7): p. 2237-2242.

54. Adanez, J., L. De Diego, and F. Garcıa-Labiano, *Calcination of calcium acetate and calcium magnesium acetate: effect of the reacting atmosphere.* Fuel, 1999. **78**(5): p. 583-592.

55. Pham, T.N., D.C. Shi, and D.E. Resasco, *Evaluating strategies for catalytic upgrading of pyrolysis oil in liquid phase.* Applied Catalysis B-Environmental, 2014. **145**: p. 10-23.

56. Alonso, D.M., J.Q. Bond, and J.A. Dumesic, *Catalytic conversion of biomass to biofuels.* Green Chemistry, 2010. **12**(9): p. 1493-1513.

57. Chheda, J.N., G.W. Huber, and J.A. Dumesic, *Liquid-phase catalytic processing of biomass-derived oxygenated hydrocarbons to fuels and chemicals.* Angewandte Chemie International Edition, 2007. **46**(38): p. 7164-7183.

58. Crossley, S., et al., *Solid nanoparticles that catalyze biofuel upgrade reactions at the water/oil interface.* Science, 2010. **327**(5961): p. 68-72.

59. West, R.M., et al., *Carbon–carbon bond formation for biomass-derived furfurals and ketones by aldol condensation in a biphasic system.* Journal of Molecular Catalysis A: Chemical, 2008. **296**(1): p. 18-27.

60. Young, S. and E. Briggs, *Distillation principles and processes.* 1922.

61. Cheng, Y.-T. and G.W. Huber, *Chemistry of furan conversion into aromatics and olefins over HZSM-5: a model biomass conversion reaction.* ACS catalysis, 2011. **1**(6): p. 611-628.

62. Cheng, Y.-T. and G.W. Huber, *Production of targeted aromatics by using Diels–Alder classes of reactions with furans and olefins over ZSM-5.* Green Chemistry, 2012. **14**(11): p. 3114-3125.

63. Carlson, T.R., et al., *Production of green aromatics and olefins by catalytic fast pyrolysis of wood sawdust.* Energy & Environmental Science, 2011. **4**(1): p. 145-161.

64. Nikbin, N., et al., *A DFT study of the acid-catalyzed conversion of 2, 5-dimethylfuran and ethylene to p-xylene.* Journal of Catalysis, 2013. **297**: p. 35-43.

65. Vaitheeswaran, S., et al., *On the Way to Biofuels from Furan: Discriminating Diels–Alder and Ring-Opening Mechanisms.* ACS Catalysis, 2013. **3**(9): p. 2012-2019.

66. Shi, J., *Catalytic Fast Pyrolysis of Biomass in a Bubbling Fluidized Bed Reactor with Gallium Promoted ZSM-5 Catalyst.* 2012.

67. Cheng, Y.T., et al., *Production of Renewable Aromatic Compounds by Catalytic Fast Pyrolysis of Lignocellulosic Biomass with Bifunctional Ga/ZSM-5 Catalysts.* Angewandte Chemie, 2012. **124**(6): p. 1416-1419.

68. Ausavasukhi, A., et al., *Hydrodeoxygenation of m-cresol over gallium-modified beta zeolite catalysts.* Journal of Catalysis, 2012. **290**: p. 90-100.

69. Zhu, X.L., et al., *Bifunctional transalkylation and hydrodeoxygenation of anisole over a Pt/HBeta catalyst.* Journal of Catalysis, 2011. **281**(1): p. 21-29.

70. Zapata, P.A., et al., *Hydrophobic zeolites for biofuel upgrading reactions at the liquid–liquid interface in water/oil emulsions.* Journal of the American Chemical Society, 2012. **134**(20): p. 8570-8578.

71. Helle, S., et al., *A kinetic model for production of glucose by hydrolysis of levoglucosan and cellobiosan from pyrolysis oil.* Carbohydrate research, 2007. **342**(16): p. 2365-2370.

72. Shafizadeh, F., et al., *Production of levoglucosan and glucose from pyrolysis of cellulosic materials.* Journal of Applied Polymer Science, 1979. **23**(12): p. 3525-3539.

73. Mettler, M.S., et al., *Pyrolytic conversion of cellulose to fuels: levoglucosan deoxygenation via elimination and cyclization within molten biomass.* Energy & Environmental Science, 2012. **5**(7): p. 7864-7868.

74. Bindwal, A.B. and P.D. Vaidya, *Kinetics of Aqueous-Phase Hydrogenation of Levoglucosan over Ru/C Catalyst.* Industrial & Engineering Chemistry Research, 2013. **52**(50): p. 17781-17789.

75. Hu, X., et al., *Mediating acid-catalyzed conversion of levoglucosan into platform chemicals with various solvents.* Green Chemistry, 2012. **14**(11): p. 3087-3098.

76. Lu, Q., et al., *Catalytic fast pyrolysis of cellulose mixed with sulfated titania to produce levoglucosenone: Analytical Py-GC/MS study.* BioResources, 2012. **7**(3): p. 2820-2834.

77. Pappa, A., et al., *TG-MS analysis for studying the effects of fire retardants on the pyrolysis of pine-needles and their components.* Journal of thermal analysis and calorimetry, 2006. **84**(3): p. 655-661.

78. Klampfl, C.W., et al., *Investigations on the effect of metal ions on the products obtained from the pyrolysis of cellulose.* Acta Chimica Slovenica, 2006. **53**(4): p. 437.

79. Agblevor, F.A., et al., *Fractional catalytic pyrolysis of hybrid poplar wood.* Industrial & Engineering Chemistry Research, 2010. **49**(8): p. 3533-3538.

80. Cooper, M., et al., *Catalytic upgrading of biomass pyrolysis vapors.* TCS, 2010.

81. Corma, A., S. Iborra, and A. Velty, *Chemical routes for the transformation of biomass into chemicals.* Chemical Reviews, 2007. **107**(6): p. 2411-2502.

82. Mukarakate, C., et al., *Real-time monitoring of the deactivation of HZSM-5 during upgrading of pine pyrolysis vapors.* Green Chemistry, 2014. **16**(3): p. 1444-1461.

83. French, R. and S. Czernik, *Catalytic pyrolysis of biomass for biofuels production.* Fuel Processing Technology, 2010. **91**(1): p. 25-32.

84. Carlson, T.R., et al., *Catalytic fast pyrolysis of glucose with HZSM-5: the combined homogeneous and heterogeneous reactions.* Journal of Catalysis, 2010. **270**(1): p. 110-124.

85. Gounder, R. and E. Iglesia, *The catalytic diversity of zeolites: confinement and solvation effects within voids of molecular dimensions.* Chemical Communications, 2013. **49**(34): p. 3491-3509.

86. Hoang, T.Q., et al., *Effects of HZSM-5 crystallite size on stability and alkyl-aromatics product distribution from conversion of propanal.* Catalysis Communications, 2010. **11**(11): p. 977-981.

87. Armaroli, T., et al., *Effects of crystal size and Si/Al ratio on the surface properties of H-ZSM-5 zeolites.* Applied Catalysis A: General, 2006. **306**: p. 78-84.

88. Li, J., et al., *Catalytic fast pyrolysis of biomass with mesoporous ZSM-5 zeolites prepared by desilication with NaOH solutions.* Applied Catalysis A: General, 2014. **470**: p. 115-122.

89. Bjørgen, M., et al., *Methanol to gasoline over zeolite H-ZSM-5: Improved catalyst performance by treatment with NaOH.* Applied Catalysis A: General, 2008. **345**(1): p. 43-50.

90. Zhu, X., et al., *Tailoring the mesopore structure of HZSM-5 to control product distribution in the conversion of propanal.* Journal of Catalysis, 2010. **271**(1): p. 88-98.

91. Dessau, R., E. Valyocsik, and N. Goeke, *Aluminum zoning in ZSM-5 as revealed by selective silica removal.* Zeolites, 1992. **12**(7): p. 776-779.

92. Wu, E., et al., *ZSM-5-type materials. Factors affecting crystal symmetry.* Journal of Physical Chemistry, 1979. **83**(21): p. 2777-2781.

93. Wan, S., et al., *Decoupling HZSM-5 Catalyst Activity from Deactivation during Upgrading of Pyrolysis Oil Vapors.* ChemSusChem, 2015. **8**(3): p. 552-559.

94. Verboekend, D. and J. Pérez-Ramírez, *Design of hierarchical zeolite catalysts by desilication.* Catalysis Science & Technology, 2011. **1**(6): p. 879-890.

95. Groen, J.C., J.A. Moulijn, and J. Pérez-Ramírez, *Desilication: on the controlled generation of mesoporosity in MFI zeolites.* Journal of Materials Chemistry, 2006. **16**(22): p. 2121-2131.

96. Van Donk, S., et al., *Generation, characterization, and impact of mesopores in zeolite catalysts.* Catalysis Reviews, 2003. **45**(2): p. 297-319.

97. Groen, J., et al., *On the introduction of intracrystalline mesoporosity in zeolites upon desilication in alkaline medium.* Microporous and Mesoporous Materials, 2004. **69**(1): p. 29-34.

98. Ogura, M., et al., *Formation of Uniform Mesopores in ZSM-5 Zeolite through Treatment in Alkaline Solution.* Chemistry letters, 2000(8): p. 882-883.

99. Caicedo-Realpe, R. and J. Pérez-Ramírez, *Mesoporous ZSM-5 zeolites prepared by a two-step route comprising sodium aluminate and acid treatments.* Microporous and mesoporous materials, 2010. **128**(1): p. 91-100.

100. Kofke, T.G., et al., *Stoichiometric adsorption complexes in H-ZSM-5, H-ZSM-12, and H-mordenite zeolites.* Journal of Catalysis, 1989. **115**(1): p. 265-272.

101. Gorte, R., *What do we know about the acidity of solid acids?* Catalysis Letters, 1999. **62**(1): p. 1-13.

102. Corma, A., et al., *Processing biomass-derived oxygenates in the oil refinery: Catalytic cracking (FCC) reaction pathways and role of catalyst.* Journal of Catalysis, 2007. **247**(2): p. 307-327.

103. Dooley, K.M., C. Chang, and G.L. Price, *Effects of pretreatments on state of gallium and aromatization activity of gallium/ZSM-5 catalysts.* Applied Catalysis A: General, 1992. **84**(1): p. 17-30.

104. Schulz, P. and M. Baerns, *Aromatization of ethane over gallium-promoted H-ZSM-5 catalysts.* Applied catalysis, 1991. **78**(1): p. 15-29.

105. Bayense, C. and J. Van Hooff, *Aromatization of propane over gallium-containing H-ZSM-5 zeolites: Influence of the preparation method on the product selectivity and the catalytic stability.* Applied Catalysis A: General, 1991. **79**(1): p. 127-140.

106. Meriaudeau, P. and C. Naccache, *Further evidence on the change of acid properties of H-ZSM-5 by Ga and Pt.* Journal of Catalysis, 1995. **157**(2): p. 283-288.

107. Meriaudeau, P., et al., *Revisiting Ga2O3/H-ZSM-5 propane aromatization catalysts.* Catalysis letters, 1994. **27**(1-2): p. 143-148.

108. Kanazirev, V., G. Price, and K. Dooley, *Preparation of Ga-Doped Zeolite Catalysts Via Hydrogen Induced Solid State Interaction Between Ga 2 O 3 and HZSM-5 ZEOLITE.* Studies in Surface Science and Catalysis, 1991. **69**: p. 277-285.

109. Ausavasukhi, A., T. Sooknoi, and D.E. Resasco, *Catalytic deoxygenation of benzaldehyde over gallium-modified ZSM-5 zeolite.* Journal of Catalysis, 2009. **268**(1): p. 68-78.

110. Huber, G.W. and J.A. Dumesic, *An overview of aqueous-phase catalytic processes for production of hydrogen and alkanes in a biorefinery.* Catalysis Today, 2006. **111**(1-2): p. 119-132.

111. Anex, R.P., et al., *Techno-economic comparison of biomass-to-transportation fuels via pyrolysis, gasification, and biochemical pathways.* Fuel, 2010. **89**: p. S29-S35.

112. Czernik, S. and A.V. Bridgwater, *Overview of applications of biomass fast pyrolysis oil.* Energy & Fuels, 2004. **18**(2): p. 590-598.

113. Prins, M.J., K.J. Ptasinski, and F.J.J.G. Janssen, *More efficient biomass gasification via torrefaction.* Energy, 2006. **31**(15): p. 3458-3470.

114. van der Stelt, M.J.C., et al., *Biomass upgrading by torrefaction for the production of biofuels: A review.* Biomass & Bioenergy, 2011. **35**(9): p. 3748-3762.

115. Chew, J.J. and V. Doshi, *Recent advances in biomass pretreatment - Torrefaction fundamentals and technology.* Renewable & Sustainable Energy Reviews, 2011. **15**(8): p. 4212-4222.

116. Climent, M.J., A. Corma, and S. Iborra, *Conversion of biomass platform molecules into fuel additives and liquid hydrocarbon fuels.* Green Chemistry, 2014. **16**(2): p. 516-547.

117. Wright, M.M., Y. Roman-Leshkov, and W.H. Green, *Investigating the techno-economic trade-offs of hydrogen source using a response surface model of drop-in biofuel production via bio-oil upgrading.* Biofuels Bioproducts & Biorefining-Biofpr, 2012. **6**(5): p. 503-520.

118. Wright, M.M., et al., *Techno-economic analysis of biomass fast pyrolysis to transportation fuels.* Fuel, 2010. **89**: p. S11-S19.

119. Brown, T.R., et al., *Techno-economic assessment (TEA) of advanced biochemical and thermochemical biorefineries*, in *Advances in biorefineries*, K. Waldron, Editor. 2014, Woodhead Publishing: Amsterdam. p. 34-66.

120. Resasco, D.E. 2015.

121. Vassilev, S.V., et al., *An overview of the organic and inorganic phase composition of biomass.* Fuel, 2012. **94**(1): p. 1-33.

122. Williams, P.T. and S. Besler, *The influence of temperature and heating rate on the pyrolysis of biomass.* Renewable Energy, 1996. **7**(3): p. 233-250.

123. Demirbas, A., *Mechanisms of liquefaction and pyrolysis reactions of biomass.* Energy Conversion and Management, 2000. **41**(6): p. 633-646.

124. Orfao, J.J.M., F.J.A. Antunes, and J.L. Figueiredo, *Pyrolysis kinetics of lignocellulosic materials - three independent reactions model.* Fuel, 1999. **78**(3): p. 349-358.

125. Gronli, M.G., G. Varhegyi, and C. Di Blasi, *Thermogravimetric analysis and devolatilization kinetics of wood.* Industrial & Engineering Chemistry Research, 2002. **41**(17): p. 4201-4208.

126. Shen, D.K. and S. Gu, *The mechanism for thermal decomposition of cellulose and its main products.* Bioresource Technology, 2009. **100**(24): p. 6496-6504.

127. Pham, T.N., D.C. Shi, and D.E. Resasco, *Reaction kinetics and mechanism of ketonization of aliphatic carboxylic acids with different carbon chain lengths over Ru/TiO2 catalyst.* Journal of Catalysis, 2014. **314**: p. 149-158.

128. Martinez, R., M.C. Huff, and M.A. Barteau, *Ketonization of acetic acid on titania-functionalized silica monoliths.* Journal of Catalysis, 2004. **222**(2): p. 404-409.

129. Pestman, R., et al., *The Formation of Ketones and Aldehydes from Carboxylic-Acids, Structure-Activity Relationship for 2 Competitive Reactions.* Journal of Molecular Catalysis a-Chemical, 1995. **103**(3): p. 175-180.

130. Doornkamp, C. and V. Ponec, *The universal character of the Mars and Van Krevelen mechanism.* Journal of Molecular Catalysis a-Chemical, 2000. **162**(1-2): p. 19-32.

131. Randery, S.D., J.S. Warren, and K.M. Dooley, *Cerium oxide-based catalysts for production of ketones by acid condensation.* Applied Catalysis a-General, 2002. **226**(1-2): p. 265-280.

132. Kikhtyanin, O., et al., *Aldol condensation of furfural and acetone on zeolites.* Catalysis Today, 2014. **227**: p. 154-162.

133. Xing, R., et al., *Production of jet and diesel fuel range alkanes from waste hemicellulose-derived aqueous solutions.* Green Chemistry, 2010. **12**(11): p. 1933-1946.

134. Salvapati, G.S., K.V. Ramanamurty, and M. Janardanarao, *Selective Catalytic Self-Condensation of Acetone.* Journal of Molecular Catalysis, 1989. **54**(1): p. 9-30.

135. Lewis, J.D., S. van de Vyver, and Y. Roman-Leshkov, *Acid-base pairs in lewis acidc zeolites promote direct aldol reactions by soft enolization.* Angewandte Chemie-International Edition, 2015. **2015**(54): p. 9835-9838.

136. Choudary, B.M., et al., *Knoevenagel and aldol condensations catalysed by a new diamino-functionalised mesoporous material.* Journal of Molecular Catalysis a-Chemical, 1999. **142**(3): p. 361-365.

137. West, R.M., et al., *Carbon-carbon bond formation for biomass-derived furfurals and ketones by aldol condensation in a biphasic system.* Journal of Molecular Catalysis a-Chemical, 2008. **296**(1-2): p. 18-27.

138. Shen, W.Q., et al., *Liquid phase aldol condensation reactions with MgO-ZrO2 and shape-selective nitrogen-substituted NaY.* Applied Catalysis a-General, 2011. **392**(1-2): p. 57-68.

139. Nie, L. and D.E. Resasco, *Improving carbon retention in biomass conversion by alkylation of phenolics with small oxygenates.* Applied Catalysis a-General, 2012. **447**: p. 14-21.

140. Zhao, C., D.M. Camaioni, and J.A. Lercher, *Selective catalytic hydroalkylation and deoxygenation of substituted phenols to bicycloalkanes.* Journal of Catalysis, 2012. **288**: p. 92-103.

141. Xu, W., et al., *Zeolite topology effects in the alkylation of phenol with propylene.* Applied Catalysis a-General, 2013. **459**: p. 114-120.

142. Corma, A., V. Martinez-Soria, and E. Schnoeveld, *Alkylation of benzene with short-chain olefins over MCM-22 zeolite: Catalytic behaviour and kinetic mechanism.* Journal of Catalysis, 2000. **192**(1): p. 163-173.

143. Li, G.Y., et al., *Synthesis of renewable diesel with hydroxyacetone and 2-methyl-furan.* Chemical Communications, 2013. **49**(51): p. 5727-5729.

144. Sartori, G. and R. Maggi, *Update 1 of: Use of Solid Catalysts in Friedel Crafts Acylation Reactions.* Chemical Reviews, 2011. **111**: p. Pr181-Pr214.

145. Chiche, B., et al., *Friedel-Crafts Acylation of Toluene and Para-Xylene with Carboxylic-Acids Catalyzed by Zeolites.* Journal of Organic Chemistry, 1986. **51**(11): p. 2128-2130.

146. Besson, M. and P. Gallezot, *Selective oxidation of alcohols and aldehydes on metal catalysts.* Catalysis Today, 2000. **57**(1-2): p. 127-141.

147. Wenkin, M., et al., *The role of bismuth as promoter in Pd-Bi catalysts for the selective oxidation of glucose to gluconate.* Journal of Molecular Catalysis a-Chemical, 2002. **180**(1-2): p. 141-159.

148. Kroger, M., U. Prusse, and K.D. Vorlop, *A new approach for the production of 2,5-furandicarboxylic acid by in situ oxidation of 5-hydroxymethylfurfural starting from fructose.* Topics in Catalysis, 2000. **13**(3): p. 237-242.

149. Pasini, T., et al., *Selective oxidation of 5-hydroxymethyl-2-furfural using supported gold-copper nanoparticles.* Green Chemistry, 2011. **13**(8): p. 2091-2099.

150. Sanna, A., T.P. Vispute, and G.W. Huber, *Hydrodeoxygenation of the aqueous fraction of bio-oil with Ru/C and Pt/C catalysts.* Applied Catalysis B-Environmental, 2015. **165**: p. 446-456.

151. Mercader, F.D., et al., *Hydrodeoxygenation of pyrolysis oil fractions: process understanding and quality assessment through co-processing in refinery units.* Energy & Environmental Science, 2011. **4**(3): p. 985-997.

152. Saidi, M., et al., *Upgrading of lignin-derived bio-oils by catalytic hydrodeoxygenation.* Energy & Environmental Science, 2014. **7**(1): p. 103-129.

153. Sutton, A.D., et al., *The hydrodeoxygenation of bioderived furans into alkanes.* Nature Chemistry, 2013. **5**(5): p. 428-432.

154. Zhao, C., et al., *Aqueous-phase hydrodeoxygenation of bio-derived phenols to cycloalkanes.* Journal of Catalysis, 2011. **280**(1): p. 8-16.

155. Zhao, C., et al., *Hydrodeoxygenation of bio-derived phenols to hydrocarbons using RANEY (R) Ni and Nafion/SiO2 catalysts.* Chemical Communications, 2010. **46**(3): p. 412-414.

156. Hong, D.Y., et al., *Hydrodeoxygenation and coupling of aqueous phenolics over bifunctional zeolite-supported metal catalysts.* Chemical Communications, 2010. **46**(7): p. 1038-1040.

157. Brewer, C.E., et al., *Characterization of Biochar from Fast Pyrolysis and Gasification Systems.* Environmental Progress & Sustainable Energy, 2009. **28**(3): p. 386-396.

158. Sternberg, J.C., W.S. Gallaway, and D.T. Jones, *The mechanism of response of flame ionization detectors.* Gas chromatography, 1962: p. 231-267.

159. Dietz, W., *Response factors for gas chromatographic analyses.* Journal of Chromatographic Science, 1967. **5**(2): p. 68-71.

160. Meier, D., A. Oasmaa, and G. Peacocke, *Properties of fast pyrolysis liquids: status of test methods*, in *Developments in Thermochemical Biomass Conversion*. 1997, Springer. p. 391-408.

161. Katritzky, A.R., et al., *Prediction of gas chromatographic retention times and response factors using a general qualitative structure-property relationships Treatment.* Analytical Chemistry, 1994. **66**(11): p. 1799-1807.

162. Dutta, A., et al., *Process design and economics for conversion of lignocellulosic biomass to ethanol: Thermochemical pathway by indirect gasification and mixed alcohol synthesis*, N.R.E. Laboratory, Editor. 2011: Golden, CO.

163. Jones, S., et al., *Process design and economics for the conversion of lignocellulosic biomass to hydrocarbon fuels: Fast pyrolysis and hydrotreating bio-oil pathway*, N.R.E.L.P.N.N. Laboratory, Editor. 2013: Richland, WA.

164. Wright, M.M., et al., *Techno-economic analysis of biomass fast pyrolysis to transportation fuels*, N.R.E. Laboratory, Editor. 2010: Golden, CO.

165. Vispute, T.P. and G.W. Huber, *Production of hydrogen, alkanes and polyols by aqueous phase processing of wood-derived pyrolysis oils.* Green Chemistry, 2009. **11**(9): p. 1433-1445.

166. Shankar Tumuluru, J., et al., *REVIEW: A review on biomass torrefaction process and product properties for energy applications.* Industrial Biotechnology, 2011. **7**(5): p. 384-401.

167. Van der Stelt, M., et al., *Biomass upgrading by torrefaction for the production of biofuels: a review.* Biomass and bioenergy, 2011. **35**(9): p. 3748-3762.

168. Zhu, Y.L., et al., *A new strategy for the efficient synthesis of 2-methylfuran and gamma-butyrolactone.* New Journal of Chemistry, 2003. **27**(2): p. 208-210.

169. Yang, J., et al., *Effects of calcination temperature on performance of Cu-Zn-Al catalyst for synthesizing gamma-butyrolactone and 2-methylfuran through the coupling of dehydrogenation and hydrogenation.* Catalysis Communications, 2004. **5**(9): p. 505-510.

170. Zheng, H.Y., et al., *Synthesis of gamma-butyrolactone and 2-methylfuran through the coupling of dehydrogenation and hydrogenation over copper-chromite catalyst.* Reaction Kinetics and Catalysis Letters, 2004. **82**(2): p. 263-269.

171. Kijenski, J., et al., *Platinum deposited on monolayer supports in selective hydrogenation of furfural to furfuryl alcohol.* Applied Catalysis a-General, 2002. **233**(1-2): p. 171-182.

172. Yang, Y.L., et al., *Conversion of furfural into cyclopentanone over Ni-Cu bimetallic catalysts.* Green Chemistry, 2013. **15**(7): p. 1932-1940.

173. Hronec, M., K. Fulajtarova, and T. Liptaj, *Effect of catalyst and solvent on the furan ring rearrangement to cyclopentanone.* Applied Catalysis a-General, 2012. **437**: p. 104-111.

174. Hronec, M., K. Fulajtarova, and T. Sotak, *Highly selective rearrangement of furfuryl alcohol to cyclopentanone.* Applied Catalysis B-Environmental, 2014. **154**: p. 294-300.

175. Zheng, H.Y., et al., *Towards understanding the reaction pathway in vapour phase hydrogenation of furfural to 2-methylfuran.* Journal of Molecular Catalysis a-Chemical, 2006. **246**(1-2): p. 18-23.

176. Scholz, D., C. Aellig, and I. Hermans, *Catalytic Transfer Hydrogenation/Hydrogenolysis for Reductive Upgrading of Furfural and 5-(Hydroxymethyl)furfural.* Chemsuschem, 2014. **7**(1): p. 268-275.

177. Komaya, T., et al., *Effects of Dispersion and Metal-Metal Oxide Interactions on Fischer-Tropsch Synthesis over Ru/Tio2 and Tio2-Promoted Ru/Sio2.* Journal of Catalysis, 1994. **150**(2): p. 400-406.

178. Resasco, D.E. and G.L. Haller, *A Model of Metal-Oxide Support Interaction for Rh on Tio2.* Journal of Catalysis, 1983. **82**(2): p. 279-288.

179. Avery, N.R., *Eels Identification of the Adsorbed Species from Acetone Adsorption on Pt(111).* Surface Science, 1983. **125**(3): p. 771-786.

180. Shekhar, R., et al., *Adsorption and reaction of aldehydes on Pd surfaces.* Journal of Physical Chemistry B, 1997. **101**(40): p. 7939-7951.

181. Davis, J.L. and M.A. Barteau, *Polymerization and Decarbonylation Reactions of Aldehydes on the Pd(111) Surface.* Journal of the American Chemical Society, 1989. **111**(5): p. 1782-1792.

182. Omotoso, T.O., Baek, B., Grabow, L. C., Crossley, S. P. , *Mechanism and Active sites for conversion of M-cresol over Ru/TiO2: An Experimental and DFT Study.* ACS Catalysis, 2014.

183. Selvaraj, V., M. Vinoba, and M. Alagar, *Electrocatalytic oxidation of ethylene glycol on Pt and Pt-Ru nanoparticles modified multi-walled carbon nanotubes.* J Colloid Interface Sci, 2008. **322**(2): p. 537-44.

184. Iwasita, T., *Electrocatalysis of methanol oxidation.* Electrochimica Acta 2002. **47**: p. 3663-3674.

185. Jiang, J. and A. Kucernak, *Electrooxidation of small organic molecules on mesoporous precious metal catalysts.* Journal of Electroanalytical Chemistry, 2003. **543**(2): p. 187-199.

Appendix A: Journal Submission to *Energy Technology*

Journal article submitted to *Energy Technology* March 2016. Responsible for torrefaction yields by pyroprobe analysis. Also added a small section on the importance of furfural conversion to methyl furan or furan for acylation and hydroxyl alkylation reactions.

Process Synthesis for Biomass Thermal Fractionation and Catalytic Upgrading to Fuels

Jeffrey A. Herron[1], Tyler Vann[2], Nhung Duong[2], Daniel E. Resasco[2],,Steven Crossley[2], Christos T. Maravelias[1*]

[1] Department of Chemical & Biological Engineering, University of Wisconsin – Madison, Madison, WI, 53706, USA

[2] School of Chemical, Biological and Materials Engineering, and, Center for Interfacial Reaction Engineering (CIRE), University of Oklahoma, Norman, OK, 73019, USA

[*] Corresponding author: Tel.: +1 608 265 9026; Fax: +1 608 262 5494.
E-mail address: maravelias@wisc.edu

Abstract. Multi-stage thermal decomposition (fractionation) of biomass with catalytic upgrading is one promising method of achieving sustainable fuels production. Though, the choice of the number of thermal decomposition stages, their conditions, and the optimal catalytic upgrading chemistries is not known. Here, using conceptual process modeling, we propose a general, systematic roadmap for the design of a biorefinery employing these technologies. The overall process considered includes a biomass pre-treatment system, a (multi-stage) thermal decomposition system where the biomass in decomposed into various fractions, a fraction upgrading system, and a combustion system. We focus primarily on the design of the thermal decomposition and fraction upgrading systems. The goal of our work is in demonstrating the key trade-offs between various process options and to identify important areas for improvement; not to perform detailed techno-economic assessment of a

particular process. In particular, we show that there are diminishing returns on the increase in product yield versus the complexity of the catalytic upgrading sequences. The choice of the number of thermal decomposition stages is not simple, requiring careful consideration of the chemistries available to upgrade different components and the relative abundances of these different components. Therefore, the optimal design of the thermal decomposition and fraction upgrading systems cannot be done independently.

1. Introduction

Biomass presents a promising source for sustainable liquid fuels production. There are three principle routes for converting biomass into liquid fuels, classified by the initial treatment of the biomass: gasification, hydrolysis, or pyrolysis and liquefaction.[81, 110, 111] The pyrolysis route involves thermal decomposition of the biomass at high temperature (500-800°C), and it has demonstrated high yields. Unfortunately, the wide range of components in the resulting pyrolysis vapor (oil) make it unstable, corrosive, and challenging to catalytically upgrade.[112] Furthermore, the high content of light (<C6) oxygenates in the pyrolysis are unsuitable for liquid fuels and are therefore of limited utility. Multi-stage torrefaction[113-115] of biomass with catalytic upgrading presents a promising method of overcoming these challenges.[55] Importantly, the decomposition of the biomass over several stages can reduce the number of product species within each *fraction*, allowing oneto mold the catalytic upgrading strategy to target a subset of the chemical functionalities.

Though the a staged thermal decomposition of biomass coupled with targeted upgrading has a number of advantages over a single stage pyrolysis with hydro-treating, there are

many unknowns regarding the best way to design such a system. Importantly, the optimization of the number and conditions of each thermal decomposition stage is a complex problem that cannot be solved without knowing the resulting influence on the final yields and process complexity resulting from the subsequent catalytic upgrading. Furthermore, there are a wide variety of chemistries[2, 56, 81, 116] available to perform upgrading. In addition to the chemistries, the reaction sequence must also be configured to optimize the overall process. In order to improve the impact of such an approach, one must also determine if general practices from this strategy may be applicable to different types of biomass feeds. In this work, we conceptualize a biorefinery that is based on multi-stage torrefaction of biomass with catalytic upgrading. The ultimate goal of this work is to design a broad roadmap that can be used to identify the key parameters and trade-offs; not to conduct a detailed techno-economic analysis of specific process configurations.[117-119] Importantly, we optimize both the number of torrefaction stages and the specific chemistries used to upgrade the thermal decomposition fractions in order to maximize the yield of fuel-grade product, while minimizing costs. We begin with a general description of the biomass to fuels plant and discuss the different configurations and options available in its design. Then, we highlight key chemistries from the literature that can be used to upgrade the torrefaction vapors and assess their merits. Finally, we describe several upgrading strategies that have been designed based on experimental torrefaction yields.[120] The detailed techno-economic analysis, focusing on a narrower design space will be the subject of future work.

2. General torrefaction-based biorefinery

The general torrefaction-based biorefinery (see Figure 444) consists of four main systems. In the first system, denoted Biomass Pre-treatment, the raw biomass is dried and ground into small particles. The dried, ground biomass is sent to a Thermal Decomposition system, which includes n sequential torrefaction stages, where the residual biomass from each torrefaction stage serves as input for the subsequent torrefaction stage. These torrefaction stages are followed by a final high-temperature pyrolysis stage. Therefore there are a total of $n + 1$ thermal decomposition stages. The temperature (T_i) of each stage, i, is different, with the temperature increasing with each subsequent stage ($T_i < T_{i+1}$). The residual char from the pyrolysis is sent to a Char Combustion system, which burns the char to provide process utilities for the rest of the plant. The vapor "fraction" that results from each of the torrefaction and pyrolysis stages is sent to the Fraction Upgrading system for catalytic upgrading to remove oxygen and improve the yield of higher hydrocarbons. Each fraction will be upgraded in a uniquely tailored process. The fraction from the first torrefaction stage is sent to the "F_1-System", while the fraction from the second torrefaction stage is sent to a "F_2-System" sub-system, and so forth. The pyrolysis fraction is upgraded in the "F_{n+1}-System."

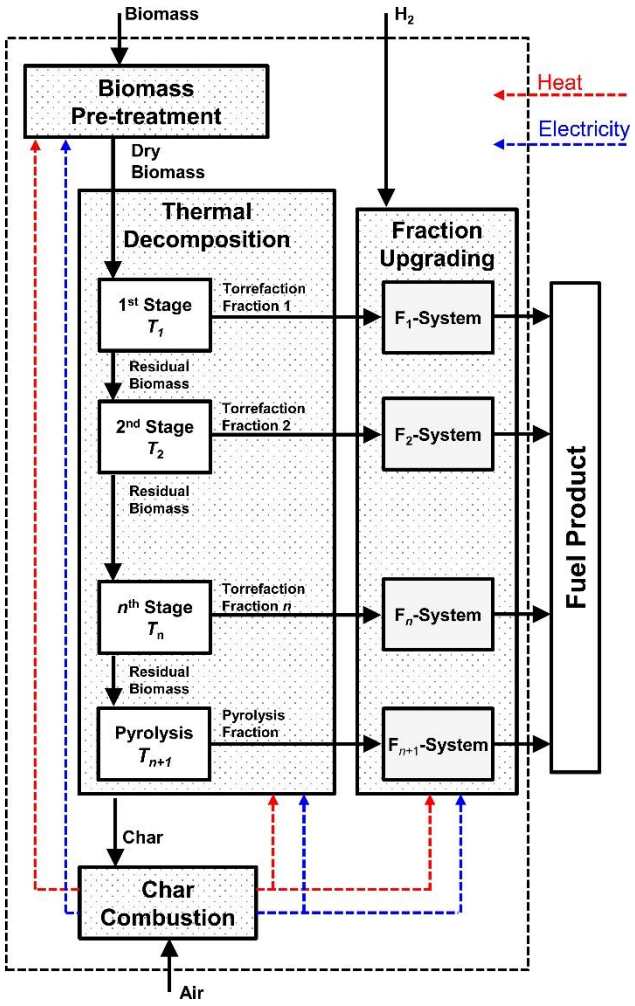

Figure 44. Block flow diagram for general process.

In this work, we describe the key decisions and trade-offs that are made in designing the torrefaction-based biorefinery. The overall goal of the design is to maximize carbon yield, while minimizing operating and capital costs. We will not be evaluating costs explicitly in this conceptual analysis, but we gauge the relative capital costs by the complexity of the processes and we evaluate hydrogen consumption as one measure of the operating costs. To quantify the *carbon yield* of the process, we calculate the total carbon in the product that is in hydrocarbons with carbon numbers between 6 and 21 (gasoline, diesel

and jet fuel range) and divide this number by the total carbon entering the process. Hereafter, the term *carbon yield* will explicitly be referring to this definition.

We focus our analysis on the Thermal Decomposition and Fraction Upgrading systems. We assume that the Biomass Pre-treatment and Char Combustion systems are designed for a given biomass input basis and that they will not differ significantly with changes in either the Thermal Decomposition or the Fraction Upgrading systems. Though, we note that their design may change with the source of biomass (switchgrass, woody biomass, etc.) used as a feed.

2.1.Thermal Decomposition System

The two main variables in designing the Thermal Decomposition System are 1) the number, n, of torrefaction stages, and 2) the temperature of each stage, T_i. Generally, from an economic perspective, the capital cost should be minimized with the fewest number of stages. Though, the subsequent upgrading may be more difficult and costly. Therefore, there are trade-offs between the complexity of the Thermal Decomposition System versus that of the Fraction Upgrading System.

Lignocellulosic biomass has three main components: cellulose, hemicellulose, and lignin; the concentration of each of these components varies with the source of the biomass.[2, 121] Since there are three biomass components, one might suggest three thermal decomposition stages, where one of these biomass constituents would decompose in each stage. This would seem ideal because the Fraction Upgrading System could be designed to upgrade the decomposition vapor of each of these components, and the design would

be applicable for different biomass feeds (though re-sized as needed to account for differences in the cellulose, hemicellulose and lignin composition).

Unfortunately, experimental results have demonstrated overlap in the decomposition temperatures of these three components, especially for lignin, which decomposes over a broad temperature range.[122-125] Still, even if the decomposition of each component could be isolated, there is no guarantee that this would yield the optimal process. Critically, one must consider the products of the decomposition reactions and the chemistries available to upgrade those products.

Decomposition products

The thermal decomposition of lignocellulosic biomass has been studied in detail and reviewed elsewhere.[2, 4] Here, we provide a brief summary of the decomposition temperatures and representative products (see Table 4). Of the three main biomass components, hemicellulose tends to decompose at the lowest temperature, between 200-260°C.[4] Typical products include light acids (e.g. acetic acid), esters, ketones, and other oxygenates (e.g. acetol).[2, 4] The decomposition of cellulose occurs between 240-350°C.[4] Principal products include levoglucosan, anhydrocellulose, furanics (e.g. furan, furfural) and pyrans.[2, 4, 126] Lignin is a polyphenolic substance which decomposes between 280-500°C.[4] Its decomposition yields phenolic compounds (e.g. guaiacol, cresol) as well as light oxygenates such as methanol, acetic acid, and acetone.[2, 4]

Table 4. Decomposition temperature and representative decomposition products for hemicellulose, cellulose and lignin.

Biomass component	Decomposition temperature (°C)	Representative products
Hemicellulose	200-260	Acetic acid, acetol
Cellulose	240-350	Furan, furfural, levoglucosan
Lignin	280-500	Cresol, guaiacol

2.2. Fraction Upgrading System

The goal of the Fraction Upgrading System is to 1) couple low carbon number species into fuel-range carbon number species and 2) remove oxygen. Both of these goals are accomplished through catalytic conversion.

The Fraction Upgrading System has the most variables in its design. One can choose the number/types of chemistries employed, and in what order to perform those chemistries. Furthermore, one can include separations in order to isolate components for specific upgrading chemistries. In the ideal case, the fractions exiting the Thermal Decomposition System would be chemically distinct and one could envision distinct upgrading strategies for each fraction. Multiple strategies could be considered for upgrading each fraction and the optimal could be identified by rigorous techno-economic analysis. Importantly, one must consider the trade-offs between improved carbon yield in the product against additional capital (and operating) costs associated with increased complexity of this system.

Chemistries

The goal of our work is develop strategies to maximize the carbon yield of fuel-range product. As such, we must take advantage of a number of different upgrading chemistries that have been developed. Recent articles have reviewed some of these strategies,[3, 55,

116] and we briefly highlight key chemistries. Since the torrefaction and pyrolysis fractions have a wide array of unique chemical species, it is generally of interest to select chemistries which have wide applicability.

Carbon-carbon coupling: The first set of reactions that we consider are for carbon-carbon coupling. In order to maximize the yield of fuel-range product, the light hydrocarbons must be coupled or integrated into larger hydrocarbons. Here, we summarize promising chemistries to achieve this coupling.

Ketonization of carboxylic acids (see Scheme 3) is one of the major chemistries considered.[20, 22, 127] In the ketonization reaction, two carboxylic acids are coupled, releasing a single molecule of H_2O and CO_2 in the process. This provides a method of coupling low carbon number species into higher carbon number species. Unfortunately, due to the formation of CO_2, the carbon yield of the reaction is affected. For ketonization between two acetic acid molecules, the only 75% of the carbon is maintained in the acetone product. Typical catalysts for ketonization include metal oxides[128-131] (TiO_2, ZrO_2, CeO_2) and metal oxides with precious metals (Ru/TiO_2).[21]

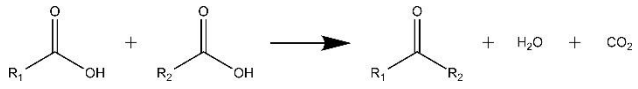

Scheme 3. General ketonization reaction.

Aldol condensation (see Scheme 4) presents a second promising chemistry for the coupling of low carbon number species. In aldol condensation, two carbonyl compounds are coupled to form a β-hydroxyketone, which is dehydrated to yield an enone.[24, 132-135] Unlike ketonization, no carbon is lost during the reaction. The reaction is base-

catalyzed, and a number of solid bases have been explored for the reaction.[132, 136-138]

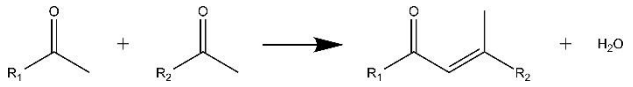

Scheme 4. General aldol condensation chemistry.

Alkylation[15, 139-142], hydroxy alkylation[143], and acylation[144, 145] (see Scheme 5) are chemistries for carbon-carbon coupling of alcohols, ketones, and carboxlyic acids, respectively, with aromatic compounds and furanics. These present attractive methods for incorporating the light oxygenated species into higher hydrocarbons. No carbon is lost during these reactions. These reactions are typically acid-catalyzed, with various zeolites having been employed as catalysts.

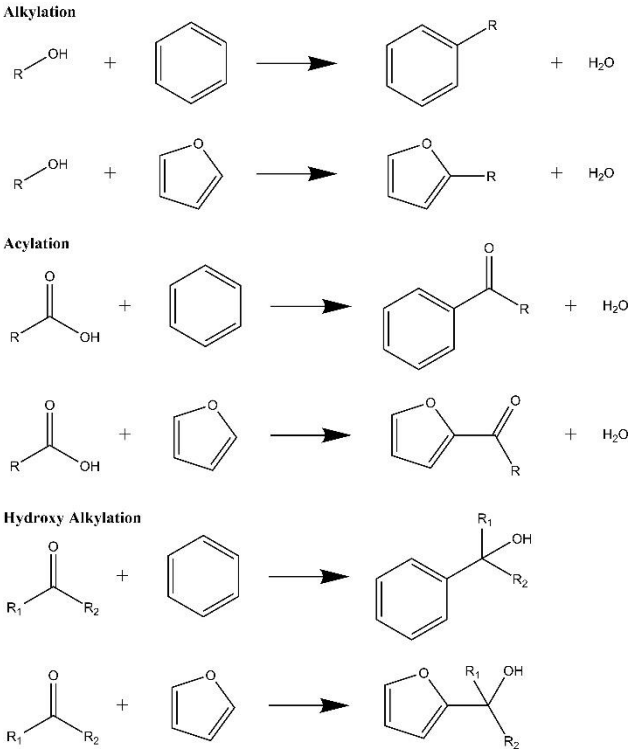

Scheme 5. General alkylation, acylation and hydroxy alkylation chemistries.

Other chemistries: In this section, we highlight some other important chemistries that are intermediate steps for carbon-carbon coupling or for the final preparation of the fuel.

Oxidation (see Scheme 6) of alcohols, aldehydes and sugar-derivatives to carboxylic acids presents a source of acids for further ketonization.[146-149] Oxidation has typically been performed over Pt and Pd catalysts. The hydrolysis of levoglucosan with solid acid Amberlyst-15, followed by oxidation in air to gluconic acid has been demonstrated over Pd/C.[52] One noteworthy disadvantage of oxidation is that it increases the oxygen content, which must subsequently be removed to form hydrocarbon products. Therefore, oxidation will generally increase the hydrogen consumption of the process.

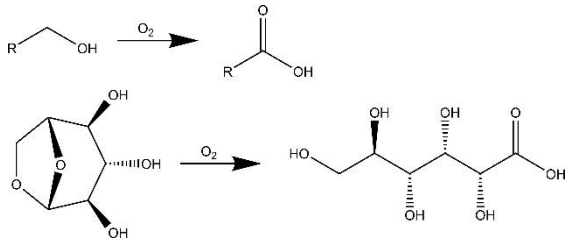

Scheme 6. Two example oxidation events. Levoglucosan oxidizes to gluconic acid.

Hydrogenation (see Scheme 7) of ketones and aldehydes to alcohols provides a method of generating alkylating species. The selective hydrogenation of such species, in the presence of aromatics, has been demonstrated on Cu/SiO_2 and $Pt\text{-}Fe/SiO_2$ catalysts.[139] Hydrogenation of levoglucosan over a Ru/C catalyst yields sorbitol and C2-C4 diols.[150]

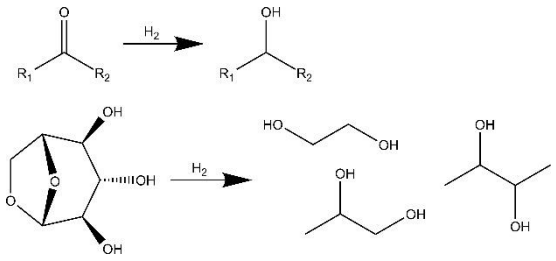

Scheme 7. Two example hydrogenation events. Levoglucosan hydrogenates to various C2-C4 diols.

Hydrodeoxygenation (HDO) is the ultimate step in fuel production.[151-153] In this reaction, the oxygen-functionalities in the oxygenated hydrocarbons are removed as water either by C-O hydrogenolysis or by dehydration followed by hydrogenation. The hydrodeoxygenation of phenolic compounds has been shown over bifunctional catalysts, featuring a noble metal (Pt, Pd, Ru) with a solid-acid.[16, 69, 154-156] Importantly, as many of the carbon-carbon coupling reactions require these oxygen functionalities, the HDO should be performed after upgrading the carbon number of the product.

Oxygen removal and hydrogen consumption

Oxygen is removed from the system through two main products: water (H_2O) and carbon dioxide (CO_2). In order to maximize carbon yield, oxygen should be removed as H_2O. However, choosing to remove oxygen as H_2O comes with an increased consumption rate of hydrogen. Therefore, there exists a trade-off between carbon yield and hydrogen consumption. We note that industrially hydrogen is produced by steam reforming of natural gas ($CH_4 + H_2O \rightarrow CO + 3H_2$) and water-gas shift ($CO + H_2O \rightarrow CO_2 + H_2$). As a result, the production of CO_2 cannot be avoided, unless the hydrogen were produced renewably. Though, this does not mean that the choice is irrelevant, careful consideration of the process economics will yield the final decision.

It is noteworthy that carbon-carbon coupling has the added benefit of lowering hydrogen consumption in the process because the H/C molar ratio decreases with increasing carbon chain length (H/C = 4 for methane and only 2.33 for hexane). Consider the hypothetical upgrading of acetone through two routes. In the first route, acetone (C_3H_6O) is merely hydrodeoxygenated to propane (C_3H_8).

$$2C_3H_6O + 4H_2 \rightarrow 2C_3H_8 + 2H_2O$$

The process consumes 2 moles of hydrogen per mole of acetone. In the second route, acetone is first converted to 2-methyl-2-penten-4-one ($C_6H_{10}O$) by self-condensation and then hydrodeoxygenated to hexane (C_6H_{14}).

$$2C_3H_6O \rightarrow C_6H_{10} + H_2O$$

$$C_6H_{10}O + 3H_2 \rightarrow C_6H_{14} + H_2O$$

This second route consumes only 1.5 moles of hydrogen per mole of acetone. Additionally, the carbon number is now in the liquid transportation fuel range, improving the carbon yield. Though, the number of upgrading steps (reactors) also increased from one to two.

This simple example illustrates that the process choices are complicated. Improving carbon yield is generally associated with increased process complexity, leading to higher capital costs. However, the hydrogen consumption can both increase with improved carbon yield due to oxygen removal as H_2O and also decrease with improved carbon yield by carbon-carbon coupling.

3. Methods

The conceptual processes are designed based on some simplifying assumptions of the torrefaction/pyrolysis fractions as well as the chemistries employed. The composition of the torrefaction/pyrolysis fractions are based on experimental yields using oak as a feedstock.[120] Representative compounds were selected to model the wide variety of different species that are present in these fractions (see Table 4): acetic acid, acetol, furan, furfural, levoglucosan, toluene, guaiacol, cresol, CO_2 and char. The elemental composition of woody biomass char is taken from a past study, in which the carbon content of the char was found to be 65 wt%.[157] The chemistries suggested in the conceptual processes are based on literature studies, though we note that most of these studies were done on model/representative compounds and not on real torrefaction/pyrolysis streams. We will generally assume that the chemistries will still work, unless there is evidence to suggest that they would not. Reaction yields and separations are idealized, based on the assumption that catalysts, reaction conditions, and the separations have been optimized. The processes are modeled assuming a 23.15 kg s^{-1} (2000 MT day^{-1}) dry biomass consumption rate.

Table 5. Yields in mass percentage for a 3-stage torrefaction process. Yields provided by Ref [120]

	3-Stage Torrefaction Process			
Species	1st Stage (270°C)	2nd Stage (360°C)	Pyrolysis (500°C)	Total
H_2O	10.1	6.8	0.0	16.9
Acetic Acid	6.9	1.9	0.5	9.3
Acetol	3.1	1.9	1.8	6.8
Furan	0.0	0.2	0.1	0.3
Furfural	1.4	4.1	0.7	6.2
Levoglucosan	0.2	7.6	4.8	12.6
Toluene	0.0	0.8	0.3	1.1
Guaiacol	1.8	2.1	1.5	5.4
Cresol	0.0	1.2	0.5	1.7
CO_2	7.2	8.5	11.5	27.2
Char	0.0	0.0	12.5	12.5
Total	30.7	35.1	34.2	100.0

In Table 5, we show the experimental torrefaction and pyrolysis yields derived from a 3-stage torrefaction process.[120] The 3-stage torrefaction process features a 1st Stage torrefaction at 270°C for 20 minutes, a 2nd Stage torrefaction at 360°C for 5 minutes and a final pyrolysis at 500°C for 1 minute. Yields were obtained from thermal treatment of 0.7-0.9 mg of raw oak, Stage 1 and Stage 2 residue in a CDS Analytical pyroprobe Model 5250. The resultant vapors were analyzed online by use of a Shimadzu QP2010 GC-MS/FID with a 60 m x 0.25 mm RTX-1701 column. For analysis of the 1st Stage and 2nd Stage torrefaction a cryogenic sorbent trap held at -50°C was used to adsorb the vapor products. This trap was then heated to 300°C for 3 minutes for desorption of the products to the GC-MS/FID. For analysis of the vapor MS is used for identification of the compounds, while FID is used for quantification of them. In order to quantify, the response factor (RF), which is the ratio between amount of the compound injected and the area of FID signal, need to be determined. RF can be obtained from experimental

calibrations of model compound injections. However, due to the large number of components, with many of them unstable and not commercially available, it is impossible to get all of the needed RFs from model compound injections. Therefore, a model to predict RF of a molecule based on its structure was developed. Sternberg et al. introduced the concept of Effective Carbon Number[158], which is the number of carbons in the molecule that are effective in producing FID signal.

$$\mathrm{ECN} = 7 * \frac{\frac{\text{area sample}}{\text{area n} - \text{heptane}}}{\frac{\text{mole sample}}{\text{mole n} - \text{heptane}}} = 7 * \frac{\mathrm{RF}_{\text{sample}} * \mathrm{MW}_{\text{sample}}}{\mathrm{RF}_{\text{n-heptane}} * 100}$$

ECN is assumed to be 7 for n-heptane. ECN values for all of hydrocarbons, such as alkanes, alkene, aromatics or polycyclic aromatics, are similar to the number to the number of carbon atom in the molecule. Therefore, each carbon atom in hydrocarbon will be counted as 1 for ECN. On the other hand, fully/partially oxidized carbon atom cannot produce FID signal as effective as a normal carbon atom, which connects to carbon or hydrogen only. Depending on the functionality, a fully/partially oxidized carbon atom will have a different ECN value, which is always less than 1.

The ECN value depends only on the structure of the molecule, the model was developed based on the data available in the literature, particularly focus on the typical functionalities in pyrolysis bio-oil, such as alcohols, carbonyls, carboxylic acids, furanics and phenolics[159-161]. The model was validated with our own experimental calibrations of 42 compounds, including typical compounds of light oxygenates, sugar derivatives and phenolics categories.

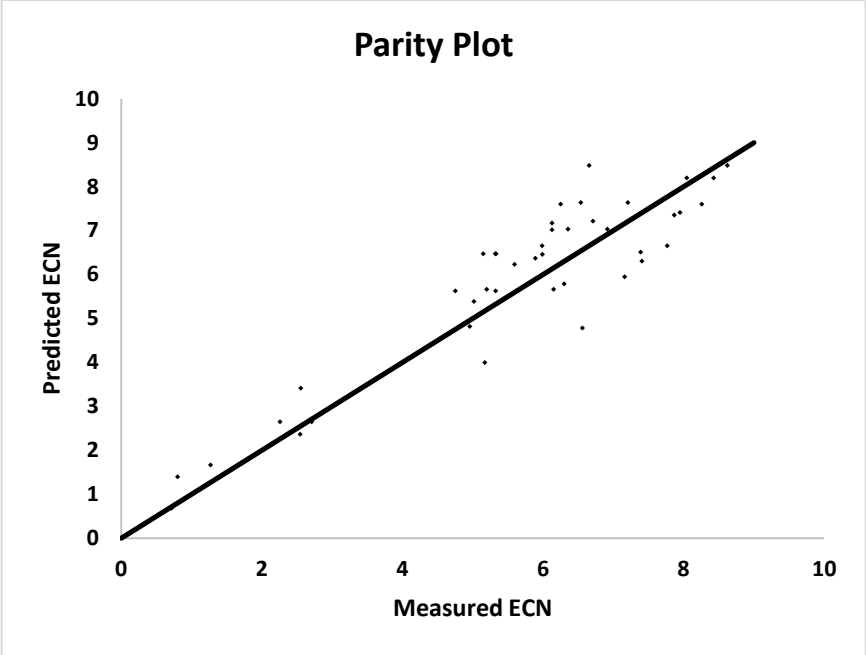

Figure 45: Parity plot between predicted ECN and measured ECN

Thermal treatment of 10-15 grams of the respective solids was completed in parallel on a scaled up reactor setup. 0.7-0.9 mg of solid from the 1st stage torrefaction on the gram scale unit was used as the feedstock for the 2nd stage experiments on the pyroprobe. Similarly, the solid from 2nd stage torrefaction on the gram scale unit was used for the final pyrolysis step in the pyroprobe. It was assumed that both reactors produced similar yields. As such, Karl Fischer titration was carried out on the resultant gram scale liquid product to determine water content. The water yields were then applied to the pyroprobe results to estimate water content. CO_2 yields could then be calculated by difference using weight loss measurements.

In constructing conceptual processes from these results, we will assume that adjacent stages can be combined into a single stage by operating at the highest temperature of the

combined stages. That is, stages 1 and 2 could be combined in a single stage operated at 360°C, all three stages could be combined in a single stage operated at 500°C, or stages 2 and 3 could be combined as a single stage operated at 500°C. However, stages 1 and 3 could not be combined without including stage 2. This assumption is motivated by experimental yields of a 1-stage pyrolysis process at 500°C (see SI) that shows reasonably close yields as that of combining the yields of all three stages of the 3-stage process.[120]

Previous ultimate analysis of woody biomass feedstock have found approximately 51 wt% carbon.[162, 163] Assuming that the carbon content of the char is 65 wt%,[157] our mass balance (and assumed representative compounds) only captures 79% of the carbon content of the literature value for woody biomass. This carbon imbalance may be due to several factors, such as the choice of overly-oxygenated representative compounds, differences in the original biomass feed stock versus the literature material, and the extent of drying prior to pyrolysis. For these reasons, we will quote all carbon yields versus the carbon content in the experimental fractions[120] shown in Table 5, assuming 65 wt% carbon in the char.

4. Process Design Philosophy

In the previous sections, we outlined the general torrefaction plant, summarized the key process options that must be considered, provided a brief review of the species involved in the process, and highlighted chemistries that have shown promise for catalytically upgrading these species. In this section, we describe our philosophy on using this information to guide the design of a torrefaction plant.

4.1. General Considerations

As mentioned in the previous sections, the main goal of our design is to maximize the carbon yield while minimizing the capital and operating costs of the process. For this conceptual analysis, the complexity will be estimated by the total number of discrete reaction operations. The only operating cost considered will be hydrogen consumption. Though, we note that due to the high temperatures required for thermal decomposition, heating/cooling costs may be substantial and the process economics will likely benefit significantly from careful heat integration.

The process design begins with an assessment of the thermal decomposition product. The first key questions to answer are:

- What chemical species/functionalities exist in the product and what chemistries/pathways are available to upgrade those species to a fuel range product?
- What are the concentrations of these species?
- Are there additional reagents/species that are also required for a particular pathway?
- Are there carbon losses along the pathway?

For example, if one of the species is acetic acid ($C_2H_4O_2$), there are several possible routes to upgrade to a fuel range product. Acetic acid can be used as an acylating agent, though an aromatic, phenolic or furanic must be available to be acylated. An alternative upgrading pathway is to first ketonize acetic acid to acetone (C_3H_6O) and then self-condense to 2-methyl-2-penten-4-one ($C_6H_{10}O$). Here, we do not need an aromatic, phenolic or furanic, but the pathway involves an additional conversion step and carbon is lost during the ketonization step. As another possibility, perhaps one finds that acetic acid

is a very minor component in the thermal decomposition product. Then, the cost of the reactor may not be worth the additional yield from its upgrading. Ultimately, the choice between these two pathways cannot be made without additional information about the abundance of the various species in the thermal decomposition product.

Once viable pathways have been assessed, it is important to consider how other species within the stream may be affected by the proposed pathways – or how the presence of those species may interfere with the proposed pathway. For example, one may wish to oxidize levoglucosan to gluconic acid and then ketonize gluconic acid to yield a C11 species. It is likely that many other components in the stream may also be oxidized to acids. Then, these species will be ketonized along with gluconic acid, and the final product may be much different than originally envisioned.

This brings up the important issue of separations. In the general scheme, the choice of the number of thermal decomposition stages provides the first instance of product separation. Without *a priori* knowledge of the chemical species, their upgrading possibilities, and the ability to isolate these species, one cannot suggest the ideal number of thermal decomposition stages. Furthermore, one may also incorporate additional separations within the upgrading process. In the above example, one may attempt to isolate levoglucosan[52] from the stream in order to upgrade the isolated component.

4.2. Upgrading Routes For Representative Compounds Of Experimental Yield

First, we calculate the molar flow rates of the representative compounds in the different fractions and assess possible C-C coupling routes, as shown in Table 3. We note that the list presented is not exhaustive of the literature nor of the possible routes from the

chemistries considered herein. For example, acetol includes a ketone functionality, which enables it to function as a hydroxy alkylating agent or to be used in aldol condensation. If acetol were oxidized to a carboxylic acid, it could undergo ketonization and then would regain its original ketone functionality. Also, to facilitate the discussion of the various routes, we will use the experimental results in Table 2, but we note that the methods and arguments are applicable to any biomass fractionation and upgrading system.

Assessment of C-C coupling routes

The fractions are composed of light components (< C6) acetic acid, acetol, furan and furfural, which must be C-C coupled in order to include their carbon in the fuel range product. Additionally, as experiments have shown that levoglucosan hydrogenates to C2-C4 alcohols, we must upgrade levoglucosan (at least stabilize versus C-C bond scission, not necessarily C-C coupling) such that its carbon is also included in the fuel product. The other components of the fractions, toluene, guaiacol and cresol are already in the fuel range.

Acetic acid can be C-C coupled through two main pathways. First, it can serve as an acylating agent with furan, furfural, toluene, guaiacol or cresol as acceptors. In the second major pathway, acetic acid is first ketonized to acetone. Then, it can be C-C coupled through aldol condensation, hydroxy alkylation by acting as an agent, or hydrogenated to isopropanol and then serving as an alkylating agent. As the ketonization step has a maximum carbon retention of only 75% (1 mole of CO_2 released per event) and these pathways have more total reaction steps, the acylation route is generally preferred.

Acetol has a variety of options available for its upgrading. The ideal case would be to use it as either an alkylatng or hydroxy alkylating agent, acting on furan, methylfuran, toluene, guaiacol or cresol because it has the fewest number of reaction steps and it should not come with any carbon losses. Alternative routes include oxidation, followed by acylation, or oxidation followed by ketonization and subsequent transformations.

Furan can serve as an acylation, hydroxy alkylation or alkyation acceptor. Alternatively, it can be converted into an alkylating agent by hydrogenation or acylating agent by oxidation. Finally, furan can be oxidized to yield an acid and then be ketonized.

Furfural has similar options as furan once deoxygenated to form methylfuran. One additional pathway, which has received considerable attention in the literature, is aldol condensation of furfural.

Levoglucosan has two principle upgrading routes that we consider. Hydrogenation of levoglucosan yields C2-C4 alcohols, which can serve as alkylating agents. Alternatively, levoglucosan can be oxidized to gluconic acid, which can be hydrodeoxygenated directly to a C6 product, ketonized to a C11 species (at an 8% carbon loss) or act as an acylating agent.

Toluene, Guaiacol, and **Cresol** can be hydrodeoxygenated to C6-C7 species, suitable for the fuel pool without any C-C coupling. However, they present import acceptors for acylating, alkylating, or hydroxy alkylating agents.

Table 6. Molar flow rate of torrefaction and pyrolysis fractions exiting the Thermal Decomposition system. Basis is 23.15 kg s^{-1} dry biomass. Possible C-C coupling routes for these representative compounds are suggested. Routes listed with an ellipsis include steps that are redundant with already presented routes.

	Molar flow rate (kmol s^{-1})				
Species	1st Stage	2nd Stage	Pyrolysis	Total	**C-C Coupling Routes**
Acetic Acid	26.62	7.33	1.93	35.88	Acylation (agent) Ketonization → Aldol condensation Ketonization → Hydroxy Alkylation (agent) Ketonization → Hydrogenation → Alkylation (agent)
Acetol	9.70	5.94	5.63	21.27	Alkylation (agent) Hydroxy Alkylation (agent) Aldol condensation Alkylation (agent) Oxidation → Acylation (agent) Oxidation → Ketonization → ...
Furan	0.00	0.68	0.34	1.02	Acylation (acceptor) Alkylation (acceptor) Hydroxy alkylation (acceptor) Hydrogenation → Alkylation (agent) Oxidation → Acylation (agent) Oxidation → Ketonization → ...
Furfural	3.38	9.89	1.69	14.95	Acylation (acceptor) Aldol condensation Alkylation (acceptor) Hydroxy alkylation (acceptor) Hydrogenation → Alkylation (agent) Oxidation → Acylation (agent) Oxidation → Ketonization → ...
Levoglucosan	0.29	10.86	6.86	18.01	Hydrogenation → Alkylation (agent) Oxidation → Acylation (agent) Oxidation → Ketonization → ...
Toluene	0.00	2.01	0.75	2.77	Acylation (acceptor) Alkylation (acceptor) Hydroxy alkylation (acceptor)
Guaiacol	3.36	3.92	2.80	10.08	Acylation (acceptor) Alkylation (acceptor) Hydroxy alkylation (acceptor)
Cresol	0.00	2.57	1.07	3.64	Acylation (acceptor) Alkylation (acceptor) Hydroxy alkylation (acceptor)

Mass balance considerations

Acetic acid and acetol can serve as acylating and hydroxy alkylating agents, respectively. Combined, there are 57.2 kmol s^{-1} of these two species entering the Fraction Upgrading System. There are 16.0 kmol s^{-1} of furanic acceptors and 16.5 kmol s^{-1} of aromatic/phenolic acceptors. Assuming that the furanics can only be acylated or hydroxy alkylated a single time (due to a limited number of acceptor sites on their 5-member ring, then the aromatics/phenolics must be acylated or alkylated, on average, 2.5 times per molecule to fully incorporate the acetic and acetol into C6+ species. The resulting furanics would be in the C6-C8 range and the aromatics/phenolics would be in the C11-C16 range.

Furanics can be oxidized to acids or hydrogenated to alcohols to serve as acylating or alkylating agents, respectively. If all of the furanics were oxidized, then to use all of these acids and the original acetic acid and acetol, the aromatics/phenolics would need to be acylated or hydroxy alkylated, on average, 4.4 times per molecule. The guaiacol and cresol already have 2 substituents on their aromatic rings and would, in theory, only have 4 sites to be acylated or hydroxy alkylated. Therefore, to fully incorporate the lights into C6+ species, additional upgrading steps would be required. Assuming 4 acylation and hydroxy alkylation events, the aromatics/phenolics would be in the C15-C27 range. Already, some of these species would be beyond the C6-C21 fuel range.

The situation only worsens if levoglucosan is oxidized or hydrogenated, to be used as an acylating or alkylating agent. Therefore, to maximize the carbon yield (C6-C21), one must explore other routes for upgrading levoglucosan and/or the other light components.

5. 1-Stage Thermal Decomposition Processes

First, we consider fraction upgrading strategies based on a single thermal decomposition stage, pyrolysis at 500°C. We consider different Fraction Upgrading scenarios, starting with the simplest design and then increasing complexity. The scenarios are denoted with two numbers, i.e. X-Y, where X is the number of thermal decomposition stages and Y is the total number of upgrading reactors. Block flow diagrams for the 1-stage thermal decomposition processes are shown in Figure 46.

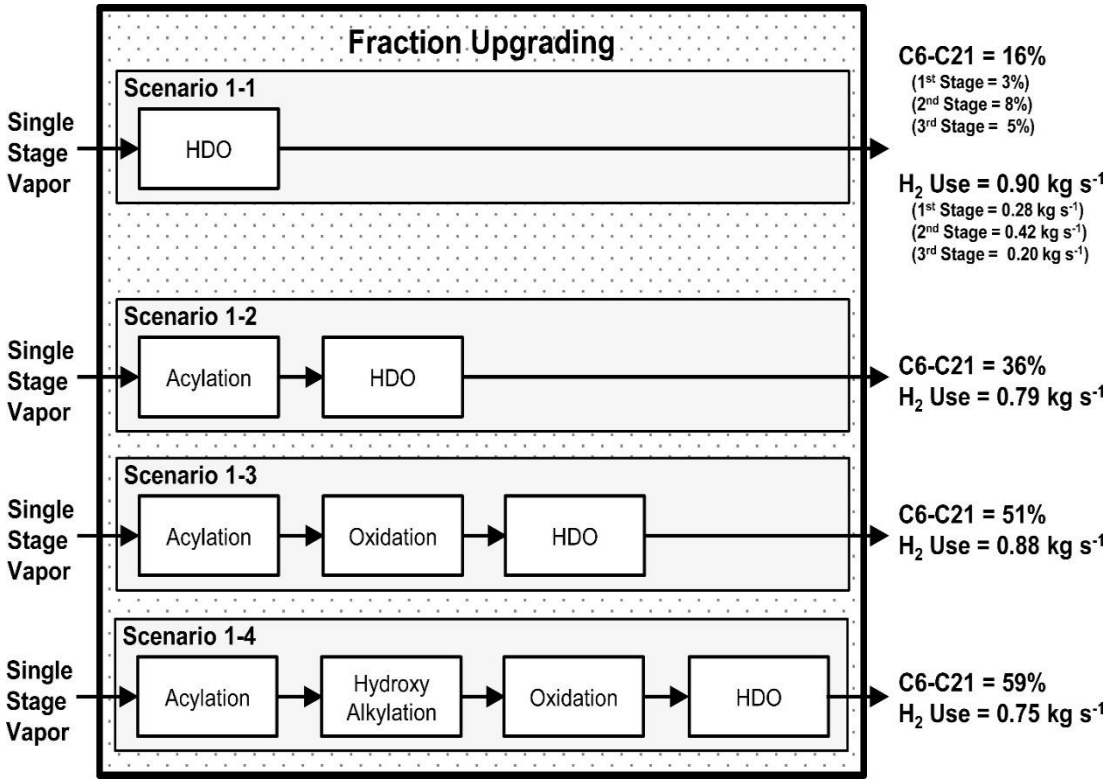

Figure 46**.** Block flow diagram of reactors in Fraction Upgrading system for various scenarios. The thermal decomposition system consists of a single stage, operating at 500°C. The C6-C21 yield and the hydrogen consumption rate are provided for each scenario. For Scenario 1-1, the C6-C21 yield and hydrogen consumption are sub-divided into the equivalent values that would be calculated by assuming that there were three fractions (270°C, 360°C, and 500°).

Scenario 1-1, base-case: The first scenario (1-1) is the base-case. This is analogous to pyrolysis with hydro-treating. The pyrolysis vapor is hydrodeoxygenated to yield the product.

The overall process mass balance is shown in Figure 47. The dry biomass entering the system is 23.15 kg s^{-1}. Assuming that the original biomass has 40 wt% moisture content,[164] the moist biomass entering the system is 38.58 kg s^{-1}. The process also consumes 0.90 kg s^{-1} of hydrogen. The hydrocarbon product includes 4.78 kg s^{-1} or alkanes: ethane, propane, butane, and pentane; and 1.52 kg s^{-1} of aromatics (toluene). The remaining mass leaves the system as H_2O (24.01 kg s-1), CO_2 (6.30 kg s^{-1}) and char (2.89 kg s^{-1}).

The C6-C21 carbon yield is only to 15.6%. Importantly, experimental studies have demonstrated that levoglucosan typically converts into C2-C4 species upon hydro-treating,[74, 165] which is outside the fuel range. Therefore, the only carbon in the product is derived from toluene, guaiacol and cresol. The total hydrogen consumed in the process is 0.90 kg s^{-1} and the total number of reactors is 2 (1 thermal decomposition reactor and 1 hydrodeoxygenation reactor). In the following scenarios, we will always assume that the last step is hydrodeoxygenation, and it will not be explicitly described in the text.

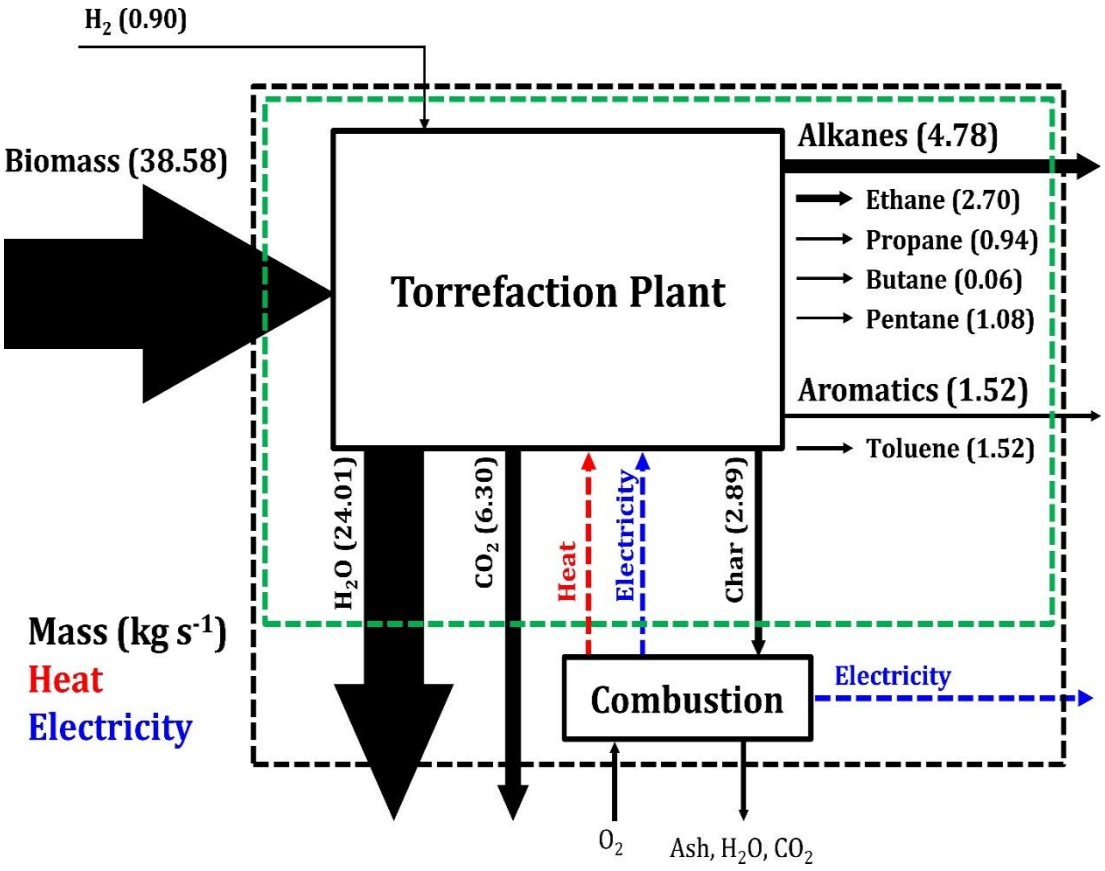

Figure 47**.** Overall mass balance of Scenario 1-1. The total (moist) biomass entering the system is 38.58 kg s^{-1} (dry biomass = 23.15 kg s^{-1}). The width of the arrows (mass flows) are proportional to the mass flow rate.

Table 7. Summary of process alternatives: C6-21 yield, hydrogen consumption, number of thermal decomposition stages (torrefaction + pyrolysis), and number of upgrading reactors.

Process	C6-C21 Yield (%)	H_2 Consumption (kg s^{-1})	Thermal Decomposition stages	Upgrading Reactors
Scenario 1-1	16	0.90	1	1
Scenario 1-2	36	0.79	1	2
Scenario 1-3	51	0.88	1	3
Scenario 1-4	59	0.75	1	4
Scenario 2-3	37	0.88	2	3
Scenario 2-5	48	0.60	2	5
Scenario 2-7	58	0.72	2	7
Scenario 3-4	37	0.88	3	4
Scenario 3-7	52	0.60	3	7
Scenario 3-10	58	0.72	3	10

Scenario 1-2: In the second scenario (1-2), we add a second upgrading reactor. We have three main choices to increase the carbon yield. We can do an acylation reaction, which will consume the acetic acid. The carbon content of the acetic acid is 71.8 $kmol_{carbon}$ s^{-1}.

There is enough acetic acid to acylate all of the furanics once and have excess to acylate the aromatics/phenolics, on average, 1.2 times per molecule. Ideally, we would like to target acylation of the furanics to move them to C6+ range, rather than the aromatics/phenolics. Depending on the kinetics of acylating these two types of species, one might require a separation of the furanics from the aromatics/phenolics to ensure that the desired species are acylated.

Alternatively, one could perform hydroxy alkylation or alkylation to consume acetol. The acetol has a carbon content that is slightly less than the acetic acid, only 63.82 $kmol_{carbon}$ s^{-1}. Already, it would seem preferable to target the acetic acid. There are enough moles of acetol to alkylate or hydroxy alkylate all of the furanics, moving them to C6+, but the excess would only be enough to acylate or alkylate the aromatics/phenolics 0.3 times per molecule. Therefore, the importance of targeting the furanics would seem more crucial.

Finally, one could oxidize levoglucosan, stabilizing it as gluconic acid. Levoglucosan has more carbon (108 $kmol_{carbon}$ s^{-1}) than either the acetic acid or acetol. However, the furanics (78.8 $kmol_{carbon}$ s^{-1}) would not be C-C coupled in this route and the overall C6-C21 yield would be lower than the previous possibilities. Furthermore, oxidation increases the hydrogen consumption.

Based on this simple analysis, it would seem that the best option is to add an acylation step. Assuming that the furanics are preferentially acylated with respect to the aromatics/phenolics, then the C6-C21 yield would be 36%. The total hydrogen consumed in the process is 0.79 kg s^{-1} and the total number of reactors is 3 (1 thermal decomposition reactor and 2 upgrading reactors).

Scenario 1-3: In the third scenario (1-3), we add an additional upgrading reactor. One could add an additional upgrading step with respect to Scenario 1-2 (1-3a), or one could start the design over (1-3b).

a) If we choose to modify Scenario 1-2, one could add a hydroxy alkylation or alkylation step to consume acetol. Alternatively, one could oxidize levoglucosan to preserve its carbon. If we choose the hydroxy alkylation or alkylation route, we can add the carbon of acetol (63.82 $kmol_{carbon}$ $s^{-}1$). Since we have already upgraded furanics through the acylation of acetic acid, we do not get the added benefit of its carbon, as we did in Scenario 1-1. Though, if the aromatics/phenolics were preferentially acylated in the first route, adding the hydroxy alkylation or alkylation step may allow one to skip the separation of furanics.

In contrast to the above gains, if we instead choose to oxidize levoglucosan, we can preserve 108 $kmol_{carbon}$ s^{-1}. Assuming that the furanics were upgraded in the acylation step, this provides a greater gain in carbon yield, and would be the preferred route. Again, we note that this does not account for the cost of any separations that may have been required to isolate the furanics from the aromatics/phenolics.

Where should we add the oxidation event? If we add the oxidation reaction after acylation but before hydrodeoxygenation, then we would gain the carbon of levoglucosan. The C6-C21 yield would increase to 51% and the hydrogen consumption would increase to 0.88 kg s^{-1}. If we oxidize before we acylate, then the acetol and furanics would also oxidize. This opens the possibility of adding the carbon of the acetol to the product as well. Unfortunately, as mentioned in earlier, this yields far too many acids that the product lies in the C15-C31 range (see Figure 48). The C6-C21 yield drops to 32% and the hydrogen

consumption is 0.85 kg s^{-1} (this value is slightly lower than the previous value because the average carbon number has increased).

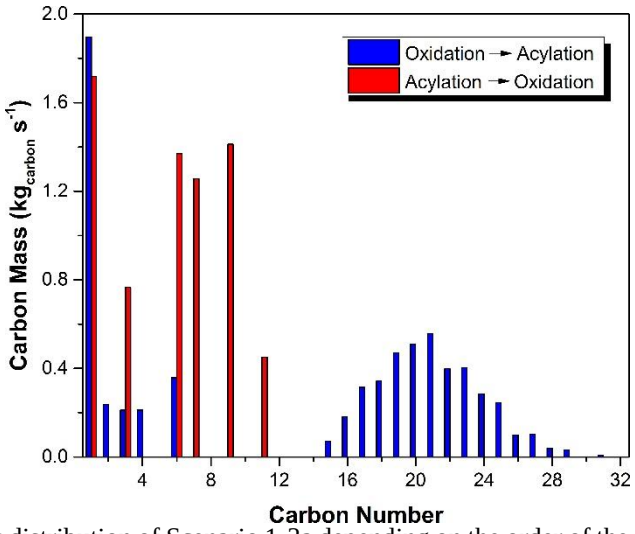

Figure 48**.** Carbon mass distribution of Scenario 1-3a depending on the order of the oxidation and acylation events. In blue bars, oxidation before acylation. In red bars, acylation before oxidation.

b) Is there a better process if the acylation step were replaced? Not for the current thermal decomposition yields, the specific chemistries considered or the assumptions used in the process design. In 1-3a, we already managed to C-C couple acetic acid, acetol, furan, furfural and even levoglucosan. One possible improvement would be to find reaction conditions such that acylation and hydroxy alkylation, which are both acid catalyzed, could be performed simultaneously in a single reactor with preference for furanics as the acceptor. This would allow one to upgrade both acetol and acetic acid in a single reactor.

Overall, Scenario 1-3 achieves a C6-C21 yield of 51%. The hydrogen consumption is 0.88 kg s^{-1} and the total number of reactors if 4 (1 thermal decomposition reactor and 3 upgrading reactors).

Scenario 1-4: In the final scenario that includes a single thermal decomposition (1-4) we add another upgrading step. Having enumerated the general design choices and decision making process in the previous scenarios, we will only comment on the "optimal" design.

Scenario 1-4 is based on Scenario 1-3a. In particular, a hydroxy alkylation step is added between the acylation and oxidation steps. This consumes acetols, adding its carbon to furanics, aromatics, and phenolics. Assuming each furanic is acylated or hydroxy alkylated a total of one time per molecule, than the aromatics/phenolics must be acylated or hydroxy alkylated approximately 2.5 times per molecule. The resulting aromatics/phenolics are only in the C11-C16 range. Oxidation of levoglucosan to gluconic acid also stabilizes the chain with respect to hydrodeoxygenation. The overall C6-C21 yield is 59% and the hydrogen consumption is 0.75 kg s^{-1}. The total number of reactors if 5 (1 thermal decomposition reactor and 4 upgrading reactors).

Additional upgrading steps and process possibilities: With Scenario 1-4, all of the carbon in the lights (<C6) has been incorporated into C6-C21, except for the carbon already in char and in CO_2. Therefore, the carbon yield cannot be increased further by increasing the number of upgrading steps. However, the hydrogen consumption could be lowered. Importantly, Scenarios 1-3 and 1-4 use oxidation to convert levogluocsan to gluconic acid; the oxygen must later be removed by hydrodeoxygenation. An alternative to avoid this step would be to hydrogenate levoglucosan to alcohols. Though, this tends to break the C-C bonds in levoglucosan, resulting in C2-C4 alcohols. These species would need to be incorporated into furanics, aromatics, or phenolics to bring the carbon into the C6-C21 fuel range. Unfortunately, the stability of the furanics with respect to hydrogenation is an issue. Therefore, as was demonstrated in Scenario 1-3, adding all of

the carbon from levoglucosan and furanics to the aromatics/phenolics would increase the carbon number beyond C21, wasting the carbon in very heavy species.

The best way to circumvent these issues are to 1) separate components prior to the chemistry in order to preserve them, and 2) to convert the lights through different processes. Either levoglucosan or the furanics must be isolated so that the furanics are not converted during hydrogenation of levoglucosan. Aldol condensation of acetol, either by self-condensation or with acetone (produced via ketonization of acetic acid) is one possibility to remove the light species without using them as hydroxy alkylation or acylating agents. We note that aldol condensation using furfural would probably not be advantageous because furfural can serve as an acceptor for the C2-C4 alcohols.

6. 2-Stage Thermal Decomposition Processes

Now we consider cases where we have two thermal decomposition stages. First, we must consider which two of the three thermal decomposition stages should be combined. Is it best to combine the first two (270°C, 360°C) or the second two (360°C, 500°C). From the yields presented in

Table 5, it seems that the second and third stage have more similarities in chemical composition than do the first and second stage. If the second and third stages are combined, we can essentially isolate levoglucosan from the first stage. Therefore, we will consider processes where the two thermal decomposition stages are at 270°C and 500°C. The yield of the first stage is assumed to be equivalent to the first stage presented in Table 5 while the yield of the new second stage is assumed to be the sum of the second and third stages of Table 5.

Block flow diagrams for the 2-stage thermal decomposition processes are shown in Figure 49. We consider only cases where there are the same number of upgrading steps for each fraction. We consider up to three upgrading steps in addition to a shared hydrodeoxygenation step. Therefore, the scenarios studied are 2-1, 2-3, 2-5, and 2-7.

Scenario 2-1: Scenario 2-1 is essentially the same as Scenario 1-1. The two fractions are upgraded by hydrodeoxygenation, in a single, shared reactor. The C6-C21 yield is 16% (3% from first stage and 13% from second stage). The overall hydrogen consumption is 0.90 kg s^{-1}. Generally, due to economies of scale, Scenario 2-1 should be inferior to Scenario 1-1.

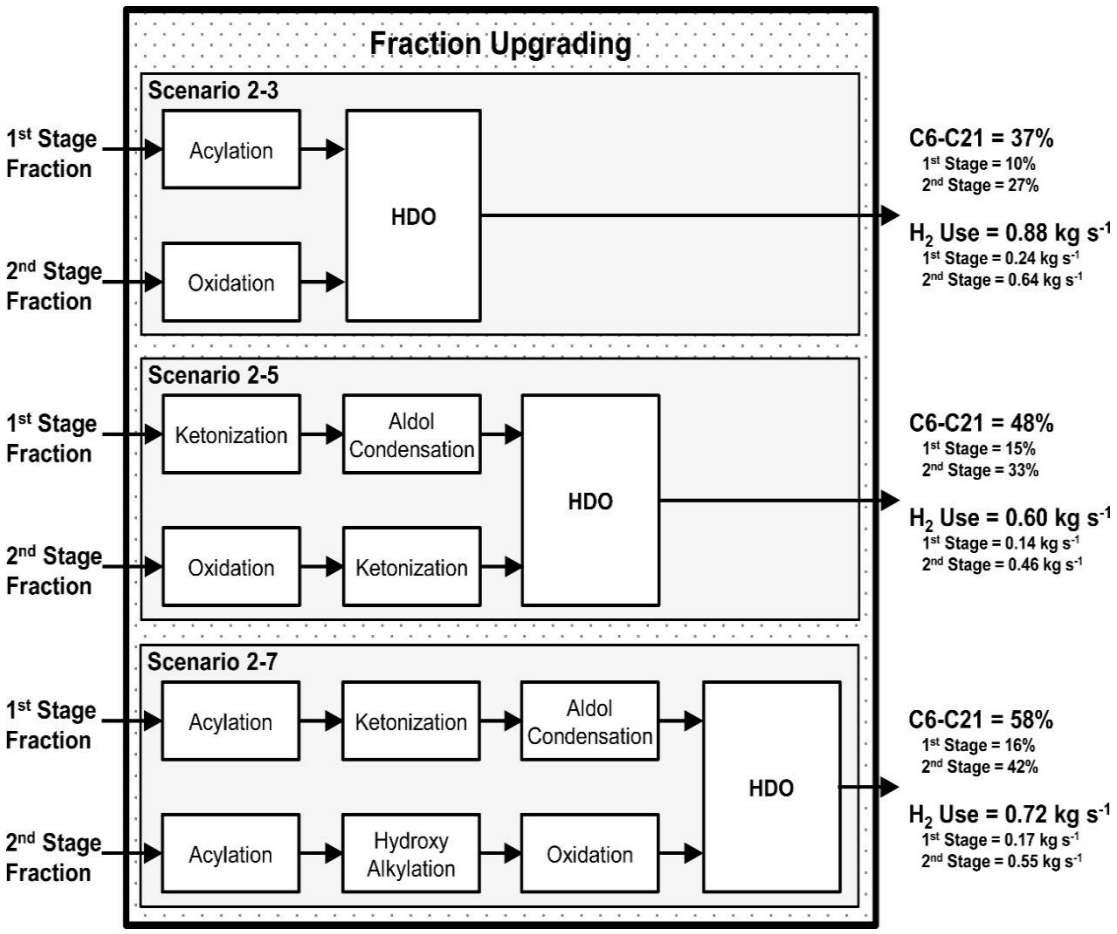

Figure 49**.** Block flow diagram of reactors in Fraction Upgrading system for various scenarios. The thermal decomposition system consists of two stages, operating at 270°C and 500°C. The C6-C21 yield and the hydrogen consumption rate are provided for each scenario. The C6-C21 yield and hydrogen consumption are also provided on a per fraction basis.

Scenario 2-3: This is the simplest scenario considered for the two-stage thermal decomposition process. The first and second stage each have a single upgrading reactor and then both share a final hydrodeoxygenation reactor.

F_1-System) The F_1-System upgrades the first stage fraction. Based on carbon content of the various species in this fraction, the most effective strategy for maximizing carbon yield is to do acylation. Acetic acid is used to acylate furan, furfural and guaiacol into C6+ species. The amount of acetic acid is too much to be fully consumed, even after acylating guaiacol four times per molecule. We note that the rate of acylation will likely

decrease with each addition to the aromatic ring, accounting for these kinetics may be an important factor in an optimal design.

F_2-System) There are two main possibilities for the upgrading the second stage fraction. Hydroxy alkylation of (preferentially) furfural and the aromatics/phenolics using acetol could recover 91.6 $kmol_{carbon}$ s^{-1}. Alternatively, oxidation of levoglucosan to gluconic acid would recover 106.3 $kmol_{carbon}$ s^{-1}. Though the oxidation route recovers more carbon, there is a penalty it consumes approximately 5% more hydrogen than the hydroxy alkylation route. With the principal goal of maximizing carbon route, we select the oxidation route in the process.

Yield) The overall C6-C21 yield is 37%. The hydrogen consumption rate is 0.88 kg s^{-1} and the total number of reactors is 5 (2 thermal decomposition and 3 upgrading). The C6-C21 yield is only slightly higher than Scenario 1-2, which also features only a single (non-hydrodeoxygenation) upgrading step. Though there are more reactors in Scenario 2-3 than in Scenario 1-2, each of the reactors should be smaller because the mass treated by each reactor is less. Since capital costs generally scale with the two-thirds rule, one would expect somewhat higher capital costs for this scenario than Scenario 1-2, but perhaps lower than Scenario 1-3.

Scenario 2-5: Again, we skip Scenario 2-4 and continue by adding another upgrading step to both the F_1-System and F_2-System.

F_1-System) In Scenario 2-3, we found that the acetic acid could not be fully utilized because there are limits on the number of times that each aromatic/phenolic compound can be acylated – that is the aromatic ring can only hold up to six substituents. As a result,

the acetol that was not used in Scenario 2-3 cannot be utilized by adding a hydroxy alkylation step. Therefore, we revise the entire strategy.

First, we employ ketonization to convert acetic acid to acetone. Though this comes with a carbon loss, it is the best option available given the streams that are available. If the process had access to an aromatic stream from a conventional refinery, this may provide an interesting synergy. Next, we perform aldol condensation between acetone, acetol, and furfural to yield C6+ species. Though the exact product distribution is not known, we assume that all of the carbon exists in at least C6 species.

F_2-System) Again, due to the high fraction of levoglucosan, oxidation remains an attractive upgrading step. After oxidation, there are two main routes to consider. First, the various acids derived from acetol, furanics and levoglucosan can serve as acylating agents with the aromatics/phenolics as acceptors. Alternatively, we can ketonize these acids to yield ketones. Though this second route appears unattractive due to carbon losses during ketonization, we have found in the past that oxidation followed by acylation often yields C22+ species, which are unsuitable for fuel use.

Yield) Employing the first strategy (F_2-System, oxidation followed by acylation), the overall (F_1-System + F_2-System) C6-C21 yield is only 26%, which actually lower than Scenario 2-3. The low yield is due to a very high fraction of C22+ species, as expected. The second strategy (F_2-System, oxidation followed by ketonization) the C6-C21 yield is 48%. This is higher than Scenario 2-3, but slightly lower than the analogous Scenario 1-3.

Though the C6-C21 yield is slightly lower, the hydrogen consumption rate is only 0.60 kg s^{-1}, as compared to 0.85 kg s^{-1} for Scenario 1-3. The much lower hydrogen consumption is due to oxygen removal as CO_2 during the ketonization step.

Scenario 2-7: A third upgrading reactor is added to each of the F_1- and F_2-Systems.

F_1-System: To improve upon Scenario 2-5, an acylation step is added to the start of the reaction series. This will consume acetic acid and minimize the carbon lost during the subsequent ketonization step. After ketonization, we again employ aldol condensation to convert acetone, acetol, and furfural to C6+ species.

F_2-System: The design of this system is analogous to that of Scenario 1-4. The process begins with acylation to couple acetic acid into the furanics, aromatics and phenolics. Next, hydroxy alkylation is used to couple acetol into these same species. Finally, oxidation of levoglucosan converts the species to gluconic acid.

Yield) The overall C6-C21 is 58%, only slightly lower than the analogous Scenario 1-4 because of some losses during the ketonization step. The hydrogen consumption rate is 0.72 kg s^{-1}. The value is higher than that of Scenario 2-5 because more oxygen is removed as H_2O rather than as CO_2.

7. 3-Stage Thermal Decomposition Processes

Finally, the case of three decomposition stages is considered: 270°C, 360°C and 500°C. The yield in each fraction is presented in Table 5.

Block flow diagrams for the 3-stage thermal decomposition processes are shown in Figure 50. Only cases where there are the same number of upgrading steps for each

fraction are considered. We consider up to three upgrading steps in addition to a shared hydrodeoxygenation step. Therefore, the scenarios studied are 3-1,32-4, 3-7, and 3-10.

Scenario 3-1: Scenario 3-1 is, again, essentially the same as Scenario 1-1. The three fractions are upgraded by hydrodeoxygenation, in a single, shared reactor. The C6-C21 yield is 16% (3% from first stage, 8% from the second stage, and 5% from third stage). The overall hydrogen consumption is 0.90 kg s^{-1}. Generally, due to economies of scale, Scenario 3-1 should be inferior to Scenario 1-1.

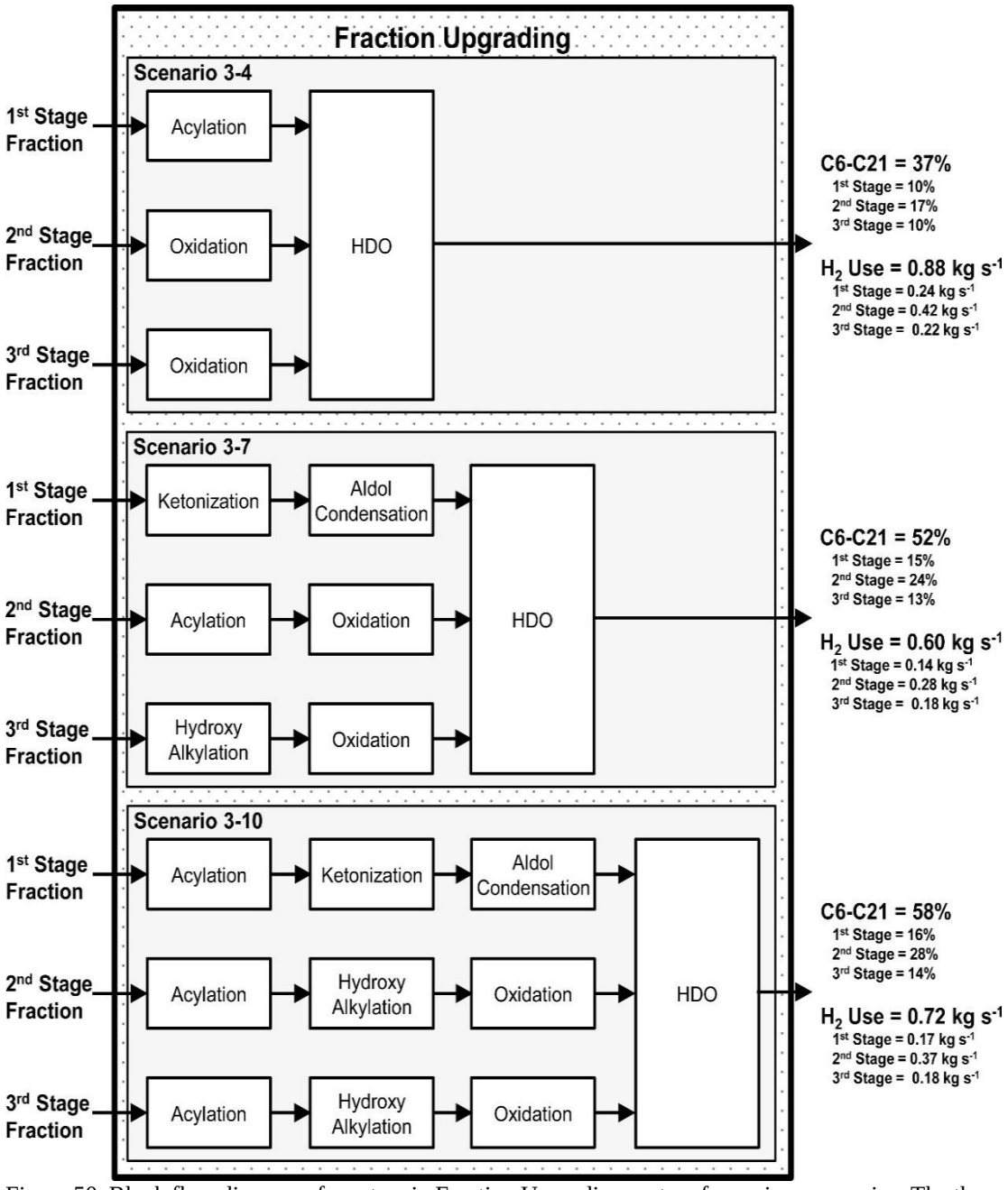

Figure 50**.** Block flow diagram of reactors in Fraction Upgrading system for various scenarios. The thermal decomposition system consists of three stages, operating at 270°C, 360°C and 500°C. The C6-C21 yield and the hydrogen consumption rate are provided for each scenario. The C6-C21 yield and hydrogen consumption are also provided on a per fraction basis.

Scenario 3-4: This is the simplest scenario considered for the three-stage thermal decomposition process. Each stage has a single upgrading reactor and a shared, final hydrodeoxygenation reactor.

F_1-System) The incoming fraction is identical to that of the F_1-System for the 2-stage thermal decomposition process. Therefore, the upgrading strategy is the same as in Scenario 2-3. That is, acylation of furanics, aromatics, and phenolics using acetic acid.

F_2-System) There are three competing options for the second fraction upgrading. First, furanics can be acylated by acetic acid, thereby incorporating the carbon in the furanics and acetic acid into C6+. The total number of moles of acetic acid is only sufficient to acylate 70% of the furfural into C6+, and the carbon recovered is only 51.3 $kmol_{carbon}$ s^{-1}. Alternatively, furanics can be hydroxy alkyated by acetol. Again, the total amount of acetol is only sufficient to upgrade 56% of the furanics. The carbon recovered into C6+ is 47.5 $kmol_{carbon}$ s^{-1}. Finally, levoglucosan can be oxidized to gluconic acid, recovering 65.2 $kmol_{carbon}$ s^{-1}. With the goal of maximizing carbon yield, the oxidation strategy is preferred. However, as oxidation increases hydrogen consumption, one might also consider the other two alternatives.

F_3-System) The amount of furanics in the 3rd stage fraction is much less than in the 2nd stage fraction. As a result, the acylation and hydroxy alkylation of furanics pathways that were competitive with oxidation of levoglucosan are no longer. Therefore, the preferred upgrading pathway is oxidation of levoglucosan.

Yield) The overall C6-C21 yield is 37% and the hydrogen consumption rate is 0.88 kg s^{-1}. The overall upgrading strategy is analogous to Scenario 2-3. Therefore, due to economies of scale, it is unlikely that Scenario 3-4 would be advantageous over Scenario 2-3.

Scenario 3-7: Scenarios 3-5 and 3-6 are skipped and another upgrading step is added to all three upgrading systems.

F_1-System) Again, the strategy is identical to that of Scenario 2-5. First, we employ ketonization to convert acetic acid to acetone. Though this comes with a carbon loss, it is the best option available. Next, aldol condensation between acetone, acetol, and furfural is conducted to yield C6+ species.

F_2-System) There are two competitive pathways for upgrading the 2nd stage fraction. The first pathway involves oxidation of acetol, furanics and levoglucosan to acids and then ketonizing those acids. In an alternative pathway, acetic acid is coupled with furanics using acylation. Then, the levoglucosan is oxidized to gluconic acid. The latter pathways recovers 15 $kmol_{carbon}$ s^{-1} more than the former pathway, and therefore is chosen as the preferred pathway.

Another pathway that could be considered is oxidation, followed by acylation using the assortment of acids to upgrade the aromatics and phenolics. Though, we find that the amount of acids far outweigh the amount of aromatics and phenolics. Therefore, the carbon yield is lower in this pathway.

F_3-System) There are two competitive pathways, that are similar to those of the F_2-System. The first pathway features oxidation followed by ketonization. The second pathway involves hydroxy alkylation to couple acetol with furanics, followed by oxidation of levoglucosan. The latter pathway recovers 15 $kmol_{carbon}$ s^{-1} more than the former pathway.

Yield) The C6-C21 yield is 52% and the hydrogen consumption rate is 0.60 kg s^{-1}. Interesting, compared to other scenarios that have two upgrading steps (plus hydrodeoxygenation), i.e. Scenario 1-3 and Scenario 2-5, this Scenario has the highest yield and the lowest hydrogen consumption. The upgrading of each fraction is able to be slightly more optimized due to the specific chemical functionalities in each stream. Importantly, the second fraction is best acylated, while the third fraction is best hydroxy alkylated.

Scenario 3-10: In the final scenario that we consider, we add another upgrading step to each of the F_1-, F_2-, and F_3-Systems.

F_1-System) Again, the F_1-System is the same as in the 2-stage process. The system begins with acylation using acetic acid. The second step is ketonization to couple residual acetic acid. Finally, aldol condensation converts acetone and acetol into C6+ species.

F_2-System) The acetic acid, acetol and furfural can all be converted into C6-C21 species. First, acetic acid is coupled with furanics by acylation. Then, the remaining furanics are converted by hydroxy alkylation using acetol. Residual acetol hydroxy alkylates the aromatics and phenolics. Finally, levoglucosan is oxidized to gluconic acid.

F_3-System) The F_3-System is of identical construction to the F_2-System.

Yield) The C6-C21 yield is 58% and the hydrogen consumption rate is 0.72 kg s^{-1}. This scenario is analogous to Scenario 2-7, except where the F_2- and F_3-Systems here are equivalent to the F_2-System of Scenario 2-7. As a result, it is likely that Scenario 3-10 would not be favorable with respect to Scenario 2-7.

8. Discussion

8.1. Number Of Upgrading Steps Versus Carbon Yield

The first key process consideration that we discuss is the choice of total number of upgrading steps. In Sections 5, 6 and 7, we considered cases where each fraction were upgraded 1, 2, 3, or 4 times. Discounting the shared hydrodeoxygenation step, there was the possibility of up to 3 C-C coupling events.

Figure 51 shows the evolution in C6-C21 yield as the number of upgrading steps increase from 1 to 4 for the 1-stage, 2-stage, and 3-stage processes. For the 1-stage processes, we see that the C6-C21 yield increases with each additional upgrading step, but the absolute change diminishes with each additional upgrading step. In particular, the yield increases as: 16%, 37%, 51% and 59%. A similar result is seen for the overall yield for the 2-stage and 3-stage processes.

For the 2-stage and 3-stage processes, we further look into the yield derived from each stage. For the 2-stage process, the first stage yield increases as: 3%, 10%, 15% and 16%; the second stage yield increases as: 13%, 27%, 33% and 42%. For the 3-stage process, the first stage yield increases as: 3%, 10%, 15% and 16%; the second stage yield increases as: 8%, 17%, 24% and 28%; and the third stage yield increases as: 5%, 10%, 13% and 14%. Again, we see that each individual stage also exhibits this diminishing returns. This is particularly noted for the first and third stage of the 3-stage processes.

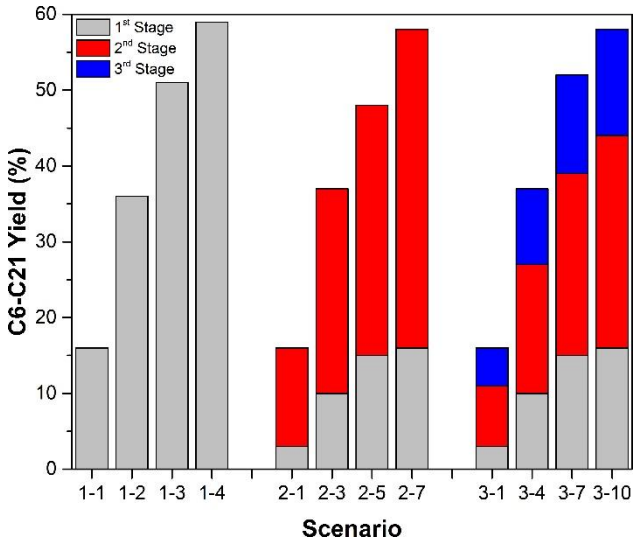

Figure 51. C6-C21 yield for different scenarios as distributed between the different torrefaction/pyrolysis fractions. The first stage is shown in grey, the second stage in red, and the third stage in blue.

Therefore, a trade-off exists between increased C6-C21 versus the number of upgrading steps. Each additional upgrading step provides less utility as the previous upgrading step. Each additional step will (likely) add to costs (though it is possible that due to the changes in the optimal chemistry, that costs could decrease).

8.2. Number Of Thermal Decomposition Stages

The second key parameter that we consider is the number of number of thermal decomposition stages. Originally, we had envisioned that the total carbon yield of a process, for a given number of upgrading steps per fraction, would increase with increasing number of thermal decomposition stages. The rationale was that each upgrading system could be uniquely tailored for a fraction's chemical composition. The results are more nuanced.

First, we examine the upgrading routes as a function of the number of upgrading steps for each fraction. In some of these scenarios, multiple fractions are upgraded in the identical

series of reactors, and it is likely that costs would be lower by combining these upgrading routes. Scenarios 2-1 and 3-1 have the same upgrading steps as Scenario 1-1, as metioned previously. Also, Scenarios 3-4 and 3-10 are the same as Scenarios 2-3 and 2-7, respectively. Therefore, the only 3-stage process that is unique is actually Scenario 3-7.

Though the upgrading steps for two different fractions may be the same, the product distribution will change if the fractions are combined before upgrading. In Figure 52 we present the carbon mass distribution of the overall product for Scenarios 2-7 and 3-10. Each of these scenarios have three upgrading steps (plus hydrodeoxygenation) for each fraction. The first fraction of both scenarios is the same and the upgrading routes are identical – therefore the yield from the first fraction is identical for these two scenarios. In Scenario 2-7, there is one additional fraction. In Scenario 3-10 there are two additional fractions, which sum to the second Scenario 2-7 fraction. The upgrading steps for the second fraction of Scenario 2-7 are identical to both the second and third fractions of Scenario 3-10. However, the components in the second and third fractions are not all equally distributed between the two fractions (see

Table **6**). For example, acetol is approximately equally distributed between the second and third stages, while acetic acid is more concentrated in the second fraction. As a result of these (and other) differences in fraction composition, the product distributions for upgrading each fraction is different and the overall product distribution for Scenario 2-7 is different from Scenario 3-10. In this case, the product all lies in the C6-C21 range, and so the C6-C21 yield is the same for both Scenario 2-7 and Scenario 3-10. Yet, it is important to note that it is possible that the yield could be different for the same set of upgrading steps if the upgrading is performed in multiple stages instead of a single stage.

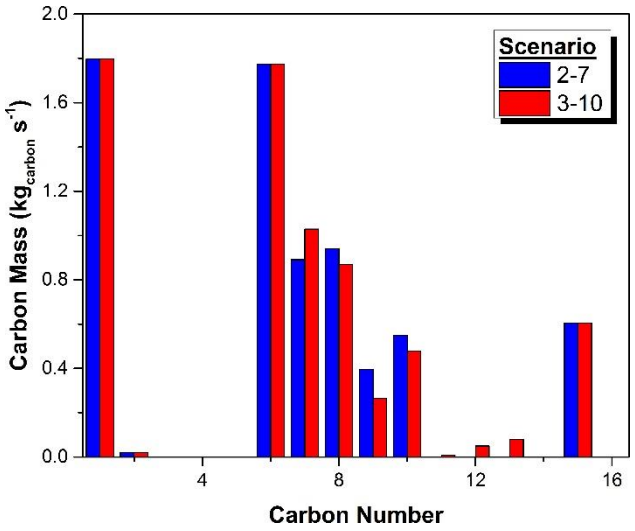

Figure 52. Carbon mass distribution of Scenarios 2-7 (blue) and 3-10 (red).

For the thermal product distribution assumed, there are no differences in C6-C21 yield for these "redundant" scenarios. Of these unique scenarios, we can identify the scenarios with the highest yield for a given number of upgrading steps per stage. For one upgrading step (hydrodeoxygenation), Scenario 1-1 is optimal (though the same yield as 2-1 and 3-1). For two upgrading steps, Scenario 2-3 is slightly ahead of the others. For three upgrading steps, Scenario 3-7 is best. Finally, for four upgrading steps, Scenario 1-4 is

best. We note that the total yield of these 2- and 3-stage scenarios is only slightly higher than the corresponding 1-stage scenario.

Though this result seems to diminish the utility of having multiple thermal decomposition stages, there are some important caveats to note. First, we note that the original 3-stage thermal decomposition yield was not optimized simultaneously with the design of the upgrading systems. It is likely that by better optimization of the thermal decomposition yield, based on feedback from process design, will enable more efficient upgrading strategies. Robust models[124, 125] for the decomposition of biomass would be a significant benefit towards this optimization.

Secondly, our process design is based on an approximation of the real thermal decomposition yield. Bio-oil from fast pyrolysis is a viscous, unstable, and corrosive mixture of many more compounds than have been considered here. It is possible that some of these compounds may poison catalysts or participate in unwanted side reactions that may alter the yields. As the fractions comprise a smaller set of compounds, the chemistries may be more well-behaved and they may be easier to process (i.e. less viscous, more stable, less corrosive, etc.), which will impact the overall economics.

Finally, we have considered only cases where the number of upgrading steps for each fraction is the same. As described in Section 8.1., there are diminishing returns with increasing number of upgrading steps. Importantly, those diminishing returns are not uniform across the different stages. For the 3-stage processes, the first and third fraction have only very small marginal increases in yield with the fourth upgrading step. Therefore, one may envision hybrid processes where the number of upgrading steps for each fraction is different.

8.3. Hybrid Processes

Here, we briefly comment on some possible hybrid processes that have a different number of upgrading steps for each fraction. In Figure 53, we show an example 2-stage possibility. Examining the change in carbon yield as a function of the number of upgrading steps (see Figure 51), it seems that the marginal benefit of adding a fourth upgrading step (counting hydrodeoxygenation as an upgrading step) to upgrade the first fraction is small. In contrast, the fourth upgrading step of the second fraction still has a reasonable marginal gain in carbon yield. This hybrid process has a C6-C21 carbon yield of 57%, as compared to the 58% achieved by including that additional upgrading step for upgrading the first fraction.

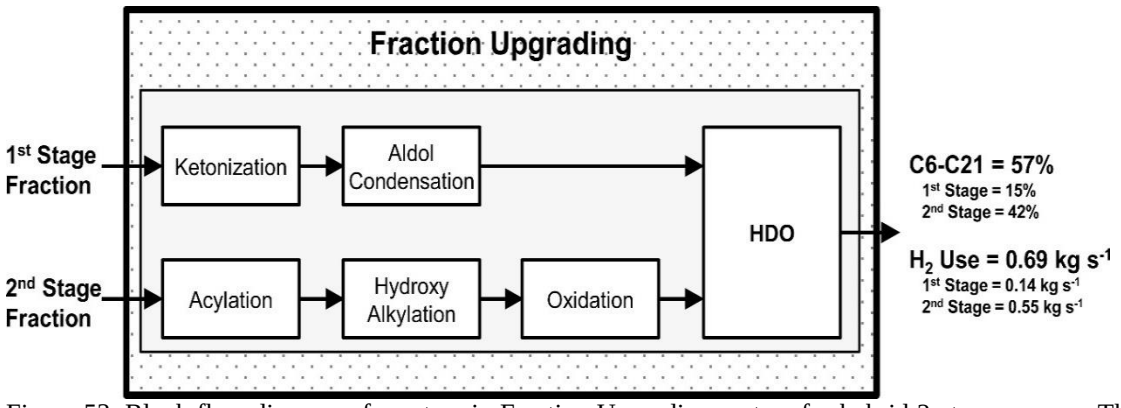

Figure 53. Block flow diagram of reactors in Fraction Upgrading system for hybrid 2-stage process. The thermal decomposition system consists of two stages, operating at 270°C, and 500°C. The overall (and on a per fraction basis) C6-C21 yield and the hydrogen consumption rate are provided.

A similar analysis of 3-stage processes suggests that the fourth upgrading step for the first and third fractions has small marginal benefits. Therefore, in Figure 54, we propose a 3-stage hybrid process where there are 4 upgrading steps for the first and third fractions and 3 upgrading steps for the second fraction. The overall C6-C21 yield is 56%.

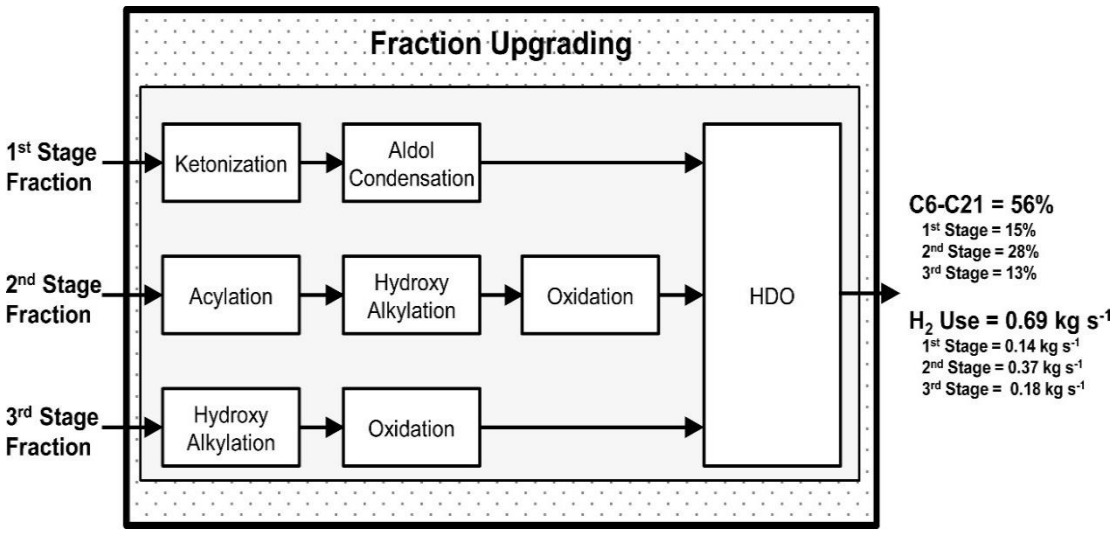

Figure 54**.** Block flow diagram of reactors in Fraction Upgrading system for hybrid 3-stage process. The thermal decomposition system consists of three stages, operating at 270°C, 360°C and 500°C. The overall (and on a per fraction basis) C6-C21 yield and the hydrogen consumption rate are provided.

These cases illustrate an important point when considering the importance of thermal fractionation. Though the yield may not necessarily be higher when fractionating, the separation allows for more precise control over the upgrading steps – not only in terms of the types of chemistries employed, but also the number of chemistries employed. When we compare Scenario 1-4 versus these two hybrid schemes, there will be a trade-off between splitting the first two upgrading steps into separate reactors versus not requiring the third upgrading step for some of the fractions.

8.4. Key Chemistries

In Table 8, we summarize the chemistries employed in the various upgrading scenarios. Of course, hydrodeoxygenation is employed in every scenario (10 scenarios), as oxygen removal is an essential part of the upgrading process. After hydrodeoxygenation, the next most employed chemistries are acylation (8 scenarios), oxidation (8 scenarios), aldol condensation (4 scenarios), hydroxy alkylation (4 scenarios), ketonization (4 scenarios), alkylation (0 scenarios), and hydrogenation (0 scenarios). We note that in general,

hydroxy alkylation is used to C-C couple acetol, and the chemistry could readily be replaced with alkylation to take advantage of the alcohol functionality in acetol.

Acylation is widely employed because there is an abundance of acetic acid, which can be C-C coupled by acylation. Other routes are available to consume acetic acid, but this is the simplest strategy and is without any inherent carbon losses (e.g. ketonization).

Oxidation is also widely used because there is an abundance of levoglucosan. The alternative strategy to process levoglucosan is via hydrogenation, which is employed zero times in the scenarios. There are two main reasons why the hydrogenation route is not favored. 1) Hydrogenation yields C2-C4 alcohols, which must later be C-C coupled in a second step. Therefore, the hydrogenation route would likely require an additional reactor with respect to the oxidation route. 2) Currently, from the mass balance, incorporating all of the resulting C2-C4 alcohols into the aromatics or phenolics would push the carbon number of these species into the C21+ range. Though these are the major disadvantages of the hydrogenation route, we note that the hydrogen consumption of a process using hydrogenation instead of oxidation will likely be lower. Oxidation adds oxygen to the species, which must later be removed at the cost of hydrogen. In the final economic evaluation, it is possible that the additional hydrogen costs of the oxidation route may outweigh the benefits of having less reactors or having a lower carbon yield. Overall, it would be beneficial if there were other strategies available to convert levoglucosan into valuable product.

Aldol condensation, hydroxy alkylation and ketonization are used in some of the processes. The aldol condensation and hydroxy alkylation routes are important for consumption of excess ketones (e.g. acetol) and aldehydes. Ideally, ketonization should

be avoided because of the stoichiometric carbon losses. Though, in some instances, for the thermal decomposition yields considered here, the processes do benefit from a ketonization step. Usually, this is the case when the fractions have excess acids that cannot be consumed by acylation.

For the acylation and hydroxy alkylation chemistry, one of the most important assumptions in designing the scenarios is that the catalyst and/or reaction conditions can be optimized so that the chemistries selectively target furanics rather than aromatics and phenolics. Due to high levels of catalyst coking for the furanic chemistries to be implemented the furfural must first be converted to furan via decarbonylation or more desirably methyl furan from hydrodeoxygenation[62]. The latter route has the advantage of maintaining the C5 structure. The selective conversion of furfural to methyl furan has been shown over silica-supported Ni-Fe catalysts.[29, 31] In general, as the aromatics and phenolics are already C6+ species, it is important to couple the light oxygenates (<C6) with the furanics (C4-C5). Additionally, as both of these reactions are acid-catalyzed, it would be useful if these two reactions could occur simultaneously within the reactor.

Table 8. Upgrading chemistries applied in each scenario.

	Scenario									
Chemistry	**1-1**	**1-2**	**1-3**	**1-4**	**2-3**	**2-5**	**2-7**	**3-4**	**3-7**	**3-10**
Acylation		x	x	x	x		x	x	x	x
Alkylation										
Aldol Condensation						x	x		x	x
Hydrodeoxygenation	x	x	x	x	x	x	x	x	x	x
Hydrogenation										
Hydroxy Alkylation				x			x		x	x
Ketonization						x	x		x	x
Oxidation			x	x	x	x	x	x	x	x

8.5. Key Separations

In the scenarios, separations were not explicitly described and it was generally assumed that the separations would be minimal. Each fraction was upgraded without removing any components from the stream. In some cases, we indicated points where it may be beneficial to remove a component in order to prevent unwanted side reactions or to protect a functionality from conversion. In addition to these reasons, separations could become an important addition to the processes to better optimize the efficiency of upgrading steps. Here, we discuss some important separations that could have a significant benefit on the process. We do not discuss the feasibility, nor the method of accomplishing these separations here, but identify key separations that could improve the overall eceonomics of the process.

One important example where component isolation may be important is for levoglucosan upgrading. Levoglucosan is upgraded either by oxidation or hydrogenation. Both of these chemistries will also target other functionalities in the systems. For example, oxidation may produce acids from acetol and furanics; hydrogenation may convert ketones and furanics into alcohols. Isolation of levoglucosan would allow one to perform these chemistries without converting these other important functionalities, allowing one to re-arrange the upgrading sequence (typically oxidation is placed at the end of the sequence). If oxidation were used, this would have the added benefit of lowering the amount of oxygen added to the system and thereby lower hydrogen consumption.

In terms of process optimization, we consider the general upgrading strategy. Light oxygenates are ideally coupled with furanics, with excess coupled to aromatics and phenolics. Levoglucosan is upgraded separately by oxidation. Therefore, one could

envision a strategy where these important components are separated and distributed to maximize the desired yield. In Figure 55, we show a general upgrading strategy, shown for 3-stage thermal decomposition, but would work for more, or less, thermal decomposition stages. We note that the choice of thermal decomposition stages should be made to simplify the subsequent separations. This strategy is designed to upgrade the specific functionalities considered here, but is applicable for different abundances of these functionalities.

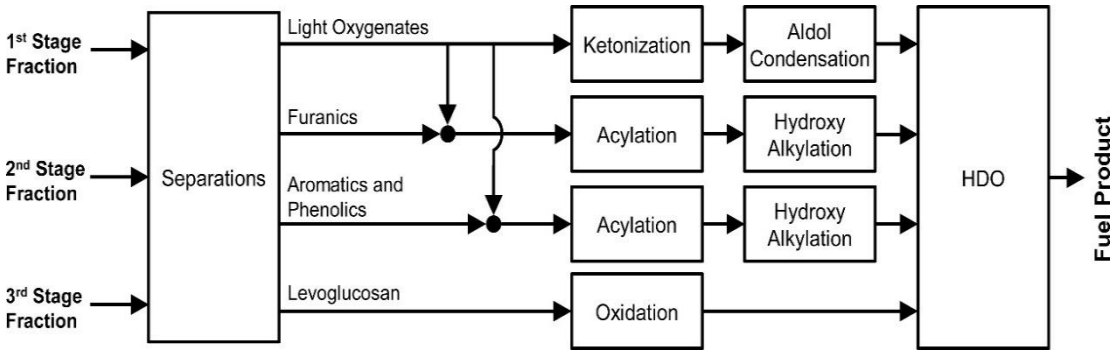

Figure 55**.** Idealized, general (3-stage) upgrading strategy with separations.

In the strategy, four principal groups are isolated, light oxygenates (including <C6 ketones, aldehydes, and acids), furanics, aromatics/phenolics, and levoglucosan. The light oxygenates are distributed between the furanics and aromatics/phenolics to be used as acylating and hydroxy alkylating agents. These light oxygenates will be distributed in order to maximize their utilization, preference given towards upgrading of the furanics. If there are any excess light oxygenates, the acids can be ketonized, with ketones and aldehydes coupled by aldol condensation. Finally, levoglucosan can be oxidized to gluconic acid.

Of course, more complicated processes could envisioned, where separations occur between upgrading steps in order to tailor the product distribution. Though, we do not note any specific cases here.

8.6. Ideal Thermal Fractionation

Finally, we return to the question of the thermal fraction. Is there an ideal, or goal, for its design? Perhaps, there is, but the "ideal" would change depending on advances in chemistries and separations. If the chemistries behave as assumed (without realizing any of the goals set in Scetion 8.4), then the ideal is close to the original conception. That is, three stages where each of the three major biomass components is decomposed in isolation: hemicellulose, cellulose, and lignin. The resulting product distribution and upgrading strategy would be similar to the streams exiting the separation block in Figure 55. Light oxygenates would be in the first stage, furanics and levoglucosan in the second stage, and aromatics/phenolics in the third stage. The main difference between this product distribution and the one shown in Figure 55 is that the levoglucosan and furanics would be combined in a single stream. The oxidation step would be added to the furanic upgrading sequence, most likely at the end of the sequence.

If there were advances in some of the chemistries, as outlined in Section 8.4, then the ideal may change. For example, if the catalyst and reaction conditions could be modulated such that furanics are preferentially acylated/hydroxy alkylated over aromatics/phenolics, then there may not be a need to separate the aromatics/phenolics from the furanics. The decomposition of the cellulose and lignin would not need to be separated.

If separations were able to target specific compounds and were reasonably cheap, perhaps thermal fractionation would not be necessary. As envisioned in Section 8.5, separations could isolate compounds groups to optimize their upgrading. Though we cannot discount the utility of thermal fractionation as a possible first step in the design of these separation systems.

9. Conclusions

We presented a conceptual process modeling assessment of biomass to fuels processes that employ multi-stage thermal fractionation of the biomass and catalytic upgrading. Using a systematic, iterative design strategy, which takes into account the abundance of various chemical functionalities within the biomass fractionation product, we derived a series of different process scenarios that differ in terms of process complexity. The main objective of this analysis was to determine the important process considerations and identify the key trade-offs. We demonstrated the important trade-off between carbon yield and process complexity. Furthermore, we showed that the choice of the number of thermal decomposition stages is not trivial; the "ideal" of decomposing each of the three main components of lignocellulosic biomass (hemicellulose, cellulose, and lignin) in their own stage may not be the best strategy. In general, more thermal decomposition stages allowed for more fine-tuning of the upgrading processes. Importantly, optimization of the decomposition conditions and number of stages must be done simultaneously with the fraction upgrading, with careful consideration of the chemistries available to upgrade those fractions.

All conceptual processes can be improved by improvements in catalytic chemistry, separations, and thermal fractionation. For the chemistry, it would be beneficial to identify catalysts and/or reaction conditions that favor acylation of furanics with respect to aromatics and pheonlics. Additionally, identifying catalysts that can perform acylation and hydroxy alkylation, using a mixture of acids/ketones could simplify the upgrading processes. Separations may be critical in realizing some of the upgrading sequences on real fractions. Furthermore, key separations can allow one to integrate the upgrading of the various fractions with one another, instead of upgrading each fraction independently.

Acknowledgements The Department of Energy is gratefully acknowledged for support under Grant DE-EE0006287 of the Bioenergy Technology Office CHASE program

Appendix B: Piancantelli Rearrangement Manuscript

Preface

In relation to the information provided in Chapter 3 on the upgrading of torrefaction vapors with Ru/TiO_2 a study was conducted with model compounds to probe the Piancatelli reaction. In conjunction with Dr. Taiwo Omotoso the following unpublished manuscript was developed. Dr. Omotoso was responsible for the model compound work and the torrefaction studies are the ones discussed in chapter 3.

Abstract

Conversion of furfural over Ru/TiO_2 in the vapor phase at 400 ^oC was studied. Results show the formation of cyclopentanone/2-cyclopentenone via the Piancatelli rearrangement. Also introduction of water in the feed shifts selectivity from 2-methylfuran to cyclopentanone/2-cyclopentenone. The addition of TiO_2 as a support led to the suppression of C-C hydrogenolysis/decarbonylation and enhancement of 2–methylfuran/cyclopentanone production when compared to pure Ru catalysts. Sites produced by interaction of Ru and TiO_2 were proposed to be active sites for this reaction. This reaction was also studied with biomass feeds. The furfurals produced from the thermal degradation of Red Oak also yielded significant amounts of cyclopentanone and 2-methylfuran.

Introduction

Torrefaction has historically been cited as a pretreatment step for the fast pyrolysis of biomass. Undergoing a mild heat treatment from 200-330 °C biomass partially decomposes, releasing mostly water and to a lesser extent organic compounds.[166, 167] This step leads to an increase in energy density of the solid residue, that is, the resulting carbon/oxygen ratio is higher than the initial biomass. An aspect of this process often over looked is the carbon loss due to torrefaction usually treated as a waste product. Utilizing this wasted energy is a promising way to increase the efficiency of the biomass to liquid fuels process.[1, 3]

Biomass used for torrefaction is composed mostly of three polymers: hemicellulose, cellulose and lignin. The specific ratios of these compounds depend on the biomass source. Red Oak is known to have compositions of 47, 27 and 21 wt % respectively.[13] During torrefaction the hemicellulose fraction begins to decompose. Not only does the moisture content decrease during this process, a significant amount of light oxygenates (acids, aldehydes, esters) and sugar derived products (furfurals, pyrans) are released. It is known that these acids are corrosive once condensed and also act to catalyze unwanted side reactions with the sugar derived products that lead to humin formation.[5] A vapor phase upgrading before condensation would provide many benefits to the overall biomass to fuels process.

While the targeted chemistry for the reaction of the acids in the torrefaction stream has been well studied, the reactions of the furfurals are still of great interest. Due to the instability of bio-oil caused by the presence of these reactive compounds, amongst others, further upgrading of bio-oil mixtures and conversion of the furfurals to

more stable and valuable molecules is desired. Furfural, for instance can be converted to 2-Methylfuran, which is a significant component in the production of fine chemicals, perfumes and medicines;[168-170] furfuryl alcohol, which is used for the synthesis of solvents and resins for ceramics processing;[171] and perhaps most importantly cyclopentanone, which is not only an important intermediate for the production of chemicals used for rubber and pharmaceutical applications[172] but can also undergo self-aldol condensation and further hydrodeoxygenation to form hydrocarbons in the jet fuel range.

The formation of cyclopentanone or its derivatives from furfural-based molecules is a desired reaction because it does not involve the loss of any carbon. Both furfural and cyclopentanone contain five carbon atoms. Initial studies on this transformation showed that it occurred via the rearrangement of a 2-furylcarbinol into 4-hydroxycyclopent-2-enone in the aqueous phase in an acidic environment.[27] This reaction is known as the Piancatelli rearrangement. It has been studied using a variety of catalysts and mainly in the liquid phase. Various starting reactant molecules have been used to demonstrate this rearrangement and it has been shown that water has to be present in the reaction mixture for the reaction to occur via key intermediates.[26, 172-174]

The vapor phase reaction for furfural conversion to cyclopentanone has not been studied as well as the liquid phase with products such as furfuryl alcohol, 2-methylfuran, furan and others obtained at mild temperatures. [171, 175] Hence this work investigates the conversion of furfural in a vapor phase flow reactor at 400 °C and atmospheric pressure over Ru/TiO_2 to understand the product distribution and get

preliminary pointers as to the nature of active sites responsible for furfural conversion. Results show that furfural can undergo the Piancatelli rearrangement to form cyclopentanone, 2-cyclopentenone and other important products such as 2-methyl furan and furfuryl alcohol. Also, water was found to play some role in shifting the selectivity from 2-methylfuran to cyclopentanone/2-cyclopentenone. The model compound studies were found to be in good agreement with the reaction of Red Oak torrefaction feeds which contained a mixture of furfurals, acids/esters and an excess of water where both cyclopentanone and 2-methylfuran were produced. Preliminary data suggests that the active sites for this reaction are formed due to the interaction of Ru and TiO_2 as seen in the change of product distribution when Ru was supported on SiO_2, CNT or TiO_2.

Experimental

Catalyst Preparation

Ru catalysts were synthesized using the incipient wetness impregnation method of an aqueous solution of Hexaaammineruthenium (III) chloride (98% Sigma Aldrich) on the TiO_2 support (Aeroxide P25, 0.25 ml/g pore volume) or SiO_2 support (Hisil-210, 0.96 ml/g pore volume). The catalysts were then dried at room temperature in air for 48 h, at 120 °C for 12 h in an oven before reducing at 400 °C for 2 h in hydrogen flow. The catalysts were pelletized and sieved to yield particles sizes from 250-420 μm.

Catalyst Characterization

ICP (Galbraith Laboratories) was utilized to determine Ru content of the synthesized catalysts. BET surface area was measured by nitrogen adsorption on a

Micromeritics ASAP 2010 instrument. Ru particle size distribution was obtained using Transmission Electron Microscopy (TEM, JEOL JEM-2100 model). Before imaging, the catalysts were pre-reduced in hydrogen flow at 400 °C for 1 h and cooled down to room temperature in nitrogen before dispersion in isopropanol and sonication to obtain a uniform suspension. Few drops of the suspension were dispersed on carbon-coated copper TEM grids. At least 200 ruthenium particles were counted in order to obtain particle size distributions.

Catalytic Activity Tests

Model compound experiments

Catalytic activity was tested in a quartz tube reactor (0.25 in OD) at atmospheric pressure and 400 °C. Catalyst particles were mixed with inert acid washed glass beads (Sigma Aldrich, Part number: G1277) with a particle size range of 212-300 μm and packed between two layers of quartz wool inside the reactor when required. In a typical experiment, pure distilled furfural (obtained from Sigma Aldrich; distilled and stored at -15 °C) with a feed flow rate of 0.1 ml/h or co-fed with water (with varying flow rates), was vaporized at the inlet zone of the reactor before introduction into a 30 ml/min hydrogen flow. The outlet stream of the reactor was heated to 250 °C to prevent condensation of compounds in the transfer lines and then flows through a six-port valve to allow for injection into a GC for product analysis. Product distribution was analyzed by online gas chromatography equipped with flame ionization detector (Agilent 5890), and HP-INNOWAX column (30 m, 0.25 μm). Identification of products was confirmed using a Shimadzu QP-2010 GCMS and standards were used to quantify the various

products in the FID. Before introduction of the feed, the Ru catalysts were reduced in situ at 400 °C for 1 h in 100 ml/min hydrogen flow. Mass balances for all the reaction runs were > 95 %.

Oak Torrefaction Experiments

For torrefaction of the raw biomass a CDS analytical pyroprobe Model 5250 with autosampler was implemented. Once the biomass was torrefied the vapors passed through 1/16" Silcosteel transfer lines at 300 °C to a separate quartz reactor setup for ex situ upgrading. An 8" quartz reactor tube placed inside a 2" ID x 6" Fibercraft Heater was connected to the pyroprobe transfer lines. 1.0 mg of Ru/TiO_2 catalyst was mixed thoroughly with 200 mg acid washed borosilicate beads (Sigma Aldrich G1145) to prevent channeling. The catalyst bed was maintained halfway through the quartz reactor by use of 30 mg of quartz wool. Temperature was measured directly outside of the quartz reactor tube by use of an Omega Type K thermocouple.

Analysis of the vapor product stream was carried out using an online Shimadzu QP2010 GCMS-FID system equipped with a RTX-1701 column (60m×0.25mm with 0.25 µm film thickness). The column oven heating ramp was set to hold at 4 min at 45 °C then ramp at 3°C/min to 280°C and hold for 20 min. A helium carrier gas was used with a total flowrate of 90 ml/min and a column flowrate of 1 ml/min. The products were identified by literature mass spectral data and quantified using FID peak area. Calibration injections of known torrefaction products were applied to determine the molar amounts of each compound in the product stream.

For these experiments using the real biomass vapors Red Oak sawdust was ground to 0.25-0.45 mm and dried in a vacuum oven (0.02 MPa) at 60 °C for 24 hours. The red oak composition of hemicellulose, cellulose and lignin has been previously found to be 47, and 27 and 21 wt % respectively. Sample sizes consisting of 0.7-1.0 mg red oak were packed in a quartz sample tube for use in the pyroprobe. The heating chamber in the pyroprobe is a quartz chamber that was heated to 270 °C for 20 min in 20 ml/min inert helium carrier gas. The vapors produced over the 20 min travel through the transfer lines where a 20 ml/min hydrogen stream is introduced. Hydrogen is introduced after the torrefaction step to ensure torrefaction is carried out under an inert environment. After passing through the catalyst bed the vapors are collected in a sorbent trap at -50 °C by use of N_2. The trap is then desorbed at 300 °C for 3 minutes with the vapors injected into the GCMS-FID.

Results and Discussion

Table 9 presents the characterization data for different catalysts used in this study. BET surface area of all catalysts as well as Ru weight percent and particle size determined from ICP and TEM respectively are shown. The particle sizes of the Ru catalysts supported on SiO_2 and TiO_2 are similar (close to 4 nm) however the particle size of the Ru supported on nanotubes (CNT) catalyst was 1.5 nm. TEM micrographs of the catalysts are shown in **Figure 56**.

Table 9: Particle size and Surfrace area for Ru/TiO_2 Characterization

Catalyst	Ru loading (wt %)	BET Surface Area (m^2/g)	Average Particle size (d_p)
Ru/TiO_2	4.4	55	3.6
Ru/SiO_2	5.3	126	4.1
Ru/CNT	1		1.5
TiO_2	-	60	-

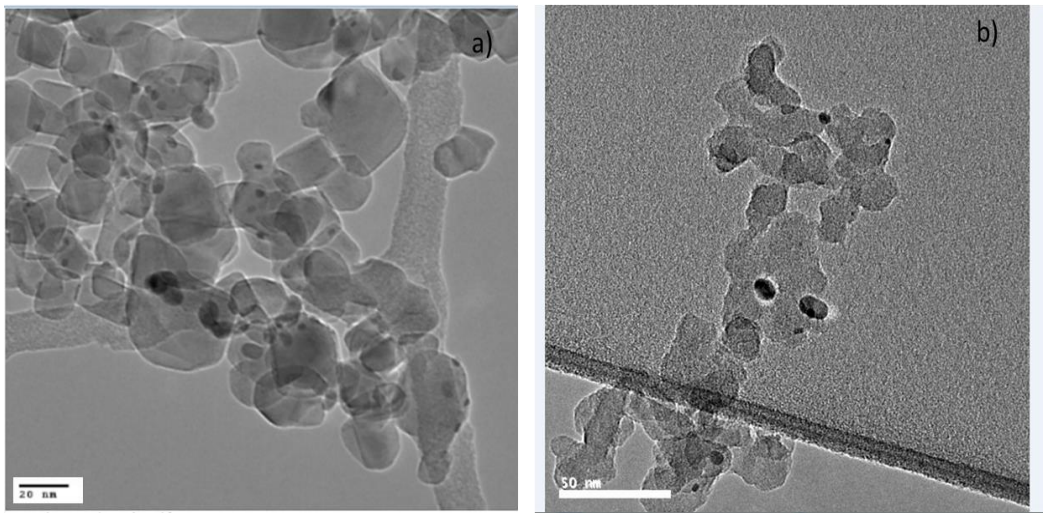

Figure 56**:** Representative TEM images for Ru catalysts a) 4.4% Ru/TiO_2 b) 5.3% Ru/SiO_2

Reaction of pure furfural over Ru/TiO_2

Product distributions for furfural conversion over Ru/TiO_2 in the vapor phase are shown in **Figure 57**. The dominant product is 2-methylfuran (2MF, yield = 59.7 % at 0.9 h). It has the highest yield at all W/F's and is produced from hydrogenolysis of the C-O bond in furfuryl alcohol (FOL) after initial hydrogenation of furfural (FAL) to furfuryl alcohol (FOL) on the Ru metal. While it is known that this hydrogenolysis can occur on metal surfaces,[29, 31, 35, 176] interfacial sites formed as a result of the

interaction between Ru and the reducible oxide TiO_2 could also play a role in the formation of 2MF from FOL as seen by the importance of these sites in reactions such as Fischer- Tropsch[177] and alkane hydrogenolysis.[178] This will be discussed further below in the paper.

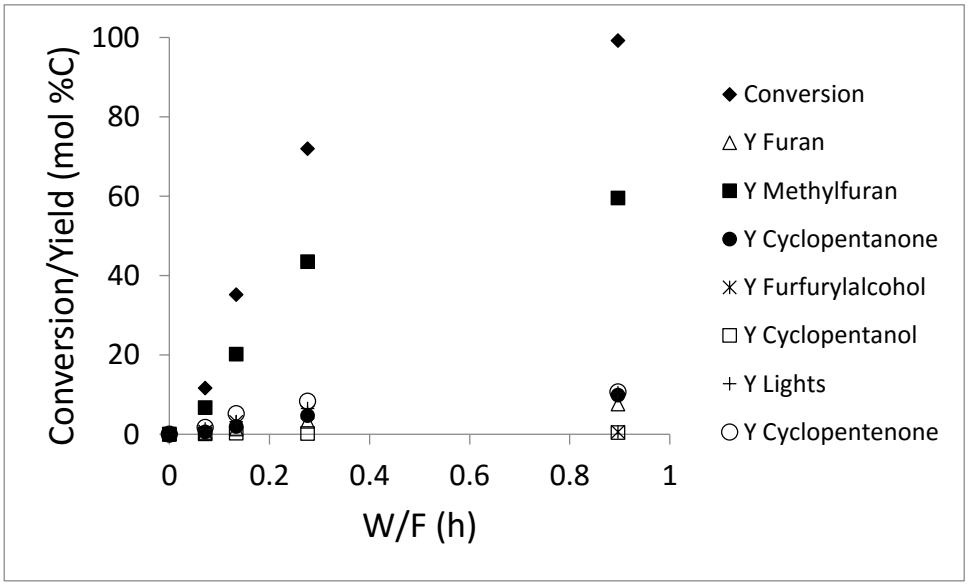

Figure 57: Furfural conversion and product yield with W/F over 4.4% Ru/TiO_2 at 400°C. 1 atm, 30 minutes time on stream

The formation of FOL passes through a maximum (yield = 5.5 % at 0.3 h) and then decreased at the highest W/F (yield = 0.6 % at 0.9 h). This could be due to the conversion of FOL to other products such as 2MF and cyclopentanone/2-cyclopentenone at higher contact times. FOL can be formed from direct hydrogenation of the carbonyl C-O bond of furfural (FAL) on the Ru metal. This reaction has been shown to occur over various metal catalysts such as Pt, Pd, Cu and Ni.[29, 31, 35, 173, 176] To obtain FOL, the O atom in the carbonyl group of FAL can adsorb on top of the Ru surface in a η^1 configuration as seen for Cu.[31, 179]. Asides from this

configuration, FAL can also adsorb on metal surfaces with both C and O atoms touching the surface in a η^2 mode as seen for Pd.[31, 180, 181] This will lead to the decarbonylation reaction whereby the CO molecule is lost and furan (FUR) formed instead of FOL. At the lowest W/F of 0.07 h, lower yields of FUR (yield = 0.4 %) as compared to FOL (yield = 0.7 %) were observed. However, as contact time increased to 0.9 h, higher yields of FUR (yield = 7.6 %) were obtained. As mentioned in the earlier discussion, FOL formed can be further converted to 2MF and cyclopentanone/2-cyclopentenone as W/F increases which could account for the low yields at this high W/F. Even at this W/F, the yield of furan is still lower than those of 2MF, cyclopentanone and 2-cyclopentenone.

Perhaps the most interesting reaction observed over this catalyst is the Piancatelli rearrangement of the furfural-based ring to form 2-cyclopentenone subsequent hydrogenation of the olefin to form cyclopentanone. From **Figure 57**, the yield of these products increase steadily with W/F from 2.3 % (W/F = 0.07 h) to 20.6 % (W/F = 0.9 h). This rearrangement is desirable due to the conservation of valuable carbon in the product stream as opposed to losing it during decarbonylation reactions since both furfural and cyclopentanone/2-cyclopentenone contain five carbon atoms. The presence of the Piancatelli rearrangement compounds in the product stream was confirmed by liquid injection of the condensed product mixture in the GC-MS and also injection of standards in the GC-FID. Small amounts of cyclopentanol (yield = 0.4 % at 0.9 h), which is produced via hydrogenation of the carbonyl group of cyclopentanone over the Ru metal is also observed from **Figure 57**. Some hydrogenolysis activity is also observed over the Ru/TiO_2 catalyst and this results in the production of light gases.

Role of water for furfural conversion to cyclopentanone

The importance of water being present in the reaction mixture for the Piancatelli rearrangement to occur in the liquid phase has been discussed in literature [26, 173, 174] therefore it was important to investigate the effect of water in this vapor phase conversion of furfural to cyclopentanone/2-cyclopentenone. Even though water was not introduced as a reactant in the results presented above, the Piancatelli rearrangement reaction was still observed even though 2-methylfuran was the most dominant product. Since water was absent in the feed, it can be produced via i) hydrogenolysis of FOL to form 2MF in which a water molecule is formed; ii) participation of OH groups on the TiO_2 surface which could facilitate this rearrangement. From the results presented earlier, it is possible that one or both of these scenarios are occurring.

To determine whether gas phase water is involved in this rearrangement, furfural was co-fed with excess water in two different molar ratios 5:1 and 12:1 and the results are presented in **Figure 58**. With the introduction of water, the sum of the Piancatelli rearrangement products CPone/CPentenone (yield = 16 %) is similar to the yield of 2MF (yield = 17 %). Comparing this with the values obtained without water in the feed, CPone/CPentenone (yield = 7 %), 2MF (yield = 20 %) an enhancement in this rearrangement is observed in the presence of water as a feed. This is in agreement with the results obtained in liquid phase systems.

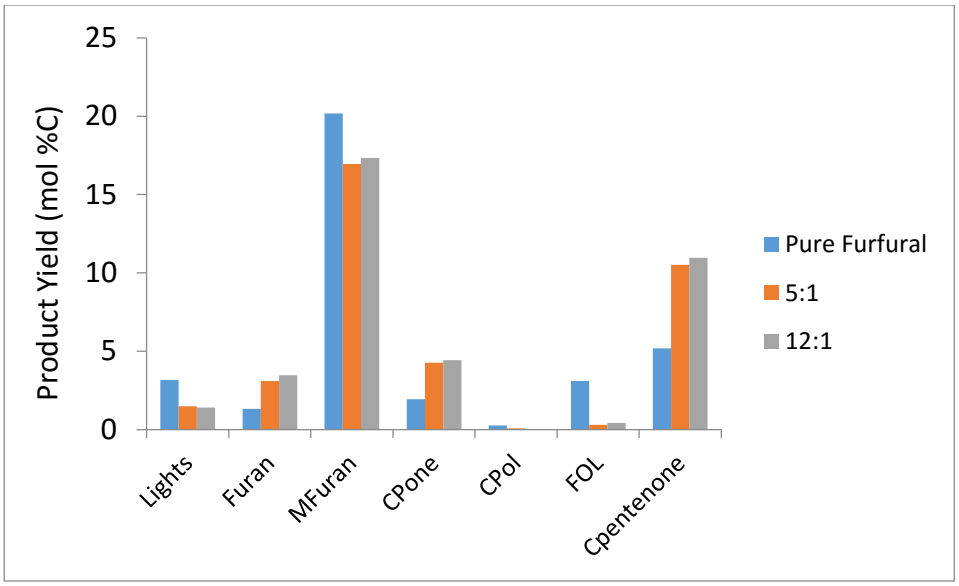

Figure 58: Product distribution for pure furfural and furfural co-fed with excess water at different molar ratios. 4.4% Ru/TiO_2 at 400°C, 1 atm, and 30 minutes time on stream. Conversion=35%

Decoupling of active sites for furfural conversion over Ru/TiO_2

After observing the product distribution, it was necessary to carry out investigations as to the nature of active sites on the Ru/TiO_2 catalyst responsible for the Piancatelli rearrangement. Our group has previously studied the conversion of various oxygenates over Ru based catalysts while changing type of support (SiO_2, C, Al_2O_3);[14] pretreatment conditions and TiO_2 support phase (anatase vs rutile)[25] to elucidate active sites responsible for the reaction. Enhanced rates observed when the reducible oxide TiO_2 was introduced as a support was attributed to the synergy between Ru and TiO_2 which led to the creation of highly active sites for guaiacol deoxygenation.[14] While it was not clear if these sites were around the perimeter of the Ru metal or defects on the TiO_2 support far away from the metal, further studies showed that while defect TiO_2 sites far away from the Ru metal are the active sites for guaiacol

conversion[25], perimeter sites around the Ru metal are the most important sites for further deoxygenation of m-cresol to toluene.[182] To investigate therefore if these sites created as a result of the interaction between Ru and TiO_2 were important for this rearrangement, pure Ru catalysts (supported on SiO_2 and CNT) and a bare TiO_2 catalyst with no metal loading were compared with Ru/TiO_2. This will help in decoupling the roles of Ru metal and effect of TiO_2 support. The results obtained from feeding a water/furfural (12:1 molar ratio) mixture over these catalysts are presented in **Figure 59**. Ru can facilitate the splitting of water leading to decoration of the metal surface with OH groups which could potentially play a role in this reaction.[183-185] We shall proceed by discussing the difference in product selectivities observed over the pure Ru catalysts (Ru/SiO_2 and Ru/CNT) and Ru/TiO_2. The following are evident: 1) CPone and CPentenone are not observed as products over the pure Ru catalysts which points to the absence of the Piancatelli rearrangement under these conditions; 2) Enhancement of FAL conversion to 2MF which is also a valuable product over Ru/TiO_2 (45.6%) compared to Ru/SiO_2 (8.9%); Ru/CNT (24.8%); 3) Suppression of decarbonylation and C-C hydrogenolysis on Ru/TiO_2 compared to the pure Ru catalysts.

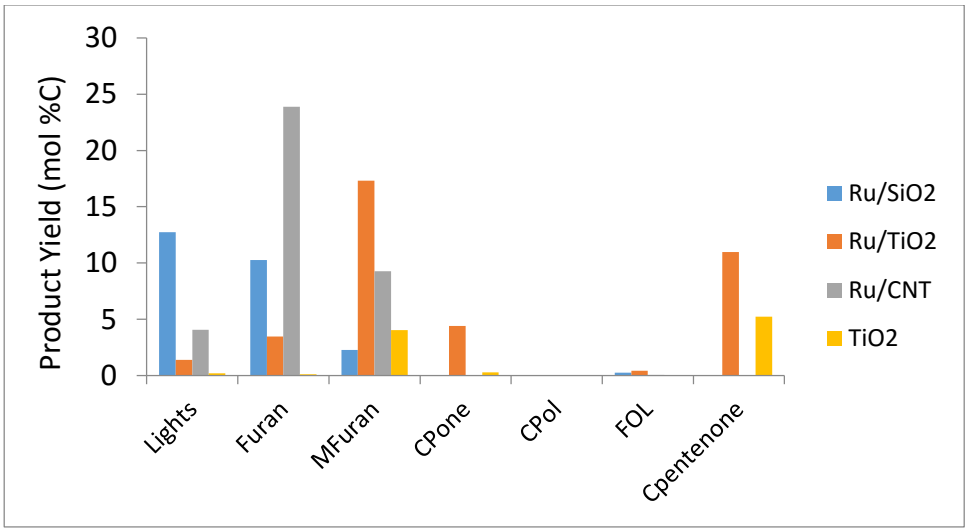

Figure 59: Product Yield for water/furfural (12:1 molar ratio) feed mixture over TiO_2, Ru/SiO_2 , Ru/CNT and Ru/TiO_2 catalysts W/F = 1.85h (TiO_2) and 0.13h (Ru/SiO_2 and Ru/TiO_2) and 0.39h(Ru/CNT) Conversion = 10% (TiO_2); 25%(5.3% Ru/SiO_2); 38% (4.4% Ru/TiO_2) and 37% (1% Ru/CNT) T = 400 °C, P = 1 atm, TOS = 30 mins

Our group observed a similar trend for the conversion of m-cresol over Ru catalysts.[182] While the rate of toluene formation was enhanced as a result of introduction of TiO_2 as a support, the hydrogenolysis of m-cresol to light gases was also greatly suppressed. One possible reason proposed for the latter was the breaking up of ensembles or sites responsible for hydrogenolysis as a result of TiO_2 decoration on Ru after high temperature reduction.[182] DFT calculations and experimental observations were in agreement showing that perimeter sites around the Ru metal were the active sites for m-cresol deoxygenation to toluene over Ru/TiO_2. This enhancement to form desired products (cyclopentanone/2-cyclopentenone and 2MF in this study/toluene in the study described above) as a result of introduction of TiO_2 as a support is similar for both furfural and m-cresol feeds therefore it is likely that the same perimeter sites responsible for m-cresol conversion are involved in FAL conversion to 2MF and cyclopentanone. However, it is also possible that defect sites on the TiO_2 support far

away from the metal are involved in this reaction. To understand this further, the reaction was run over pure TiO_2 without the Ru metal. As seen in **Figure 59**, similar product distributions are observed over TiO_2 and Ru/TiO_2 with an order of magnitude higher W/F for pure TiO_2. This was also observed for guaiacol conversion in which the addition of Ru generated more active sites for the reaction hence the increased conversion observed over Ru/TiO_2.[14] At this point therefore, it is only known that the active sites to form 2MF and CPone/CPentenone are created as a result of the interaction between Ru and TiO_2. Both types of sites – perimeter sites and defect sites on TiO_2 could be playing important roles for formation of these products especially as they are observed on TiO_2 without the presence of Ru. Other reactions such as hydrogenation (FAL to FOL, cyclopentanone to cyclopentanol) and decarbonylation/C-C hydrogenolysis reaction (FAL to Furan and light gases) occur over the Ru metal.

Oak Torrefaction Experiments

As this reaction showed promise in model compound studies, it was of great interest to study if the reactions would take place with the oak torrefaction vapor stream. In pyroprobe pulse studies red oak was torrefied at 270 °C. The resultant vapor stream consisted primarily of water and C2-C3 acids and esters. Torrefaction of 1 mg of red oak also importantly yielded 0.11 μmol of furfural. In addition, a pyranic species that is dehydrated to furfural with increased residence time in the heated transfer lines is seen with a yield of 0.17 μmol. Along with the small amount of furfuryl alcohol and furan increases the total furanic ring composition in the vapors to 0.30 μmol per milligram of red oak torrefied. It should be noted that this stream also contains a large

amount of water that is not quantified by FID analysis. The condensed liquid from this torrefaction process has been found to have a water content of 65 wt%.

As expected the acids and esters underwent ketonization reactions under these conditions to form C3-C4 ketones. Once condensed these compounds are stable and limit acid catalyzed reactions. In addition to ketonization of the acids, remarkably, the furfural species reacted to produce ring re-arrangement products 2-cyclopenten-1-one and cyclopentanone, as well as the dehydration product 2MF similar to the model compound studies. Furfural conversion levels of 91% were observed in the initial biomass pulse. Competitive adsorption due to the many compounds in the torrefaction vapor stream could be playing a major role in shifting the product selectivity with these real feeds. It is important to note that molar ratios of water/furfural levels are even higher with this feed than with model compound studies. It would be expected that water and acids have a significant role in shifting product selectivity as discussed previously. With the real torrefaction stream an increased selectivity to ring re-arrangement products (47 %) was observed compared to dehydration products 2MF (12 %). A summary of product selectivities can be seen in **Figure 60**. Converted furfural not accounted for in **Figure 60** is likely cracked into light gases over the metal catalyst.

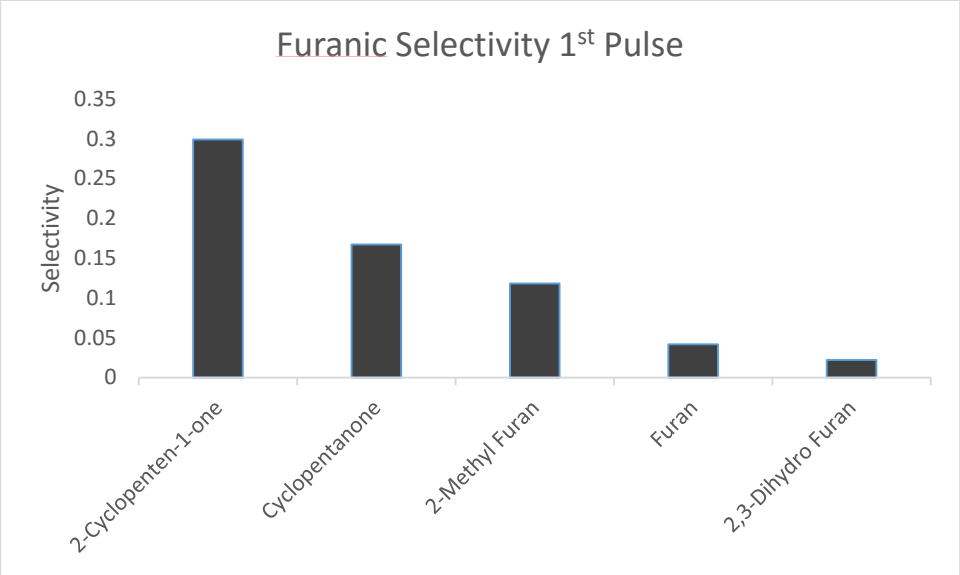

Figure 60: Furanic and Pyranic product selectivity for the initial pulse of oak torrefaction. Selectivity as defined as moles product/mol of furfural+pyranic in blank reaction

During pulse experiments ten pulses of red oak was torrefied approximately two hours apart, each time the vapors passed through the reactor with the Ru/TiO_2 catalyst. As it can be seen in **Figure 61**, the conversion to cyclopentenone/cyclopentanone and 2MF is fairly stable throughout the pulses. It was also observed that the ketonization reactions stayed at a stable conversion as well. It would be expected scaling up this upgrading process would lead to a stable liquid product. These results also show the promise of the torrefaction process. This is the first evidence of a Piancatelli type rearrangement using actual biomass feeds. It is well known if a full pyrolysis of oak was carried out catalyst deactivation would be significant and unwanted side reactions would dominate. As this strategy limits the amount of different organic compounds that pass over the catalyst surface, targeted chemistries can occur. This promising product

could then be upgraded in the liquid phase as discussed previously to form gasoline and/or diesel range products.

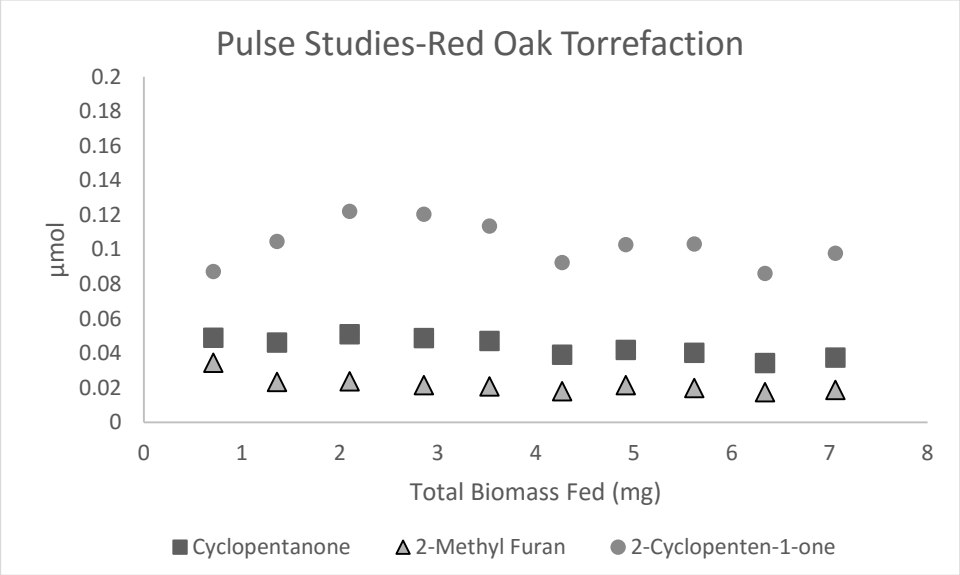

Figure 61: Yield of the major product from furfural reaction over Ru/TiO_2. Red Oak was torrefied at 270°C for 20 minutes using an analytical pyroprobe with ex situ catalytic reactor.

Conclusion

Conversion of furfural in vapor phase at 400 ^oC has been studied over Ru/TiO_2 and a number of reactions such as hydrogenation, decarbonylation, hydrogenolysis were observed over the catalyst to form products such as furfuryl alcohol, furan and 2-methylfuran. The carbon efficient Piancatelli rearrangement of furfural to produce cyclopentanone/2-cyclopentenone was also observed with subsequent hydrogenation to form cyclopentanol occurring over the Ru metal. Water was demonstrated to play a role in shifting the selectivity from the dominant 2-methylfuran to cyclopentanone/2-cyclopentenone. Also, the support plays an important role in determining the product distribution as pure Ru catalysts produced mainly light gases and furan when compared

with Ru/TiO_2. The active sites for this reaction are either perimeter sites or defects on TiO_2 created as a result of interaction between Ru and TiO_2. Using Red Oak as a biomass source, the reaction was also observed with real torrefaction feeds in a pulse reactor. With the biomass feeds the selectivity to cylcopentanone was enhanced due to the adsorption effects of the numerous compounds found in the vapor stream.

Appendix C: Supplemental Figures

Chapter 7

Product Distributions

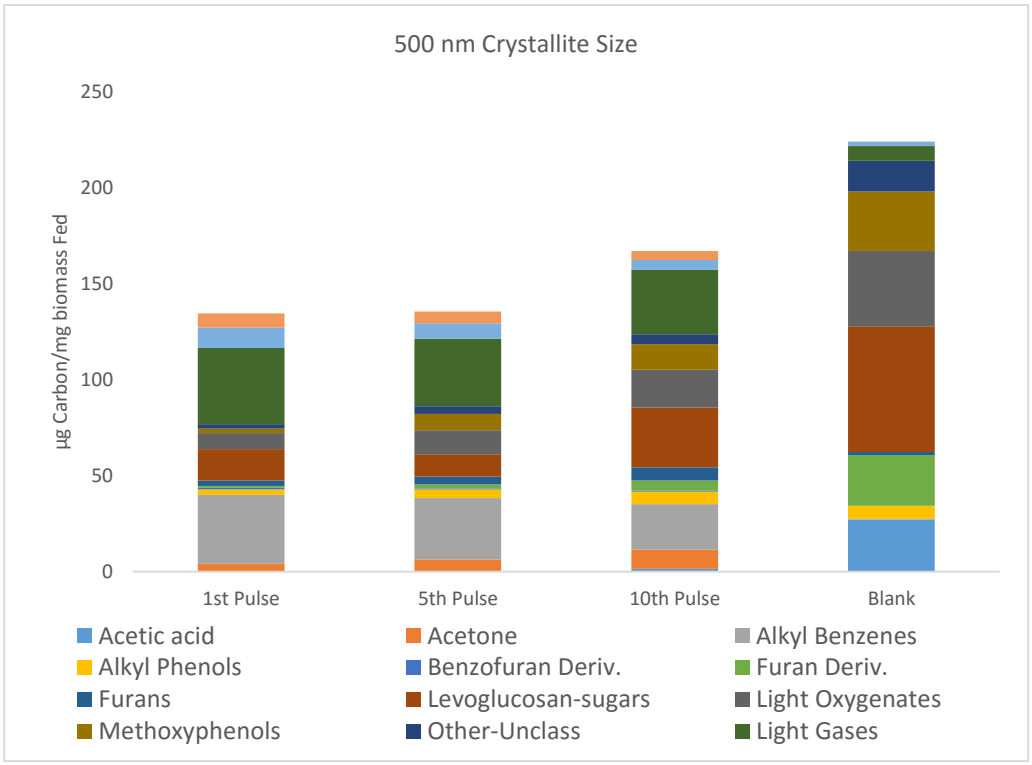

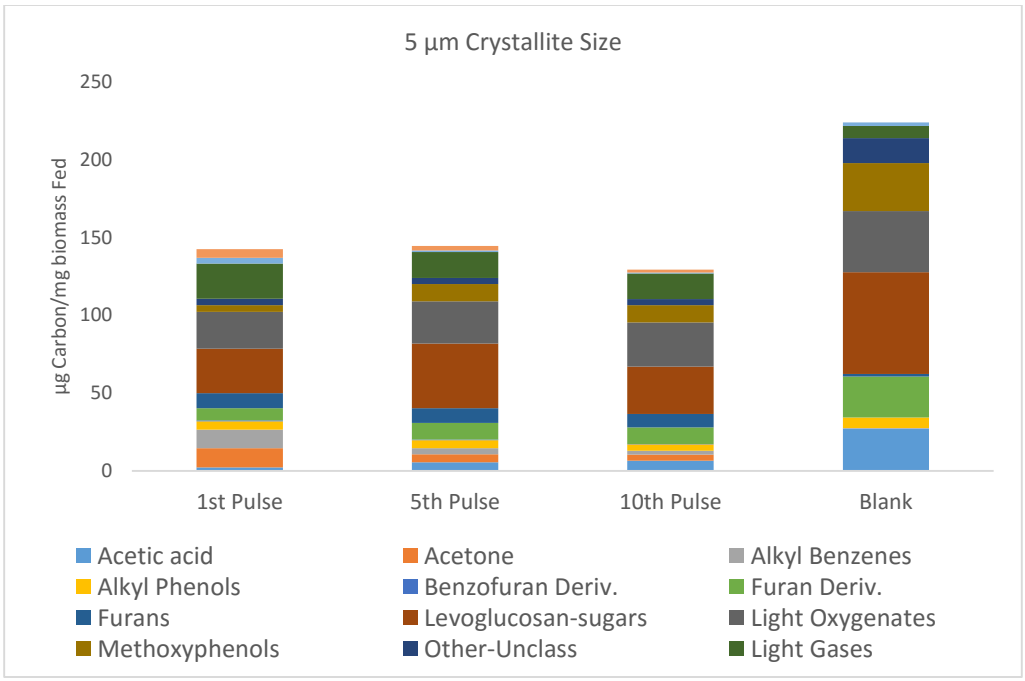
5 µm Crystallite Size
µg Carbon/mg biomass Fed
250
200
150
100
50
0
1st Pulse
5th Pulse
10th Pulse
Blank
Acetic acid
Acetone
Alkyl Benzenes
Alkyl Phenols
Benzofuran Deriv.
Furan Deriv.
Furans
Levoglucosan-sugars
Light Oxygenates
Methoxyphenols
Other-Unclass
Light Gases

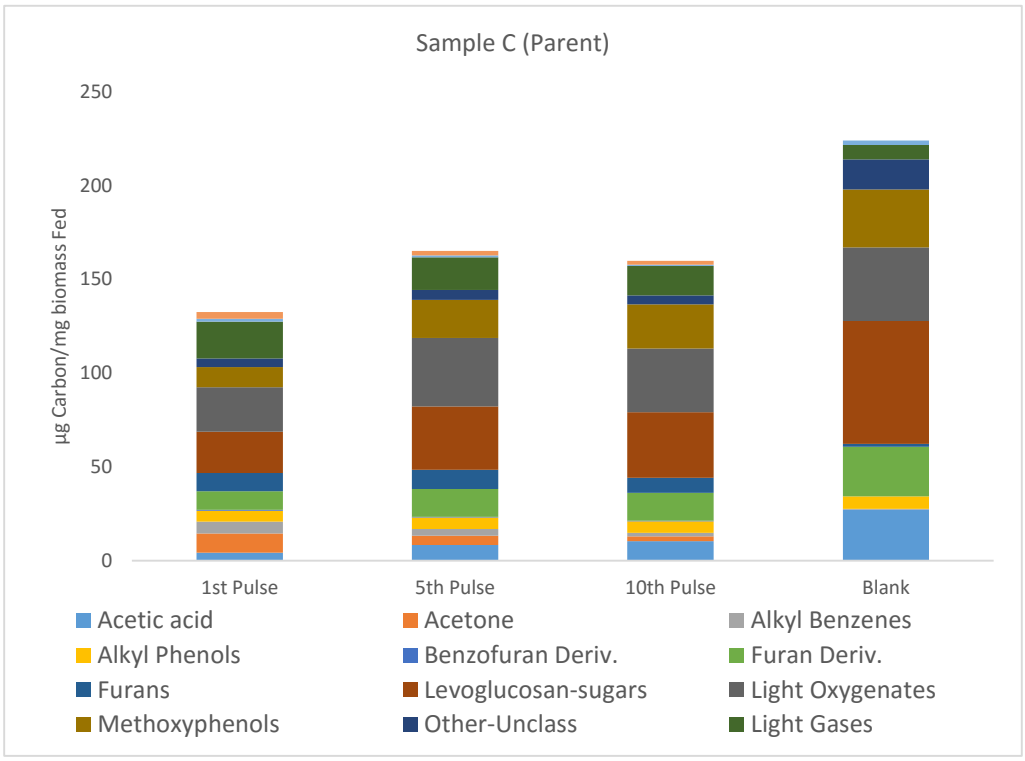
Sample C (Parent)
µg Carbon/mg biomass Fed
250
200
150
100
50
0
1st Pulse
5th Pulse
10th Pulse
Blank
Acetic acid
Acetone
Alkyl Benzenes
Alkyl Phenols
Benzofuran Deriv.
Furan Deriv.
Furans
Levoglucosan-sugars
Light Oxygenates
Methoxyphenols
Other-Unclass
Light Gases

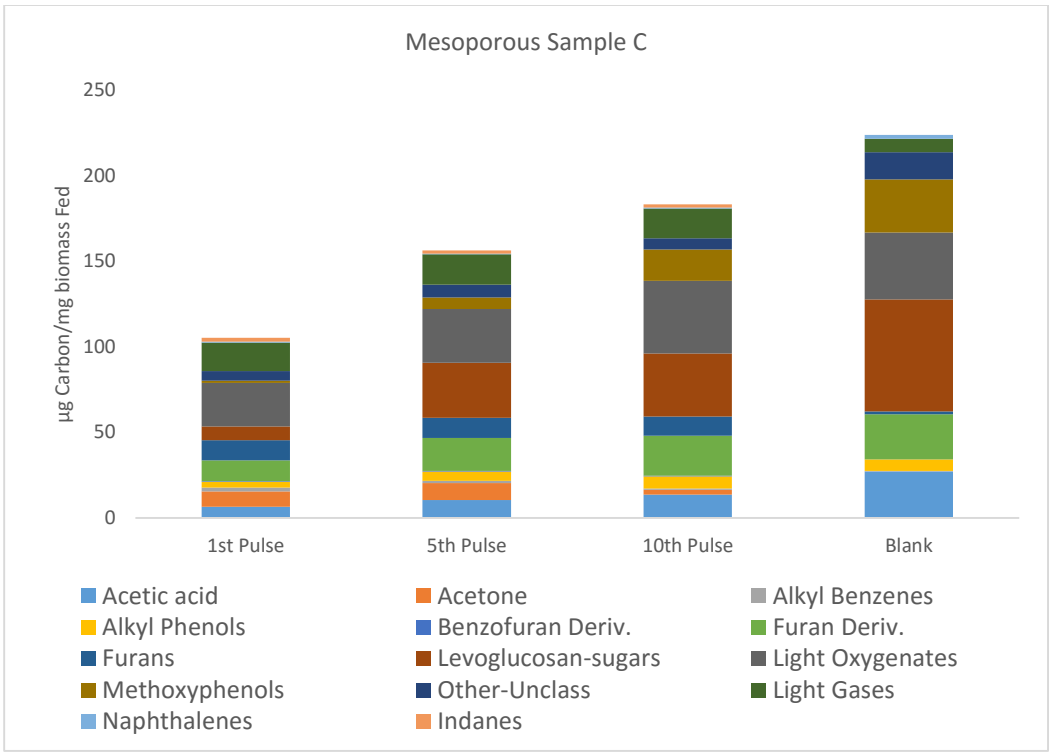
Mesoporous Sample C
250
200
150
100
50
0
µg Carbon/mg biomass Fed
1st Pulse
5th Pulse
10th Pulse
Blank
Acetic acid
Acetone
Alkyl Benzenes
Alkyl Phenols
Benzofuran Deriv.
Furan Deriv.
Furans
Levoglucosan-sugars
Light Oxygenates
Methoxyphenols
Other-Unclass
Light Gases
Naphthalenes
Indanes

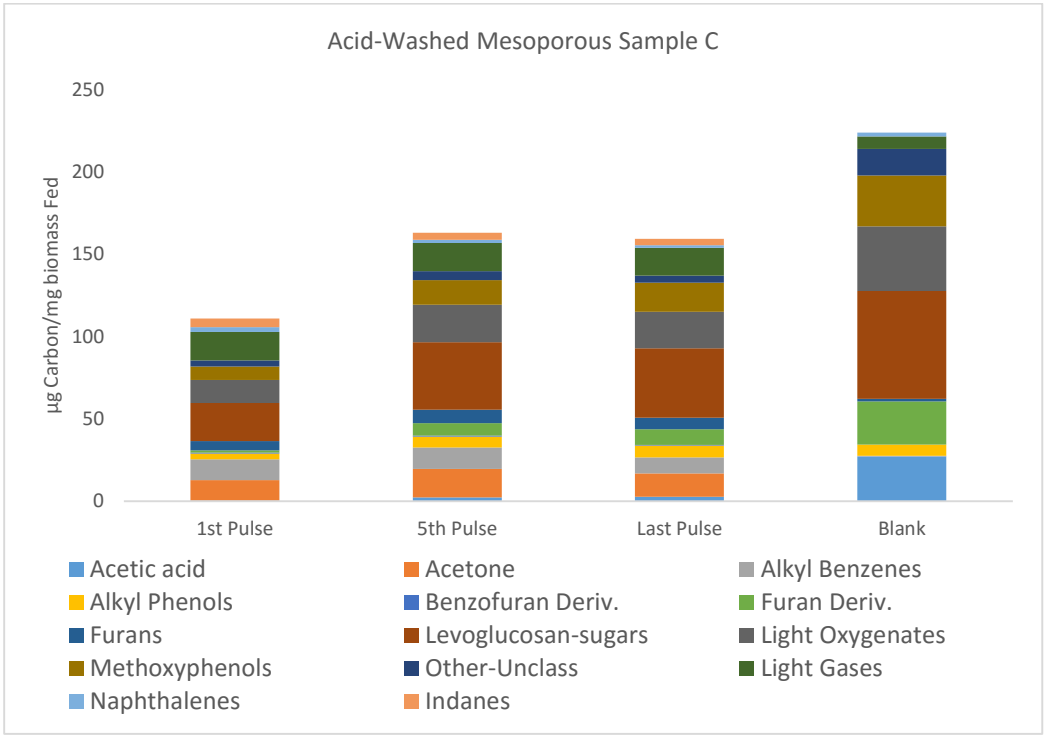
Acid-Washed Mesoporous Sample C
250
200
150
100
50
0
µg Carbon/mg biomass Fed
1st Pulse
5th Pulse
Last Pulse
Blank
Acetic acid
Acetone
Alkyl Benzenes
Alkyl Phenols
Benzofuran Deriv.
Furan Deriv.
Furans
Levoglucosan-sugars
Light Oxygenates
Methoxyphenols
Other-Unclass
Light Gases
Naphthalenes
Indanes

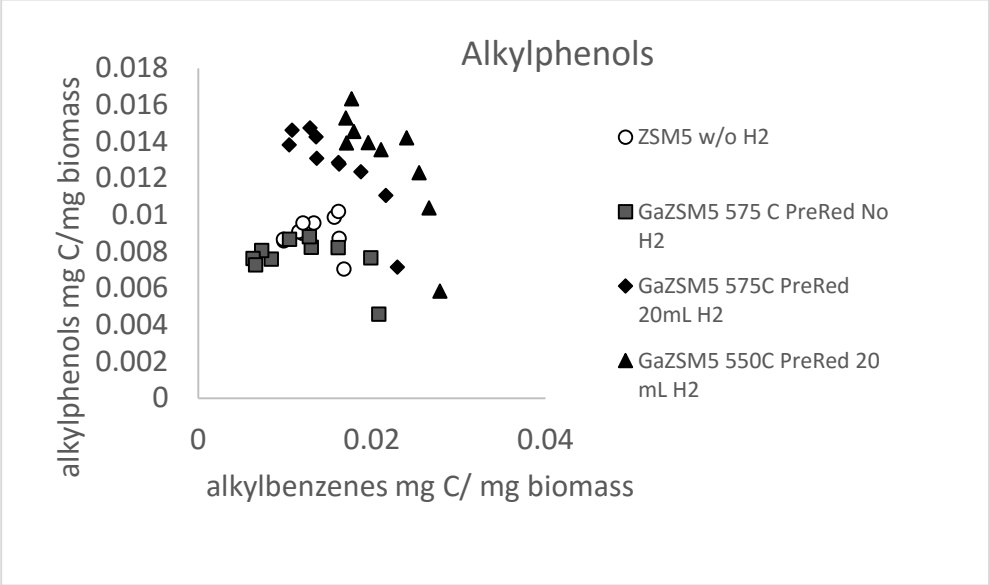
Alkylphenols
alkylphenols mg C/mg biomass
0.018
0.016
0.014
0.012
0.01
0.008
0.006
0.004
0.002
0
0
0.02
0.04
alkylbenzenes mg C/ mg biomass
ZSM5 w/o H2
GaZSM5 575 C PreRed No H2
GaZSM5 575C PreRed 20mL H2
GaZSM5 550C PreRed 20 mL H2

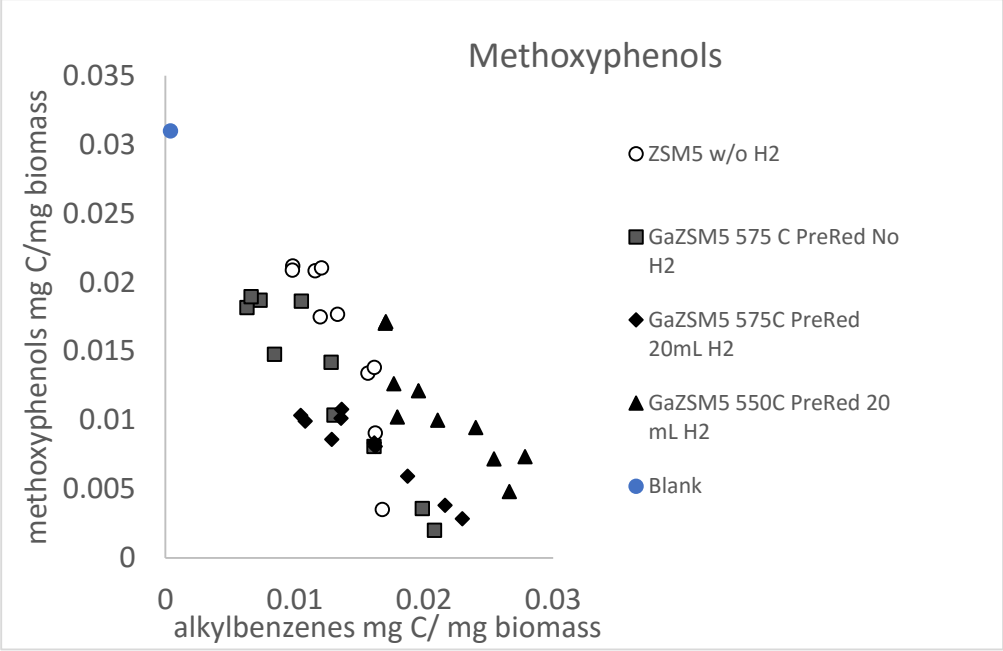
Methoxyphenols
methoxyphenols mg C/mg biomass
0.035
0.03
0.025
0.02
0.015
0.01
0.005
0
0
0.01
0.02
0.03
alkylbenzenes mg C/ mg biomass
ZSM5 w/o H2
GaZSM5 575 C PreRed No H2
GaZSM5 575C PreRed 20mL H2
GaZSM5 550C PreRed 20 mL H2
Blank

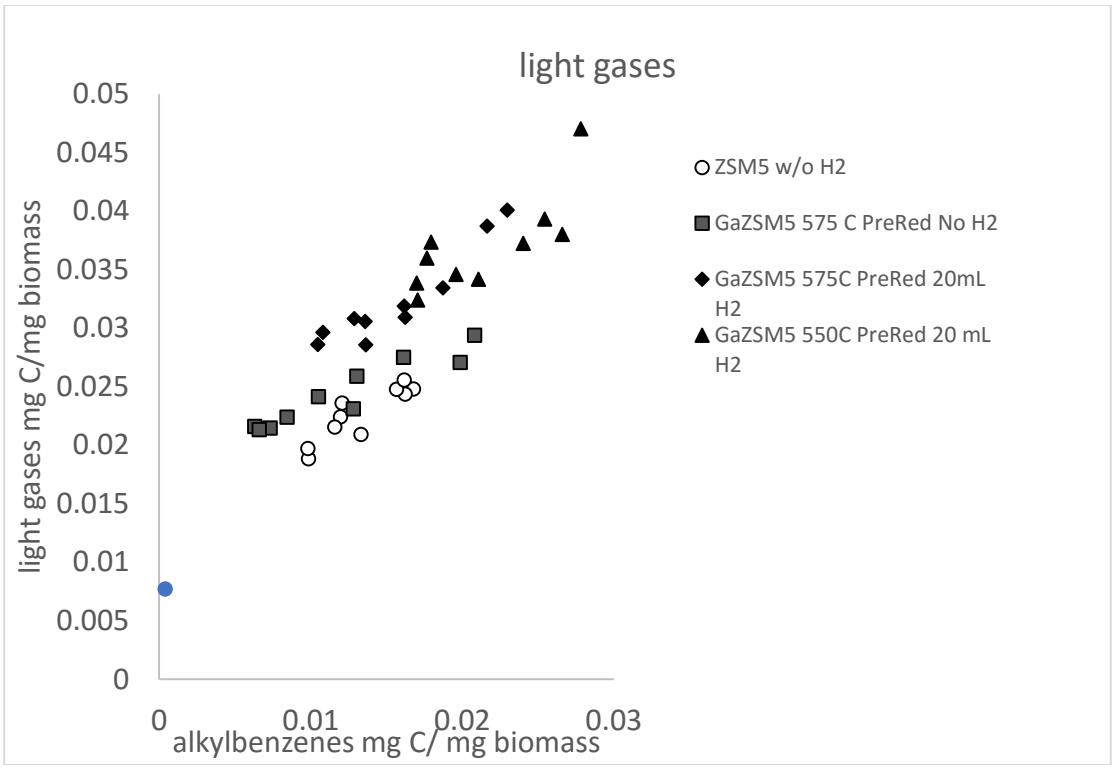
light gases
0.05
0.045
0.04
0.035
0.03
0.025
0.02
0.015
0.01
0.005
0
light gases mg C/mg biomass
0
0.01
0.02
0.03
alkylbenzenes mg C/ mg biomass
ZSM5 w/o H2
GaZSM5 575 C PreRed No H2
GaZSM5 575C PreRed 20mL H2
GaZSM5 550C PreRed 20 mL H2

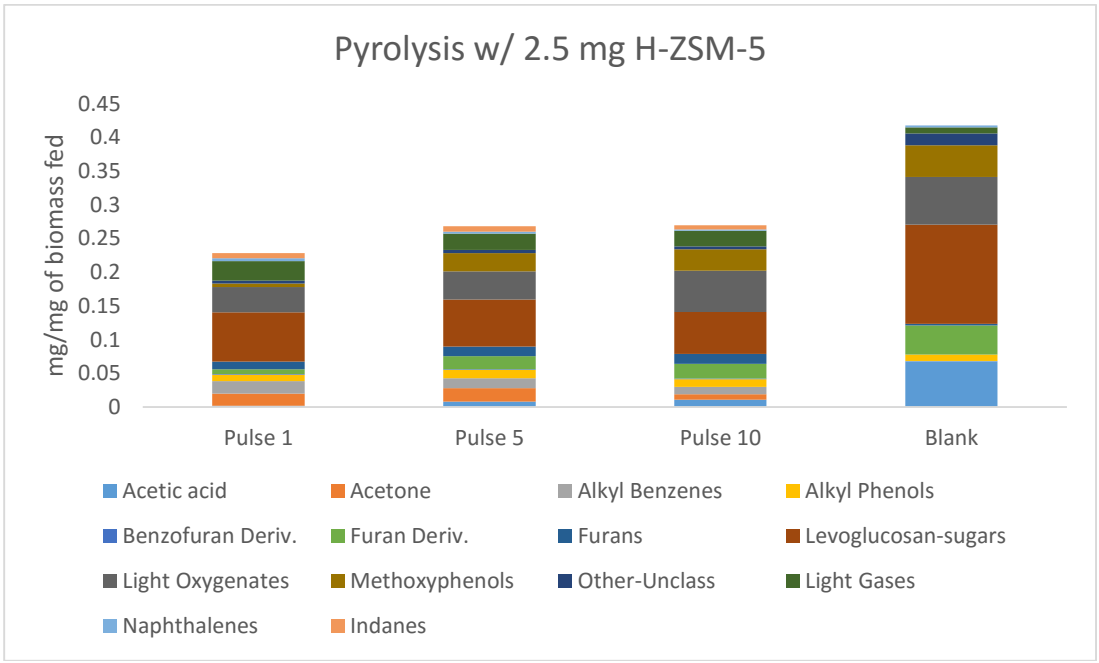
Pyrolysis w/ 2.5 mg H-ZSM-5
0.45
0.4
0.35
0.3
0.25
0.2
0.15
0.1
0.05
0
mg/mg of biomass fed
Pulse 1
Pulse 5
Pulse 10
Blank
Acetic acid
Acetone
Alkyl Benzenes
Alkyl Phenols
Benzofuran Deriv.
Furan Deriv.
Furans
Levoglucosan-sugars
Light Oxygenates
Methoxyphenols
Other-Unclass
Light Gases
Naphthalenes
Indanes

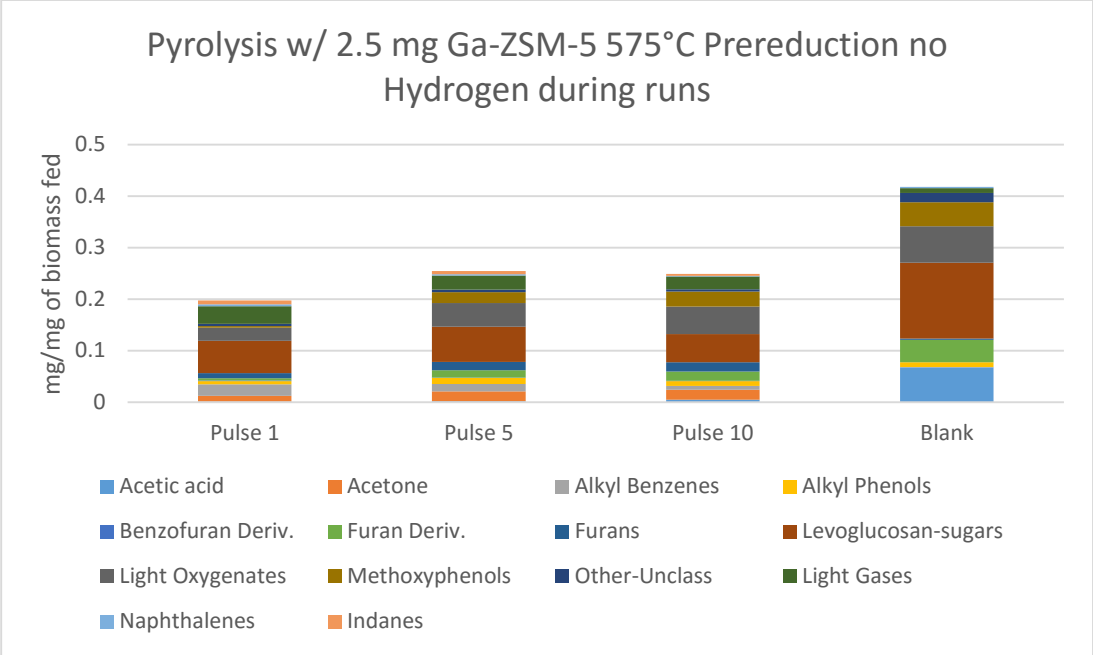
Pyrolysis w/ 2.5 mg Ga-ZSM-5 575°C Prereduction no Hydrogen during runs
mg/mg of biomass fed
0.5
0.4
0.3
0.2
0.1
0
Pulse 1
Pulse 5
Pulse 10
Blank
Acetic acid
Acetone
Alkyl Benzenes
Alkyl Phenols
Benzofuran Deriv.
Furan Deriv.
Furans
Levoglucosan-sugars
Light Oxygenates
Methoxyphenols
Other-Unclass
Light Gases
Naphthalenes
Indanes

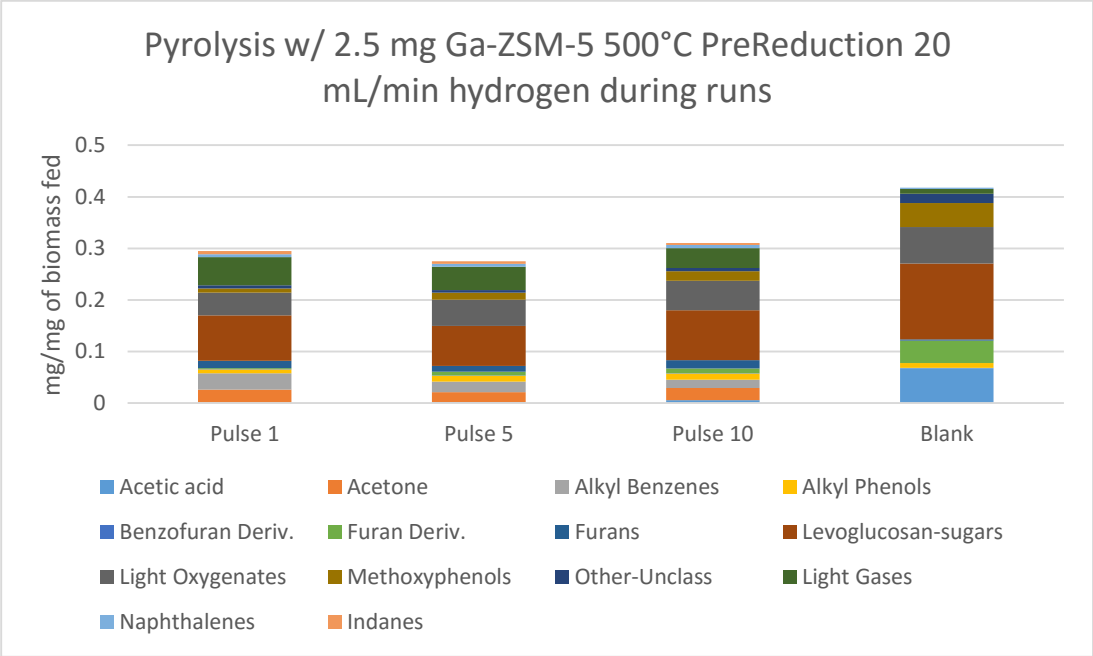
Pyrolysis w/ 2.5 mg Ga-ZSM-5 500°C PreReduction 20 mL/min hydrogen during runs
mg/mg of biomass fed
0.5
0.4
0.3
0.2
0.1
0
Pulse 1
Pulse 5
Pulse 10
Blank
Acetic acid
Acetone
Alkyl Benzenes
Alkyl Phenols
Benzofuran Deriv.
Furan Deriv.
Furans
Levoglucosan-sugars
Light Oxygenates
Methoxyphenols
Other-Unclass
Light Gases
Naphthalenes
Indanes

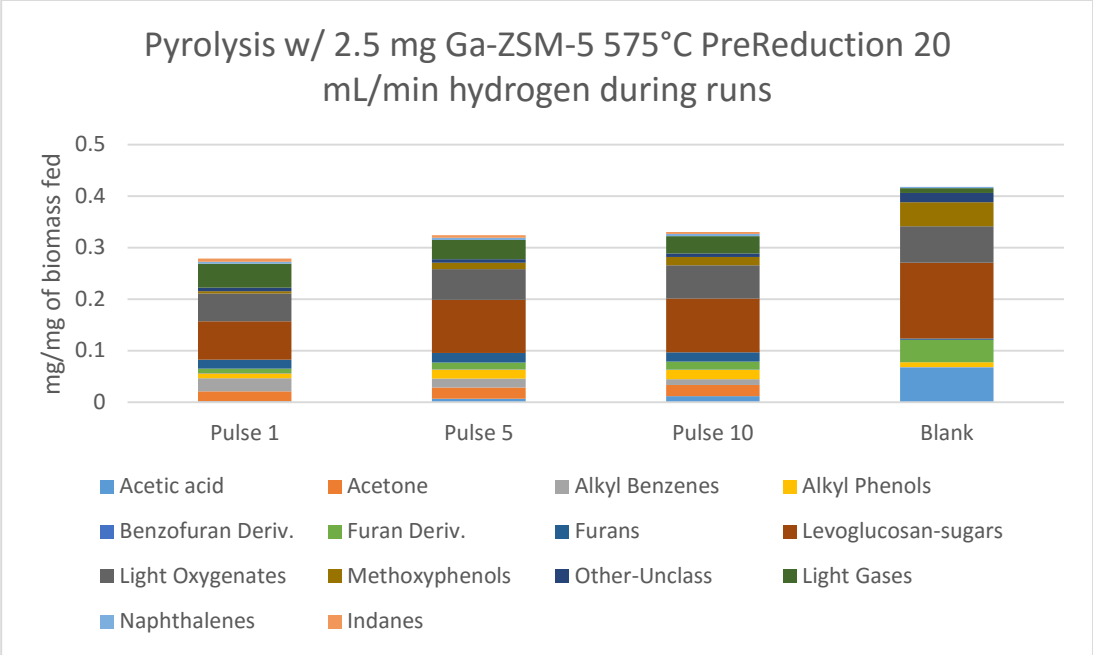
Pyrolysis w/ 2.5 mg Ga-ZSM-5 575°C PreReduction 20 mL/min hydrogen during runs
mg/mg of biomass fed
0.5
0.4
0.3
0.2
0.1
0
Pulse 1
Pulse 5
Pulse 10
Blank
Acetic acid
Acetone
Alkyl Benzenes
Alkyl Phenols
Benzofuran Deriv.
Furan Deriv.
Furans
Levoglucosan-sugars
Light Oxygenates
Methoxyphenols
Other-Unclass
Light Gases
Naphthalenes
Indanes

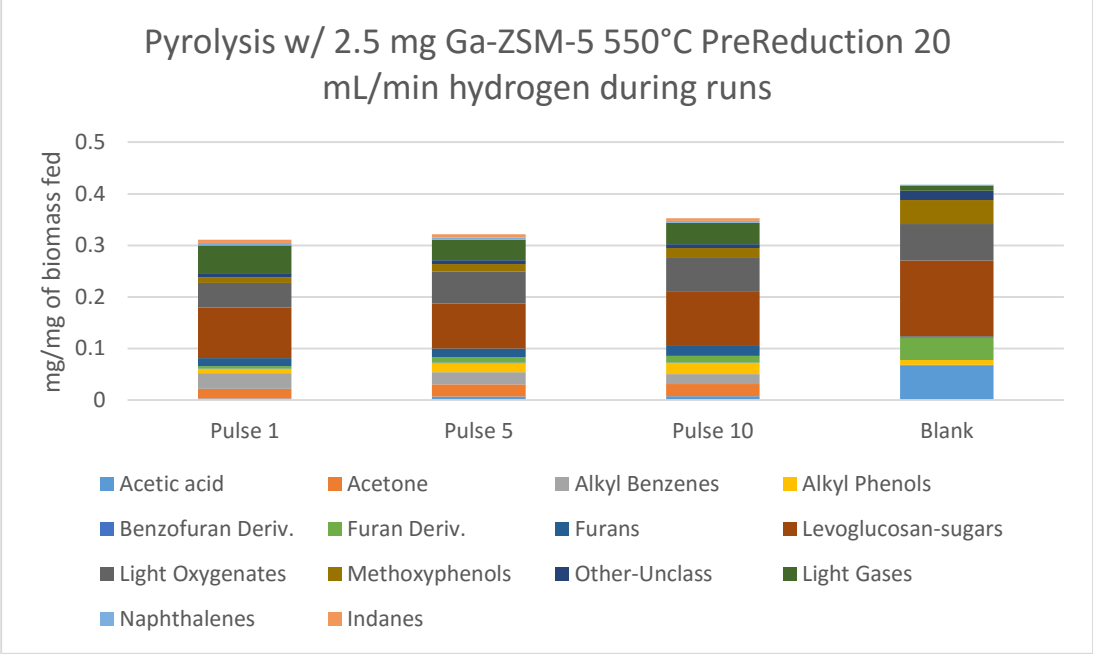
Pyrolysis w/ 2.5 mg Ga-ZSM-5 550°C PreReduction 20 mL/min hydrogen during runs
mg/mg of biomass fed
0.5
0.4
0.3
0.2
0.1
0
Pulse 1
Pulse 5
Pulse 10
Blank
Acetic acid
Acetone
Alkyl Benzenes
Alkyl Phenols
Benzofuran Deriv.
Furan Deriv.
Furans
Levoglucosan-sugars
Light Oxygenates
Methoxyphenols
Other-Unclass
Light Gases
Naphthalenes
Indanes